



Universities Press

EDUCATIONAL MONOGRAPHS



Jawaharlal Nehru Centre for
Advanced Scientific Research

Electrostatics of Atoms and Molecules



S R Gadre and R N Shirsat

Educational Monographs

Electrostatics of Atoms and Molecules

S R Gadre

Department of Chemistry
University of Pune

R N Shirsat

Department of Chemistry
University of Goa



Jawaharlal Nehru Centre for
Advanced Scientific Research



Universities Press

Universities Press (India) Limited

Registered Office

3-5-819 Hyderguda, Hyderabad 500 029 (A.P.), India

Distributed by

Orient Longman Limited

Registered Office

3-6-272 Himayatnagar, Hyderabad 500 029 (A.P.), India

Other Offices

Bangalore / Bhopal / Bhubaneshwar / Calcutta / Chandigarh

Chennai / Ernakulam / Guwahati / Hyderabad / Jaipur

Lucknow / Mumbai / New Delhi / Patna

© Universities Press (India) Limited 2000

First published 2000

ISBN 81 7371 296 4

Typeset by

Venture Graphics, Chennai 600 031

Printed in India at

Orion Printers, Hyderabad 500 004

Published by

Universities Press (India) Limited

3-5-819 Hyderguda, Hyderabad 500 029

Contents

CHAPTER 1

Electrostatics	1
1.1 Preamble	1
1.2 Electrostatic Field and Potential due to Discrete Charges	4
1.3 Visual Display of Electrostatic Potential and Field due to Discrete Charges	8
1.4 Potential and Field of a Dipole: Moments of a Charge Distribution	9
1.5 Basic Theorems in Electrostatics	12
1.6 Electrostatic Potential of Molecules	17
References	18

CHAPTER 2

Molecular Electrostatic Potential: Theoretical Computation, Experimental Determination and Graphics Visualization	19
2.1 Introduction	19
2.2 Theoretical Evaluation via Multipole Moments	20
2.3 Point Charge Models for MESP Evaluation	22
2.4 MESP Using <i>Ab Initio</i> Molecular Wave Function	26
2.5 MESP from Semi-Empirical and other Approximate Methods	29
2.6 Experimental Determination of Electrostatic Potentials	30
2.7 MESP Visualization	33
2.7.1 Two-dimensional visualization	33
2.7.2 Three-dimensional visualization	34
References	36

CHAPTER 3

Some General Results Regarding Atomic and Molecular Electrostatic Potentials	39
3.1 Molecular Non-binding Theorems within Statistical Theories	39
3.2 ESP at Nuclei and Electronic Energies of Atoms and Molecules	44
3.3 Similarities in Contour Maps of Molecular Electron Densities, Electrostatic Potentials and Bare-Nuclear Potentials	47
3.4 Maximal and Minimal Characteristics of Atomic and Molecular Electrostatic Potentials	49
3.5 Atomic and Molecular Anions	51
3.6 Topography of Molecular Electrostatic Potentials	55
References	60

CHAPTER 4

Applications of Molecular Electrostatic Potential	63
4.1 Introduction	63
4.2 MESP as a Reactivity Parameter in Chemistry	63
4.3 Electrostatics-Based Models for Intermolecular Interactions	67
4.4 High-Energy Molecules	70
4.5 MESP Applications to Catalysis	72
4.5.1 Zeolites, oxides and related materials	72
4.5.2 Enzyme catalysis	73
4.6 Structure–Property and Structure–Activity Relationships	75
4.7 Treatments Based on Poisson–Boltzmann Equation	77
4.8 Biological and Medicinal Chemistry	79
References	81

Appendix A

Some Biographical Notes on Pioneering Contributors to Electrostatics	85
References	88

Appendix B

B.1 A list of some useful fundamental and derived physico-chemical constants	89
B.2 Atomic units and their conversion to SI units	90

Appendix C

Introduction to Vectors	91
References	99

Appendix D

<i>Ab Initio</i> Methods and Gaussian Basis Sets	100
References	108

Appendix E

Introduction to Semi-Empirical Methods	110
References	113

Appendix F

Molecular Electron Density and Density Functional Theory	115
F1 Molecular Electron Density	115
F2 Density Functional Theory	118
F3 Topographical Features of MED	121
References	123

Appendix G

Topographical Concepts	125
References	130

Index	131
-------------	-----

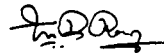
Foreword

The Jawaharlal Nehru Centre for Advanced Scientific Research was established by the Government of India in 1989 as part of the centenary celebrations of Pandit Jawaharlal Nehru. Located in Bangalore, it functions in close academic collaboration with the Indian Institute of Science.

The Centre functions as an autonomous institution devoted to advanced scientific research. It promotes programmes in chosen frontier areas of science and engineering and supports workshops and symposia in these areas. It also has programmes to encourage young talent.

In addition to the above activities, the Centre has undertaken a programme of publishing high quality Educational Monographs written by leading scientists and engineers in the country. These are short accounts of interesting areas in science and engineering addressed to students at the graduate and postgraduate levels, and the general research community.

This monograph is one of the series being brought out as part of the publication activities of the Centre. The Centre pays due attention to the choice of authors and subjects and style of presentation, to make these monographs attractive, interesting and useful to students as well as teachers. It is our hope that these publications will be received well both within and outside India.



C N R Rao
President

Preface

One of the key physical quantities which has found wide-ranging applications in many branches of chemistry, physics and biology is the molecular electrostatic potential (MESP). The purpose of this monograph is to introduce the subject of molecular electrostatics to postgraduate students, teachers, and young researchers in the above disciplines. Keeping this in view, an attempt has been made here to discuss rigorous as well as applied aspects of the MESP. An essence of relevant mathematical arguments has been provided, although detailed derivations have been avoided. Wherever possible, illustrations have been introduced to bring out the salient features of MESP in a pictorial way. Many of the illustrations are taken from the work done at the authors' laboratory with an indigenously developed package called UNIVIS. This is done due to the easy accessibility and flexibility of such graphics visualization.

The outline of this monograph is as follows. Chapter 1 introduces the subject of electrostatics and provides a connection with the molecular world through the definition of MESP. We have, however, dropped out any formal introduction to Maxwell's equations due to limitations of space. The experimental determination, theoretical calculation as well as three-dimensional visualization of the MESP are taken up in Chapter 2. Chapter 3 presents a variety of general results regarding electrostatics of atoms and molecules. Chapter 4 is aimed at briefly summarizing the applications of MESP in diverse areas of chemistry, biology, materials science, etc.

A series of appendices providing an introduction to several topics appearing in the main text of the monograph are also included. Readers uninitiated in a given topic may gainfully refer to the corresponding appendix. Optionally available from the authors is a compact disk containing colour graphics displays of the MESP features of a large number of molecules. Readers having access to a computer with a colour monitor can benefit from this visualization.

It is expected that a chemist/physicist with adequate mathematical background would find the entire monograph of interest. However, Chapter 3 may be omitted during the first reading by those who are less mathematically oriented. Due to limitations of space, we are constrained to drop out details

of certain topics and have attempted to provide just a flavour of a subject which is of great utility in physics, chemistry and biology.

It is a pleasure to acknowledge the help and advice from several colleagues and friends. In particular, we are thankful to several referees (introduced to us through the organization of XII ICCCRE in Pune) and the entire quantum chemistry research group at Pune University for their assistance, critical comments and suggestions. In particular, we are grateful to Professors D R Salahub, K Hirao, S B Jonnalagadda, J Gosper, N Sathyamurthy, R Vertivel, B L Tembe, R K Pathak, M Swift, E Ludeña and J J P Stewart for reviewing the manuscript. The responsibility for errors which may have still remained in the monograph, is certainly ours. Recalling Professor Coulson's words, "We would like to be told of places where we could do better".

We thank the Jawaharlal Nehru Centre for Advanced Scientific Research for the sponsorship. In particular, the constant encouragement and support from Professors C N R Rao and N Mukunda is gratefully acknowledged.

It is our hope that students, teachers and researchers working in various cross-disciplinary areas in science will find this monograph useful.

Rajendra N Shirsat
Taleigao Plateau, Goa

Shridhar R Gadre
Pune, Maharashtra

1

Electrostatics

1.1 Preamble

It was known to Thales of Miletus [1–3] (ca. 600 BC) that a rubbed piece of amber attracts pieces of straw. The term ‘electric’, derived from the Greek word ‘electron’ (amber), seems to have been first used by Gilbert around AD 1600 [3]. Later, Cabeo documented that electrified bodies attract or repel each other, which implied that there were two types of electricity. The terms positive and negative were suggested by Benjamin Franklin and Watson independently in 1747 [3]. The historical development of electrostatics makes fascinating reading. Some biographical notes on this aspect are presented in Appendix A.

Similar empirical observations, that natural magnetic ores called lodestones, attract iron filings were also known for a long time. After developing separately, the sciences of electricity and magnetism were coupled in 1820 by Ørsted, who noticed that an electric current flowing through a wire can deflect a magnetic needle. The new science of electromagnetism was developed by Michael Faraday and James Clerk Maxwell.

In this monograph, we shall deal directly only with the electrostatic aspects. The most fundamental quantitative law in electrostatics describing the force of attraction or repulsion between two point charges was given by Charles Augustin de Coulomb in 1784. Experimental investigations were made by him on a torsion balance [1, 2] of the type that was later used by Henry Cavendish for studying gravitational forces. However, the existence of such a law bearing an inverse square form was apparently known [3] to Aepinus, Cavendish and Priestley. Coulomb’s law may be mathematically expressed as

$$F = \frac{q_1 q_2 \hat{\mathbf{r}}}{4\pi\epsilon_0 r^2} \quad (1.1)$$

where q_1, q_2 are point charges separated by a distance r in vacuum; $\hat{\mathbf{r}}$ is a unit vector joining the position vectors of q_1 and q_2 and $4\pi\epsilon_0$ is the constant

2 Electrostatics of Atoms and Molecules

of proportionality in SI units. In a medium, ϵ_0 in the denominator of Eq. 1.1 is replaced by an appropriate constant ϵ , called the permittivity of the medium. The free-space value ϵ_0 equals $8.854 \times 10^{-12} \text{C}^2\text{N}^{-1}\text{m}^{-2}$ (see Appendix B for a list of some useful fundamental and derived constants). It is assumed in Eq. 1.1 that both the charges are sufficiently localized within regions that are small compared to the distance r between them. Further, if a charge has some internal structure [4], then it cannot be described by a mere scalar quantity, q .

It may be re-emphasized that Coulomb's law bears the inverse square form, analogous to that of Newton's law of gravitation, discovered about a century earlier. The main difference is that the gravitational force is always attractive, whereas the electrostatic force could be attractive or repulsive. It is commonly known that like charges repel and unlike charges attract each other. Charges are thus characterized into two classes: positive and negative. It may be noted that the currently used labels of positive and negative for the charges of a proton and an electron, respectively, are rather arbitrary. This choice of signs is perhaps a historical accident [4]. Two other properties of electrical charges described below are significant.

- i) Conservation of charge: The total electrical charge in an isolated system is conserved, i.e., the algebraic sum of the positive and negative charges does not change.
- ii) Quantization of charge: Electrical charges occur in units of e , the electronic charge. This 'graininess' of electricity, however, does not show up in macroscale experiments due to the tiny numerical value of e . Several experimental verifications of the charge quantization principle have been recorded [4]. For example, in order to appraise the validity of proton–electron charge balance, Zorn *et al.* [5] passed a sharply defined beam of cesium atoms *in vacuo* through a strong electric field. In the absence of any deflection, it was concluded that the net charge on a cesium atom does not exceed $10^{-16}|e|$. In recent years, it has been stipulated [6] that charge quantization takes place in units of $\pm e/3$. Thus, protons, neutrons and some other subatomic particles may be made of such fractionally charged particles called quarks.

The fact that the exponent in Coulomb's law is 2 (and not a number close to 2, e.g. 2.00001 or 1.99999) has been verified through many carefully devised experimental investigations. The first one was reported in 1772 by the British experimental genius [1] Henry Cavendish, followed later by Maxwell. These investigations were based on the result that the field inside a closed conductor is zero if the inverse square law holds exactly. Two

concentric spherical shells separated by air, but connected by a wire, were initially charged to a high potential. The outer sphere was then earthed and the inner one was tested for charge by an electrometer (for this purpose, a small hole was made in the outer sphere). It was found that the inner sphere did not carry any appreciable charge, amounting to the verification of Coulomb's law to within 2 per cent. Plimpton and Lawton [7] verified in 1936 the validity of Coulomb's law to a few parts in 10^9 by employing a refined version of the same experiment. The deviation of the value of the exponent from 2 is estimated to be less than 3×10^{-16} from more recent experimental studies [7]. A related question deals with the domain of distances over which Coulomb's law breaks down [4]. There is no evidence that Coulomb's law holds at very short distances, for instance, 10^{-12} m or less. Further, this law has, as yet, not been proven by experimentation for distances ranging from geographical to astronomical [4]. Thus the domain of validity of Coulomb's law seems to extend from about 10^{-11} metres to several kilometres (or perhaps more). Electrostatic considerations may thus be applied to relevant aspects of atomic, molecular and solid state phenomena, wherein the typical distances involved may range from 1 to 100 Å.

If there are two (or more) charges exerting forces on a given charge, similar to the situation in a tug-of-war contest, the principle of superposition viz. the force with which two charges interact, is not changed by the presence of a third one [4], is applicable. In other words, the resultant force experienced by the reference charge equals the vector sum of the individual forces.

Both the coulombic and gravitational forces bear an inverse square dependence on the distance. Substituting the value of $4\pi\epsilon_0$ and the gravitational constant G , their magnitudes turn out to be $|F_{coul}| \equiv 9 \times 10^9 \frac{q_1 q_2}{r^2}$ N and $|F_{grav}| \equiv 6.67 \times 10^{-11} \frac{m_1 m_2}{r^2}$ N (where N stands for Newtons). How do the coulombic and gravitational forces between two electrons, separated by a distance r , compare with each other? Taking the values of the electronic charge and mass from Appendix B, one obtains

$$|F_{coul}| \equiv \frac{9.0 \times 10^9 \times (1.6 \times 10^{-19})^2}{r^2} = \frac{2.304 \times 10^{-28}}{r^2} \text{ N}$$

$$|F_{grav}| \equiv \frac{6.7 \times 10^{-11} \times (9.1 \times 10^{-31})^2}{r^2} = \frac{5.548 \times 10^{-71}}{r^2} \text{ N}$$

yielding

4 Electrostatics of Atoms and Molecules

$$\left| \frac{F_{\text{coul}}}{F_{\text{grav}}} \right| \cong 4.2 \times 10^{42}$$

One often wonders whether gravitational forces could play any role in chemical phenomena. The above analysis shows that the gravitational forces could safely be ignored while dealing with even the weakest chemical interactions such as van der Waals attraction or hydrogen bond formation [8]. Yet another dramatic example of the strength of electrical forces has been given by Feynman [9], in his unparalleled style: "If you were standing at arm's length from someone and each of you had one per cent more electrons than protons, the repelling force would be incredible. How great? Enough to lift the Empire State Building? No! To lift Mount Everest? No! The repulsion would be enough to lift a weight equal to that of the *entire earth!*"

1.2 Electrostatic Field and Potential due to Discrete Charges

One may define the intensity \mathbf{E} of an electric field as the force acting on a unit test charge placed at the reference point in the field. Thus, the field due to a fixed point charge q produced at a site \mathbf{r} is given by

$$\mathbf{E} = \frac{q\mathbf{r}}{4\pi\epsilon_0|\mathbf{r}|^3} \quad (1.2)$$

The value of the electric field is expressed in NC^{-1} (Newton per Coulomb) since a unit electric field exerts a force of 1 N on a test charge of 1 C. This field is also equivalent to 1 volt/metre. The source charge q should be held fixed since the introduction of the test charge may cause the former to move. In view of this, sometimes the concept of electric field is introduced by referring to an infinitesimal test charge q_0 , followed by taking the limit as $q_0 \rightarrow 0$. This definition appears to be more rigorous [4] but is actually not, if one keeps in mind the quantization of charge mentioned earlier. Note that, being a vector quantity (see Appendix C for an introduction to vectors), the electric field at a given point requires a magnitude as well as a direction for its description.

We are now ready to invoke the principle of superposition. For a system of two or more charges $\{q_\alpha\}$, the electric field is given by the vector sum of the fields \mathbf{E}_α produced by the individual charges, viz.

$$\mathbf{E}(\mathbf{r}) = \sum_{\alpha} \mathbf{E}_{\alpha}(\mathbf{r}) = \frac{1}{4\pi\epsilon_0} \sum_{\alpha} \frac{q_{\alpha}(\mathbf{r} - \mathbf{r}_{\alpha})}{|\mathbf{r} - \mathbf{r}_{\alpha}|^3} \quad (1.3)$$

Consider an electrical field \mathbf{E} in which a positive charge q is to be moved from A to B as shown in Fig. 1.1. The electrical field exerts a force $q\mathbf{E}$ on the charge. An external force $-q\mathbf{E}$ should thus be applied for preventing acceleration of the charge. Thus, the work done by an external agent in moving the charge through $|d\mathbf{l}|$ is (cf. Fig. 1.2) $-q\mathbf{E} \cdot d\mathbf{l}$. The work done in displacing the charge q from A to B is obtained by a suitable integration, viz.

$$W_{AB} = -q \int_A^B \mathbf{E} \cdot d\mathbf{l} \quad (1.4)$$

where $d\mathbf{l}$ is an infinitesimal displacement vector along AB . Such an integral is called a line integral. The work done on a unit charge while moving it

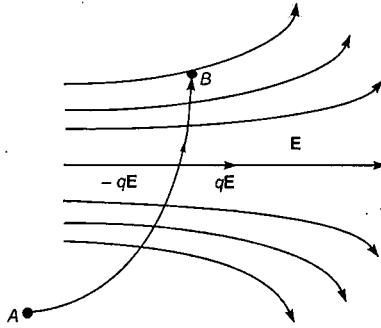


Fig. 1.1 An electrical field \mathbf{E} in which a positive charge q is moved from A to B .

from A to B is termed the potential difference, $V_B - V_A$. Thus, in the field of a point charge q_0 , the work done is given by (cf. Fig. 1.2)

$$q(V_B - V_A) = -q \int_A^B \mathbf{E} \cdot d\mathbf{l} = -q \int_{r_A}^{r_B} \frac{q_0 dr}{4\pi\epsilon_0 r^2} = \frac{qq_0}{4\pi\epsilon_0} \left\{ \frac{1}{r_B} - \frac{1}{r_A} \right\} \quad (1.5)$$

6 Electrostatics of Atoms and Molecules

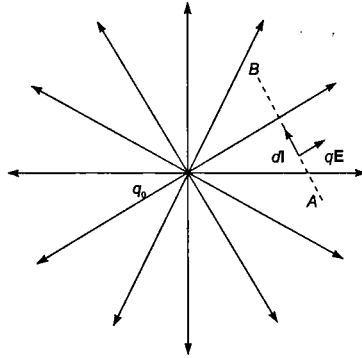


Fig. 1.2 The work done in moving a charge q from A to B in the field set up by a fixed point charge q_0 .

A significant result obtained from Eq. 1.5 is that both W_{AB} and the potential difference ($V_B - V_A$) are independent of the path chosen between the points A and B . This means that the electrostatic field is conservative. Further, if the points A and B coincide, then

$$\oint_c \mathbf{E} \cdot d\mathbf{l} = 0 \quad (1.6)$$

where c denotes a closed curve. Equation 1.6 in conjunction with Stokes' theorem (cf. Appendix C) yields the result that $\nabla \times \mathbf{E} = 0$. This formula shows that the electrostatic field is irrotational. The relation $\nabla \times \mathbf{E} = 0$ is satisfied by any \mathbf{E} which is expressible as the gradient of a scalar field, viz. $\mathbf{E} = \pm \nabla V$. As noted above, this scalar field is called the electrostatic potential. Yet another definition of this quantity (V) is as follows. V at a reference point is the work done in bringing a unit positive test charge from infinity to that reference point. For example, when the field is produced by a single point charge q_0 the potential at a distance r_B from the point charge is given as

$$V_B = - \int_{\infty}^{r_B} \frac{q_0}{4\pi\epsilon_0 r^2} dr = \frac{q_0}{4\pi\epsilon_0 r_B} \quad (1.7)$$

Thus, on dropping the subscript B , the potential produced by a point charge q_0 at a distance r from it is given by $V = q_0/(4\pi\epsilon_0 r)$. The principle of superposition is applicable to the electrostatic potential as well. The potential

at a point \mathbf{r} due to a set of fixed point charges $\{q_\alpha\}$ located at $\{\mathbf{r}_\alpha\}$ is given by the sum of the individual contributions, i.e.,

$$V = \frac{1}{4\pi\epsilon_0} \sum_{\alpha} \frac{q_\alpha}{|\mathbf{r} - \mathbf{r}_\alpha|} \quad (1.8)$$

Given a scalar field such as V , some related scalar/vector fields can be generated by using differential operators. These include, as seen above, the electric field $\mathbf{E} = -\nabla V = -\text{grad}(V)$ and the Laplacian of V , viz. $\nabla^2 V = \text{div grad}(V)$ (cf. Appendix C).

The points in space at which the electric potential is constant, constitute an equipotential surface. Figure 1.3 depicts schematically two such equipotential surfaces S_0 and S_1 corresponding to the potential values V_0 and V_1 respectively. Let us now consider the work done when a unit positive charge is moved between a pair of points lying on S_0 and S_1 . For example, the work done in displacing a unit charge from the point A to B is zero since the points A and B lie on an equipotential surface of value V_0 . Similarly there is no net work done in moving the charge from the point C to D . Further, the work done along the paths GH and EF are identical and equal to $V_1 - V_0$, even though the individual paths differ.

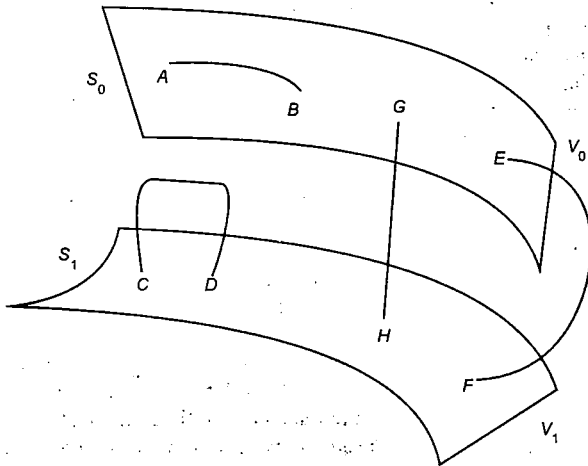


Fig. 1.3 Two equipotential surfaces S_0 and S_1 corresponding to electrostatic potentials of V_0 and V_1 . Points A, B, G and E lie on S_0 and C, D, H and F are located on S_1 .

1.3 *Visual Display of Electrostatic Potential and Field due to Discrete Charges*

Several equipotential surfaces generated by a set of point charges are depicted in Plate 1. For simplicity, atomic units are used throughout. These are rather convenient, although apparently strange units for dealing with atomic-level phenomena, wherein magnitude of the electronic charge e , mass m_e , $4\pi\epsilon_0$ as well as \hbar are assigned a unit value. The commonly used atomic units along with the respective conversion factors to SI units are presented in Appendix B. The cross-sections of such equipotential surfaces by planes, displayed in Plate 1, lead to contours in two dimensions. These contour plots are given in Plate 2 with the corresponding electric field $\mathbf{E} = -\nabla V$ superimposed. The field at a point is represented by an arrow whose head bears a colour according to the magnitude of the field; blue to red variation corresponds to successive increase in the field value from zero upwards.

In Plate 1(a), one can see the isopotential surfaces generated by two point charges of magnitude $+1$, kept a unit distance apart. For the same configuration of charges, various contours can be seen in Plate 2(a) along with the electric field in the form of vectors. The field is seen to be always directed away from the point charges in the present case.

Equipotential surfaces for a pair of charges $(+1, -1)$ kept a unit distance apart are shown in Plate 1(b). The magnitude of the potential goes on decaying as one moves away from either the positive or the negative charge. It approaches zero towards the plane equidistant from these charges. This set of charges gives rise to planar contours, some of which are displayed in Plate 2(b). The blue contours are negative valued while the red ones are positive valued. The shape of the contours becomes more and more circular as the absolute magnitude of the contour value is increased, i.e., as one approaches the charge sites. The potential generated by a quadrupole, i.e., a set of four charges, two with magnitude $+1$ and the other two with -1 , resident at the corners of a square of unit length is shown in Plate 1(c). The charges of identical polarity are diagonally opposite to each other. The general features of electrostatic potential and field observed earlier in the case of a dipole $(+1, -1)$ in Plate 1(b) are more vivid in this case. This is true even for the contour and electric field plot in Plate 2(c) (compare this with Plate 2(b)). It can also be seen from this figure that the electric field vectors, emanating from the positive charge and terminating at the negative charge, build up along the line joining negative charges and deplete along the line joining positive charges.

A look at Plates 1 and 2 reveals the following 'common sense' [10] features.

- i) Electric fields originate from the positive charge and terminate at the negative end.
- ii) The symmetry features of charges are retained by the electrostatic potentials as well as electric fields.
- iii) Two equipotential surfaces (corresponding to two different V values) never cross each other.
- iv) Equipotential surfaces become more and more spherical as one approaches the positive or the negative point charge.
- v) The electric field at a point on an equipotential surface is normal to the surface at that point.

Feynman [9] has made an interesting observation on the definition of an electric field: "All this business of fluxes and circulations is pretty abstract. There are electric fields at every point in space; then there are these 'laws'. But what is *actually* happening? Why can't you explain it, for instance, by whatever it is that goes between the charges? The best way is to use the abstract field idea. That it is abstract is unfortunate, but necessary. The attempts to try to represent the electric field as the motion of some kind of gear wheels, or in terms of lines, or of stresses in some kind of material, have used up more effort of physicists than it would have taken simply to get the right answers about electrodynamics."

1.4 Potential and Field of a Dipole: Moments of a Charge Distribution

The potential and field due to a dipole, i.e. two charges $+q$ and $-q$ separated from each other by a small distance d , can be readily worked out. Consider these charges located on the Z axis at $(0, 0, d/2)$ and $(0, 0, -d/2)$ respectively as shown in Fig. 1.4. The potential at a point $P(x, y, z)$ due to this dipole is given by

$$V = \frac{1}{4\pi\epsilon_0} \left[\frac{q}{\sqrt{x^2 + y^2 + (z - d/2)^2}} - \frac{q}{\sqrt{x^2 + y^2 + (z + d/2)^2}} \right]$$

When d is small in comparison with the distance of the charges from the point P , the above expression reduces to

$$V = \frac{1}{4\pi\epsilon_0} \frac{z}{r^3} \cdot qd = \frac{\mathbf{p} \cdot \mathbf{r}}{4\pi\epsilon_0 r^3} \quad (1.9)$$

10 Electrostatics of Atoms and Molecules

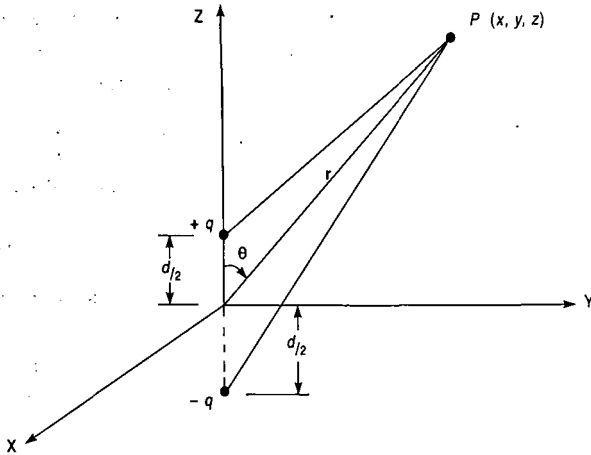


Fig. 1.4 The potential generated at a point $P(x, y, z)$ by a dipole, viz. two charges $+q$ and $-q$ separated by a distance d .

where \mathbf{p} is a dipole vector whose magnitude p is $q \cdot d$, along the axis of the dipole, and \mathbf{r} is the vector joining the centre of the dipole to the reference point P . The corresponding electrical field components can be deduced by differentiating Eq. 1.9.

$$\left. \begin{aligned} E_z &= \frac{p}{4\pi\epsilon_0} \left\{ \frac{3z^2 - r^2}{r^5} \right\} \\ E_x &= \frac{3pzx}{4\pi\epsilon_0 r^5} \\ \text{and } E_y &= \frac{3pzy}{4\pi\epsilon_0 r^5} \end{aligned} \right\} \quad (1.10)$$

The contour and vector plots depicted in Plate 1(b) and Plate 2(b) indeed depict the potential and electric field respectively due to a unit dipole.

Let us now consider a continuous charge distribution $\rho(\mathbf{r}) = \rho(x, y, z)$ as depicted in Fig. 1.5. The charge contained in an infinitesimal volume element d^3r' around a point \mathbf{r}' is $\rho(\mathbf{r}')d^3r'$. This generates a potential of $\rho(\mathbf{r}')d^3r'/|\mathbf{r} - \mathbf{r}'|$ at a reference point \mathbf{r} . The potential

generated by the entire charge distribution is obtained by integration (analogous to Eq. 1.8 which involves a summation for discrete charges), viz.

$$V(\mathbf{r}) = \frac{1}{4\pi\epsilon_0} \int \frac{\rho(\mathbf{r}')}{|\mathbf{r} - \mathbf{r}'|} d^3r' \quad (1.11)$$

The potential V at a point $P(x, y, z)$ outside this distribution is given, on Taylor expansion [11] of the $1/|\mathbf{r} - \mathbf{r}'|$ term in Eq. 1.11, by

$$V = \frac{1}{4\pi\epsilon_0} \left\{ \frac{Q_0}{r} + \frac{Q_1}{r^2} + \frac{Q_2}{r^3} + \dots \right\} \quad (1.12)$$

where Q_0 is the net charge of the distribution.

$$Q_0 = \int \rho(\mathbf{r}') d^3r';$$

$$Q_1 = \int \rho(\mathbf{r}')(lx' + my' + nz') d^3r';$$

$$Q_2 = \frac{1}{2} \int \rho(\mathbf{r}') [6(mny'z' + nlz'x' + lmx'y') + (3l^2 - 1)x'^2 + (3m^2 - 1)y'^2 + (3n^2 - 1)z'^2] d^3r' \dots \text{ and so on.} \quad (1.13)$$

Here, l , m and n denote direction cosines of the line joining P to the origin and d^3r' is the volume element $dx'dy'dz'$. The integrals $\langle x \rangle = \int \rho(\mathbf{r}')x'd^3r'$ etc. are the components of the dipole moment. Those of types $\langle x^2 \rangle = \int \rho(\mathbf{r}')x'^2 d^3r'$ or $\langle xy \rangle = \int \rho(\mathbf{r}')x'y' d^3r'$ constitute the components of quadrupole moment. Using these definitions of moments, it turns out that

$$Q_1 = l \langle x \rangle + m \langle y \rangle + n \langle z \rangle \text{ and}$$

$$Q_2 = 3mn \langle yz \rangle + 3nl \langle zx \rangle + 3lm \langle xy \rangle + 1/2 [(3l^2 - 1) \langle x^2 \rangle + (3m^2 - 1) \langle y^2 \rangle + (3n^2 - 1) \langle z^2 \rangle]$$

Equation 1.13 tells us that the potential due to an arbitrary charge distribution at a point outside the distribution is the sum of the contributions due to

- i) a point charge equal to the net charge
- ii) the dipole moment of the distribution
- iii) a quadrupole and so on,

12 Electrostatics of Atoms and Molecules

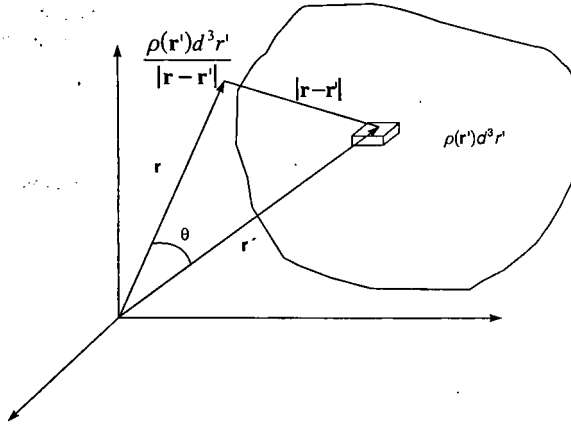


Fig. 1.5 Electrostatic potential generated by a continuous charge distribution $\rho(\mathbf{r}')$. The potential generated at \mathbf{r} is due to an infinitesimal charge $\rho(\mathbf{r}')d^3r'$ ($4\pi\epsilon_0$ is assumed to be unity for convenience).

where all the moments are located at the origin. For a distribution that possesses cylindrical symmetry around the Z axis, $\langle xy \rangle$, $\langle xz \rangle$, $\langle yz \rangle$ are zero and $\langle x^2 \rangle = \langle y^2 \rangle$. In this case, it is convenient to define a quadrupole moment $Q = \langle 3z^2 - r^2 \rangle$ and the corresponding contribution to the potential is hence given by $Q(3\cos^2\theta - 1)/(16\pi\epsilon_0r^3)$. It may be noted that some moments depend upon the choice of origin, though the monopole term always equals the net charge of the system. The dipole term is independent of the choice of the origin in the case where the system is electrically neutral, i.e., it possesses no net charge.

1.5 Basic Theorems in Electrostatics

The electrostatic potential for a combination of discrete charges $\{q_a\}$ placed at $\{\mathbf{r}_a\}$ and a smeared distribution $\rho(\mathbf{r})$ can be written by employing the superposition principle and combining Eqs. 1.8 and 1.11, as

$$V(\mathbf{r}) = \frac{1}{4\pi\epsilon_0} \left\{ \sum_a \frac{q_a}{|\mathbf{r} - \mathbf{r}_a|} + \int \frac{\rho(\mathbf{r}')}{|\mathbf{r} - \mathbf{r}'|} d^3r' \right\} \quad (1.14)$$

The electric field $\mathbf{E}(\mathbf{r})$ due to this combination of charges is obtained by taking the gradient of $V(\mathbf{r})$ in Eq. 1.14 and employing $\mathbf{E}(\mathbf{r}) = -\nabla V(\mathbf{r})$. This yields

$$\mathbf{E}(\mathbf{r}) = \frac{-1}{4\pi\epsilon_0} \left\{ \sum_{\alpha} \frac{q_{\alpha}(\mathbf{r} - \mathbf{r}_{\alpha})}{|\mathbf{r} - \mathbf{r}_{\alpha}|^3} + \int \frac{\rho(\mathbf{r}')(\mathbf{r} - \mathbf{r}')}{|\mathbf{r} - \mathbf{r}'|^3} d^3r' \right\} \quad (1.15)$$

There exists yet another relation in integral form, viz. Gauss' law, for this purpose. This is expressed as

$$\oint \mathbf{E} \cdot d\mathbf{S} = \frac{1}{\epsilon_0} \sum_i q_i \quad (1.16)$$

where q_i 's are the charges enclosed *inside* the surface S , and \mathbf{E} denotes the corresponding electric field. The surface integral on the l.h.s. equals $\oint \mathbf{E} \cdot \mathbf{n} ds$ where \mathbf{n} is the outward normal, and ds is an infinitesimal area as shown in Fig. 1.6. As a special case, it is clear that $\oint \mathbf{E} \cdot d\mathbf{S} = 0$ if the surface encloses no net charge (cf. Fig. 1.7). Gauss' law as expressed by Eq. 1.16 is also called the fundamental theorem of electrostatics. Its integral form for a continuous charge density distribution is given by

$$\oint_S \mathbf{E} \cdot d\mathbf{S} = \frac{1}{\epsilon_0} \int \rho(\mathbf{r}) d^3r \quad (1.17)$$

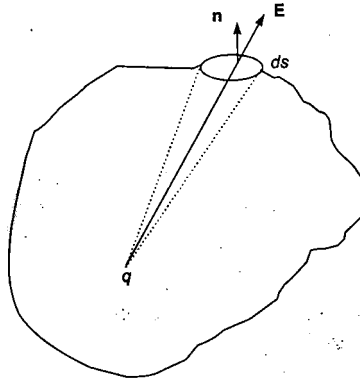


Fig. 1.6 Illustration of Gauss' law for a charge enclosed in a closed surface S . Here, ds is a small surface element and \mathbf{n} is a unit outward normal to the surface element ds .

14 Electrostatics of Atoms and Molecules

Note that Eqs. 1.16 and 1.17 are based on the inverse square law [6] (which implicitly implies the central nature of the force) and the principle of superposition. Since all these conditions hold good for the gravitational field as well, a relation similar to Eq. 1.17 is valid for the gravitational case also, if $\rho(\mathbf{r})$ is treated as matter density.

It is possible to reduce Gauss' law to its differential form by employing the so-called divergence theorem (see Appendix C)

$$\oint \mathbf{A} \cdot d\mathbf{S} = \oint \mathbf{A} \cdot \mathbf{n} \, ds = \int_{\Omega} \nabla \cdot \mathbf{A} \, d\tau \quad (1.18)$$

for a closed surface S which encloses a volume Ω . In order to obtain a "local" version of Gauss' law, consider an infinitesimally small cube. The flux out of such a cube is given by $\nabla \cdot \mathbf{E} \, d\tau$ where $d\tau$ is the volume of the cube. The charge inside the tiny volume $d\tau$ is $\rho d\tau$. Equating these, one obtains the differential form of Gauss' law, viz.

$$\nabla \cdot \mathbf{E} = \rho / \epsilon_0 \quad (1.19)$$

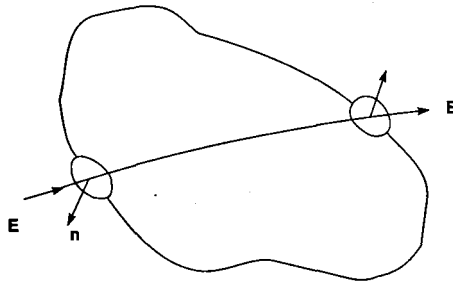


Fig. 1.7 Schematic representation of Gauss' law for a closed surface containing no charges inside.

Equation 1.19 is very useful for solving problems in electrostatics [12]. A related form, called the Poisson equation, is obtained by substituting $\mathbf{E} = -\nabla V$ in Eq. 1.19:

$$\nabla^2 V(\mathbf{r}) = -\rho(\mathbf{r}) / \epsilon_0 \quad (1.20)$$

What is the energy associated with an electric field? Consider, for simplicity, a set of point charges $\{q_\alpha\}$ placed at $\{\mathbf{r}_\alpha\}$. The energy associated with this assembly of charges is given by

$$U = \frac{1}{2} \sum_{i \neq j} \frac{q_i q_j}{4\pi\epsilon_0 r_{ij}} \quad (1.21)$$

This may be alternatively written as

$$U = \frac{1}{2} \sum_j q_j \sum_{i \neq j} \left\{ \frac{q_i}{4\pi\epsilon_0 r_{ij}} \right\} \quad (1.22)$$

Note that inclusion of the factor 1/2 is necessary in Eqs. 1.21 and 1.22 in order to avoid double counting of the electrostatic interactions. Further, the term in curly brackets in Eq. 1.22 is just the electrostatic potential V_j at \mathbf{r}_j generated by point charges $\{q_i\}$ located at sites $\{\mathbf{r}_i\}$. Hence,

$$U = \frac{1}{2} \sum_j q_j V_j \quad (1.23)$$

For the continuous case wherein the charge distribution is described by a function $\rho(\mathbf{r})$, the summation in the energy expression 1.23 is replaced by a suitable integration

$$U = \frac{1}{2} \int \rho(\mathbf{r}) V(\mathbf{r}) d^3r \quad (1.24)$$

This may be written in yet another form, by employing the Poisson equation and vector integral theorems described in Appendix C, as

$$U = \frac{1}{2\epsilon_0} \int |\nabla V|^2 d^3r \quad (1.25)$$

If the charge density at a point \mathbf{r} is zero, Eq. 1.20 reduces to Laplace's equation, viz.

$$\nabla^2 V(\mathbf{r}) = 0 \quad (1.26)$$

16 Electrostatics of Atoms and Molecules

Thus, for a system containing only point charges, $\nabla^2 V(\mathbf{r}) = 0$ at all points, except at the charge sites. This shows that for such a system of charges, the electrostatic potential cannot show a maximum or minimum (cf. Chapter 3) except at those points where the charges are located. For a (nondegenerate) maximum (minimum) in $V(\mathbf{r})$ to occur at a point, a necessary condition is that $\nabla^2 V(\mathbf{r}) < 0$ (> 0) which is in violation of Eq. 1.26 above (see Appendix G for an introduction to topography). Using this property, it can be shown that no charge can be in *stable* equilibrium in an electric field produced by a collection of charges. This result is known as Earnshaw's theorem. For a test positive charge q to be in equilibrium at a point, the field there must be zero, and moving the charge away from P in any direction should lead to a restoring force opposing the displacement [9]. This situation is depicted schematically in Fig. 1.8.

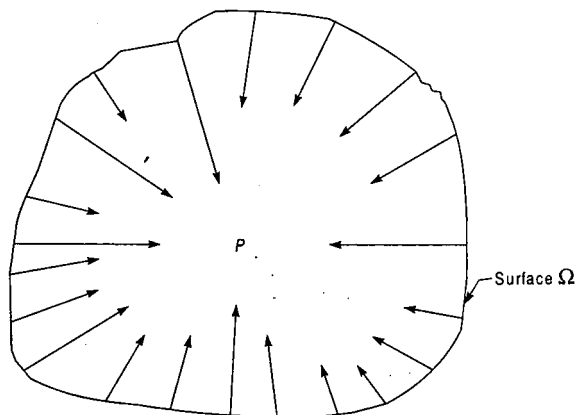


Fig. 1.8 Electric field in the neighbourhood of a point P , position of a stable equilibrium for a positive charge.

It may be seen from this figure that $\mathbf{E} = -\nabla V$ must point inwards to the point P . Thus, $\int_{\Omega} \nabla V \cdot d\mathbf{S}$ must be negative, which contradicts Gauss' theorem since there is no negative charge in this infinitesimally small region. Note that the test charge is not to be counted explicitly. Furthermore, it is positive rather than negative, as implied by Gauss' theorem. One may have a charged particle in equilibrium in an electrical field: for example, at those points P where $\mathbf{E} = 0$ in Fig. 1.8. However, such an equilibrium is *not* a stable one [4].

1.6 Electrostatic Potential of Molecules

Equation 1.14 is applicable to a molecular charge distribution which is essentially a collection of (static) positive discrete nuclear charges $\{Z_\alpha\}$ and a continuous negative electron density distribution described by $\rho(\mathbf{r})$. The MESP thus generated is given in atomic units (cf. Appendix B for a table of constants in SI units and their conversion to atomic units) as

$$V(\mathbf{r}) = \sum_{\alpha} \frac{Z_{\alpha}}{|\mathbf{r} - \mathbf{r}_{\alpha}|} - \int \frac{\rho(\mathbf{r}')}{|\mathbf{r} - \mathbf{r}'|} d^3r' \quad (1.27)$$

The MESP defined by Eq. 1.27 bears some interesting characteristics. The first term therein is the bare-nuclear potential, V_{bn} , which is always non-negative. As shown earlier in Section 1.5, V_{bn} is incapable of exhibiting (non-nuclear) maxima, as well as minima. At the (point) nuclei, V_{bn} tends to assume infinite value, which could be treated as a pseudo maximum. Some interesting characteristics of V_{bn} will be discussed later in Chapter 3. The second term in Eq. 1.27 is the negative potential engendered by the continuous electron charge density. The resultant total MESP thus generated can attain positive as well as negative values through zero, a feature which is rather unique and not exhibited individually by the electronic or the bare-nuclear contributions to the total potential.

In summary, we have given a brief introduction to electrostatic concepts in this Chapter. We are now ready to take off on a voyage through the atomic and molecular world wearing electrostatic eyeglasses! The atomic and molecular electrostatic potentials introduced in this Chapter are the key quantities for this exploration.

Chapter 2 presents an introduction to theoretical and experimental methods for obtaining MESP distributions. Like the proverbial statement, here also, a picture is better than a thousand words (or a million bytes)! Various ways for visualization of MESP are also discussed in Chapter 2. Apart from these visual features, MESP has a direct link with energetic aspects. It represents the interaction energy of the system with a test positive charge. Some interesting general rigorous and semi-rigorous results regarding atomic and molecular ESPs emerge from this connection as well as from the spatial characteristics of the latter. These will be presented in Chapter 3.

Yet another salient feature of MESP brought out by Eq. 1.27 is the amplification of the second term in the vicinity of an electron-rich region. This amplification effect may be attributed to the $1/|\mathbf{r} - \mathbf{r}'|$ weight attached within the electronic term of that equation. Thus, attainment of negative

MESP values in a region of space is an indicator of electron localization therein. These characteristics [13, 14] make the MESP a very attractive tool for studying the molecular reactivity patterns which are described in Chapter 4. Many other applications of MESP are also summarized in that Chapter.

References

1. (a) D Halliday and R Resnick, *Fundamentals of Physics*, John Wiley, New York (1981). (b) G B Arfken, D F Griffing, D C Kelly and J Priest, *University Physics*, Academic, New York (1984).
2. F W Sears, M W Zemansky and H D Young, *University Physics*, Indian Edition, Narosa, New Delhi (1985).
3. D K Sinha and R Bandyopadhyaya, *The Mathematical Theory of Electricity and Magnetism*, Macmillan (1977).
4. E M Purcell, *Electricity and Magnetism, Berkeley Physics Course, Vol. 2*, McGraw Hill (1981).
5. (a) J C Zorn, G E Chamberlain and V W Hughes, *Phys. Rev.*, **129**, 2566 (1963). (b) J G King, *Phys. Rev. Letters*, **5**, 562 (1960).
6. L B Leipuner, W T Chu, R C Larsen and R K Adair, *Phys. Rev. Letters*, **12**, 423 (1964).
7. (a) S J Plimpton and W E Lawton, *Phys. Rev.*, **50**, 1066 (1936). (b) For more recent experiments, see E R Williams, J E Faller and H A Hill, *Phys. Rev. Letters*, **26**, 721 (1971).
8. C A Coulson, *Valence*, Oxford University, Oxford (1952).
9. R P Feynman, R B Leighton and M Sands, *Lectures on Physics*, Vol. 2, p. 1, Addison-Wesley, New York (1964).
10. L Solyman, *Lectures on Electromagnetic Theory*, Oxford University, Oxford (1987).
11. P Lorrain and D Corson, *Electromagnetic Fields and Waves*, Freeman, New York (1970).
12. J D Jackson, *Classical Electromagnetism*, Wiley Eastern, New Delhi (1978).
13. (a) For a recent review on molecular electrostatics, see G Náráy-Szabo and G G Ferenczy, *Chem. Rev.*, **95**, 829 (1995). (b) Earlier comprehensive reviews have been given by E Scrocco and J Tomasi, in *Adv. Quantum Chem.*, Ed. P-O Löwdin, Academic, New York **11**, 115 (1978). (c) For a comprehensive short article emphasizing the importance of MESP in biology, see B Pullman, *Intern. J. Quantum Chem. Quantum Biology Symp.* **17**, 81 (1990).
14. (a) For an excellent collection of articles on atomic and molecular electrostatic potentials, cf. P Politzer and D G Truhlar, ed. *Chemical Application of Atomic and Molecular Electrostatic Potentials*, Plenum, New York (1981). (b) J Murray and K Sen, ed. *Molecular Electrostatic Potentials: Concepts and Applications*, Elsevier, Amsterdam (1996).

2

Molecular Electrostatic Potential: Theoretical Computation, Experimental Determination and Graphics Visualization

2.1 Introduction

We have seen in Chapter 1 that the MESP, $V(\mathbf{r})$, is a three-dimensional scalar function that can be evaluated, by a numerical quadrature, from the corresponding electron density distribution (cf. Eq. 1.27). A picture of the molecule as 'seen' by a non-interfering unit positive charge can then be obtained by visualizing the MESP over a sufficiently large region of space surrounding the nuclear framework. Such a picture is found to be very useful for capturing the essential features of molecular structure and reactivity. However, for such a study, $V(\mathbf{r})$ has to be theoretically calculated or experimentally determined [1] over a large number of points (for example $\sim 10^6$ to 10^9 i.e. points over a three-dimensional grid of 100 to 1000 points in each dimension, for a medium-sized molecule). The estimation and enumeration of $V(\mathbf{r})$ over such a large number of points as well as visualization of these three-dimensional data are both computer-intensive jobs.

The integration in Eq. 1.27 could be implemented numerically over a three-dimensional mesh. However, the values of MESP extracted in this fashion are susceptible to errors due to the use of numerical quadrature procedures. On the other hand, in many modern quantum-chemical programs, the electron density is expressed as a linear combination of Gaussians as described in Appendix F. This facilitates computation of many molecular properties, including the MESP and molecular electrostatic field (MEF), which can be evaluated with the help of closed-form algebraic expressions. MESP can also be directly obtained by numerical integration of electron densities available from X-ray diffraction data. However, it is possible, by using suitably weighted $\rho(\mathbf{r})$'s, to circumvent the intermediate step of enumeration of $\rho(\mathbf{r})$ followed by a numerical quadrature for extracting MESP.

The MESP thus computed directly from the X-ray diffraction data for crystals of small as well as large molecules [1–9] can be tested against the corresponding theoretically computed value, and the salient features compared.

A chemist is particularly interested in probing the electron-rich sites in a molecule as brought out by the negative MESP regions. Many theoretical approaches, rigorous as well as approximate, have therefore been developed for MESP computation. We review these approaches in the following Sections.

2.2 Theoretical Evaluation via Multipole Moments

As mentioned earlier, the theoretical evaluation of MESP may be effected by a quadrature of the corresponding electron density. In the wave function-based methods, $\rho(\mathbf{r})$ is extracted from the corresponding many-particle wave function. On the other hand, the density functional theory (DFT) directly yields $\rho(\mathbf{r})$ since it employs the latter as a basic variable within the theory as outlined in Appendix F. MESP can also be evaluated classically using molecular moments. This classical evaluation of MESP is based on the multipole expansion of the electrostatic potential, which has been briefly introduced in Chapter 1. We shall now discuss the multipole expansion for a special case wherein the molecular charge density distribution, $\rho(\mathbf{r})$, is described as a sum of Gaussians [10, 11, 12]. Let $\rho(\mathbf{r}) = \sum \rho_N(\mathbf{r})$ where $\rho_N(\mathbf{r})$ is a single Gaussian placed at an appropriate centre. The electrostatic potential $V(\mathbf{r}) = \sum V_N(\mathbf{r})$ from such a distribution may be expanded [13] in terms of the multipoles of corresponding molecular electron density, $\rho(\mathbf{r})$ as

$$V_N(\mathbf{r}) = \frac{1}{\epsilon_0} \sum_{l,m} \frac{1}{(2l+1)!} Q_{l,m} Y_{l,m}(\theta, \phi) \frac{1}{r^{l+1}} \quad (2.1)$$

where l may take values upto $l_i + l_j$, the sum of individual l values for the individual Gaussians, and $Y_{l,m}(\theta, \phi)$ is defined [11] in the same co-ordinate system as $\rho_N(\mathbf{r})$. Here $\sqrt{4\pi} Q_{0,0}$ represents the total charge in $\rho_N(\mathbf{r})$; $Q_{1,m}$'s represent cartesian dipoles multiplied by $4\sqrt{3}\pi$; $Q_{2,m}$'s represent quadrupolar terms ($2z^2 - x^2 - y^2$), $(x^2 - y^2)$, xy , yz and zx . MESP can thus be evaluated in terms of the moments around appropriate Gaussian product centres. This is essentially an alternate representation of the multipole expansion discussed in Section 1.4. As seen earlier, the expansion 2.1 implicitly assumes that the reference point \mathbf{r} at which the MESP is evaluated lies *outside* the charge distribution itself, an assumption which is certainly not true for a realistic molecular charge distribution.

Further, the expansion in Eq. 2.1 is operationally unwieldy for the following two reasons.

- i) As the basis set becomes more elaborate, progressively higher moments are required for calculating MESP. For instance, for an *sp* basis, only the quadrupole moments suffice, whereas for an *spd* basis, octupole and hexadecapole moments are also required [13(b)].
- ii) Too many Gaussian centres ($\sim N^2/2$ for N primitive Gaussian functions) are needed for such an evaluation. For example, when the number of primitive Gaussians (PGs) is ~ 500 , typically 125,000 centres are to be handled.

For these reasons, it is convenient to redistribute various contributions to *atom-based* ones with an appropriately chosen weight. For example, in Sokalski's cumulative atomic multipole moments (CAMM) scheme [14], a radically simple choice is made. If both the PGs belong to the same centre, the weight is assigned as unity. The weights for both centres are 'democratically' assigned as 1/2 if two distinct centres are involved. As pointed out by Ángyán and Chipot [13(b)], this is certainly not an optimal choice since half the moments in the vicinity of a centre are shifted to a distant atom. According to Stone's method [15] the overlap moments are shifted to the closest centre. Vigne-Maeder and Claverie, on the other hand, have advocated the assignment of a continuously changing weightage that is inversely proportional to the distance from a centre [12].

Typical errors in the MESP produced by employing the multipole moment values (as compared to the corresponding *ab initio* MESP) turn out to be about 5%, but they rise to 10% for aliphatic hydrocarbons and sulfur compounds [14]. A method has been proposed by Köster *et al.* [16(a)] that employs the exact MESP value at the nuclei for supplementing the multipole expansion which is traditionally found useful for large distances. They showed that in this method the MESP as well as its topography (see Appendix G for an introduction to topographical concepts) are reproduced quite well. Jug and Kölle [16(b)] have found that, generally, the topography within CAMM matches reasonably with the actual *ab initio* topography. However, in some cases (such as benzene), significantly fewer critical points are obtained for the CAMM-based MESP in those regions where the MESP varies slowly. Distributed multipole moments were also employed for studying weakly bonded complexes by Buckingham and Fowler [17]. In fact, the Buckingham–Fowler model (cf. Chapter 4) has now attained the status of a celebrated work.

In addition to the general multipole expansion method discussed above, a special case involving the use of point charges for fitting MESP

distributions has been extremely popular in the literature. The following Section briefly summarizes some of these models.

2.3 Point Charge Models for MESP Evaluation

In point charge models, the MESP, $V(\mathbf{r})$, is expanded in terms of a set of fixed charges appropriately chosen so as to represent the overall molecular charge distribution. These point charge models are popular in the literature since $V(\mathbf{r})$ can be readily evaluated from them by using Coulomb's law via Eq. 1.8. Various methods are available for evaluating point charges for this purpose. The point charges are conventionally taken as the effective atomic charges derived directly on the basis of Mulliken or Löwdin population analysis without any fitting procedure. The Mulliken ($\alpha = 0$) and Löwdin ($\alpha = 0.5$) charges assigned to atom A are defined as

$$q_A = Z_A - \sum_{i \in A} (\mathbf{S}^\alpha \mathbf{P} \mathbf{S}^{1-\alpha})_{ii} \quad (2.2)$$

where \mathbf{S} and \mathbf{P} denote the overlap and density matrices respectively (see Appendix D). The $V(\mathbf{r})$ computed using these charges generally agrees fairly well with the quantum mechanical results [18]. However, it has been found that these charges depend heavily on the choice of the basis set and do not necessarily reproduce the molecular dipole moments well. Further, these atomic charges do not normally reflect the conformational change [19]. For these reasons, this method has been replaced by other schemes wherein the charges are fitted to mimic various molecular electrostatic properties. The classical evaluation involves computation of the charges by minimizing f , the square of the difference between the potential due to multipole $V^{ME}(\mathbf{r})$ and that due to the point charges $V^{PC}(\mathbf{r})$, i.e.,

$$f = \sum_{i=1}^N [V^{ME}(\mathbf{r}_i) - V^{PC}(\mathbf{r}_i)]^2 \quad (2.3)$$

where N is the number of points over which the fit is effected. The charges thus obtained are known to reproduce the molecular moments quite well. However, since the quantum mechanical MESP can now be readily evaluated, why should one use the approximate one for fitting purposes? Hence a better strategy is adopted in the potential-derived atomic charge (PD-AC) method wherein the full quantum mechanically computed $V(\mathbf{r})$ is employed for effecting such a fit, by minimizing the deviation Δ defined by

$$\Delta = \sum_{i=1}^N [V^{PC}(\mathbf{r}_i) - V(\mathbf{r}_i)]^2 \quad (2.4)$$

These charges are indeed superior in that they generate better $V(\mathbf{r})$ than that obtained from charges calculated from multipole expansion or Mulliken population analysis, as expected—not surprising since the charges are indeed derived so as to fit the correct $V(\mathbf{r})$! The PD-ACs are used in molecular dynamics studies and found to be useful for probing intermolecular interactions. Further, they depend on the conformation and are useful for a conformational study [14]. On the other hand, the PD-ACs do not generally show transferability, and one has to add more site charges in addition to atom-centred ones in order to ensure transferability of charges [20]. Also, one may get multiple sets of charges giving rise to a fit of a similar quality. This may be seen from Figs. 2.1(a) and 2.1(b) wherein two sets of point charges are shown for methanol and formaldehyde molecules, giving comparable root mean square deviation (RMSD) $\sigma = \{\Delta/(N-1)\}^{1/2}$ from the *ab initio* (6-31G** level) $V(\mathbf{r})$ values for identical grid points, which is defined in Eq. 2.4. For example, the RMSDs for an appropriately defined outer region for the methanol molecule are 5.7×10^{-4} and 5.6×10^{-4} . However, the charges on carbon and oxygen atoms are seen to be quite different in these two sets. Similarly, two different charge models for HCHO yielding comparable RMSDs are displayed in Fig. 2.1(b).

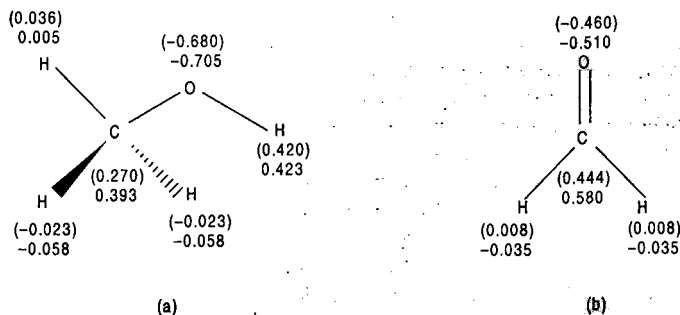


Fig. 2.1 Two sets of point charges for (a) methanol and (b) formaldehyde, giving comparable RMSDs. The first set of charges for methanol gives $\text{RMSD} = 5.7 \times 10^{-4}$ and the second set (values shown in parentheses) gives $\text{RMSD} = 5.6 \times 10^{-4}$ for the same set of grid points at HF/6-31G** level. The corresponding values for the formaldehyde molecule are 4.3×10^{-4} and 2.9×10^{-4} (all values are in a.u.).

A set of point charges may also be obtained by fitting the molecular electrostatic field (MEF) over the outer region of space surrounding the molecule [7, 13(b)]. The general consensus, however, seems to be that the sets of MESP- and MEF-fitted charges are quite similar, though the former is computationally less expensive. Choosing MEF for fitting may, however, yield more sensitive directional information. Procedures have been developed for implementing least-squares fitting by imposing additional constraints, such as the higher molecular moments (cf. Ref. 13(b) for a summary). Since the fitting is done over a grid of points, it is necessary to choose the grid carefully. Some of the relevant issues are as follows.

- i) Symmetry-related grid points are avoided since their inclusion may increase their weight unduly.
- ii) The points lying inside the van der Waals' (or related) envelope as well as those outside a suitably chosen parallelepiped, are deleted. Sometimes, the grid points sandwiched between two (scaled) van der Waals' surfaces are selected. In any case, a strong grid-dependence of charges has been noted [20(c)]. Ferenczy [20(d)] has developed a method which circumvents the explicit use of a grid. The latter is replaced by a region over which analytical integration is carried out for effecting a fit.

Several commercial as well as public domain packages are available [21] for obtaining MESP/MEF-fitted point charges. Such charges are used routinely for molecular simulations. It may be re-emphasized here that these point charges, however good otherwise, are incapable of mimicking the topographical features of MESP due to the lack of a continuous component in the charge distribution (cf. Section 1.3). For fulfilment of this, Hall and Smith [22] and, more recently, Shrivastava and Gadre [23] have developed a model wherein a set of point charges along with a continuous component, in the form of one or more spherical Gaussians, are fitted for reproducing the three-dimensional information described by the MESP as well as MEF. If desired, the second derivative information may be incorporated in terms of the electron density value. Such a connection is offered by the Poisson equation $\nabla^2 V(\mathbf{r}) = 4\pi\rho(\mathbf{r})$ at a non-nuclear site, as seen in Chapter 1. The MESP evaluation using topography-driven charge models is certainly more expensive than that obtained from PD-ACs due to the presence of one or more Gaussians. However, the advantage here is that these models reproduce the essential topographical features of $V(\mathbf{r})$ and hence are expected to represent intermolecular interactions more faithfully.

A comparison of the MESP obtained employing point-charge models with those incorporating one or more Gaussians is presented in Fig. 2.2.

It may be seen from this Figure that the Gaussian-supplemented point charge model for the water molecule mimics the $V(\mathbf{r})$ *ab initio* topography better than the PD-AC one. The point charge model shows negative potential around the oxygen atom but fails to show minima. Figure 2.2(a) shows $V(\mathbf{r})$ for the H_2O molecule evaluated from PD-AC in the molecular plane. The MESP values are positive around hydrogen and negative around oxygen atom. The $V(\mathbf{r})$ maps evaluated from topography-driven charge model and that from *ab initio* HF/6-31G** wave function are depicted in Figs. 2.2(b) and (c) respectively. Here the potential around the molecular framework is positive and that around the lone pair sites of oxygen atom is negative. It may be seen that the qualitative features of *ab initio* MESP contours as described by Fig. 2.2(c) are borne out better by the Gaussian-based ones depicted in Fig. 2.2(b) rather than the point charge one shown in Fig. 2.2(a).

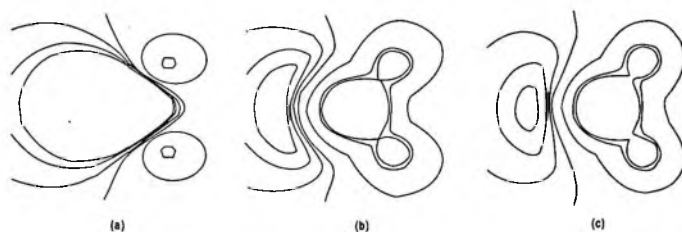


Fig. 2.2 MESP contours for H_2O molecule in the molecular plane evaluated from (a) Point charge model (b) Topography-driven charge model and (c) HF/6-31G** level wave function. The MESP values for successive contours are 1.0, 0.8, 0.2, 0.0, -0.04 , -0.07 and -0.09 a.u. respectively.

Mohan *et al.* [24] have recently developed a method which uses a combination of the Löwdin charges (cf. Sec. 2.2) and (the so-called) hybridization displacement charges (HDC) at the semi-empirical MNDO (modified neglect of differential overlap) level (see Appendix E for an introduction to semi-empirical procedures) to reproduce topographical features. This method seems to work quite well again since it describes the electron density as a continuous function.

Apart from the use of various approximate theoretical methods, the MESP can also be rigorously computed by *ab initio* quantum mechanical methods. This is possible due to the advent of otherwise faster CPUs (e.g. PENTIUM or RISC-based workstations). Further, superior algorithms enriched by mathematical inequalities can be employed for improving the performance of such methods. Since the present monograph mainly describes $V(\mathbf{r})$ within the *ab initio* framework, the following Section is devoted to this topic.

2.4 MESP Using *Ab Initio* Molecular Wave Function

The *ab initio* method of obtaining the approximate molecular wave function by solving the Schrödinger equation is briefly outlined in Appendix D. The MESP is then evaluated using the density matrix \mathbf{P} (obtained from the corresponding wave function) and the atomic orbitals $\{\phi_\mu\}$, as

$$V(\mathbf{r}) = \sum_{A=1}^N \frac{Z_A}{|\mathbf{r} - \mathbf{R}_A|} - \sum_{\mu,\nu} P_{\mu\nu} \int \frac{\phi_\mu(\mathbf{r}') \phi_\nu^*(\mathbf{r}')}{|\mathbf{r}' - \mathbf{r}|} d^3r' \quad (2.5)$$

Here ϕ_μ 's are atomic orbitals and $P_{\mu\nu}$'s denote the corresponding density matrix elements, defined by Eq. D.13 (Appendix D). In fact, the MESP from a wave function beyond SCF (self consistent field) level (e.g. MP2 or CI) could also be computed by employing the corresponding density matrix \mathbf{P} in conjunction with Eq. 2.5. Within a density functional scheme, the Kohn-Sham orbitals could similarly be used in order to compute MESP.

Even after obtaining the molecular wave function using a typical HF-SCF program, the *ab initio* MESP calculations for larger molecules are often prohibitively slow due to the large number of atoms involved, the extensive basis set employed, as well as the number of grid points over which the MESP is to be evaluated. For a molecular orbital (MO) made up of N atomic orbitals (AOs), the number of such one-electron, (predominantly) three-centre integrals is $N(N+1)/2$. Since this large number of integrals must be evaluated at each of the grid points for describing $V(\mathbf{r})$, the computer time required for these calculations often exceeds that required for even the HF-SCF calculations! For instance, Rohmer *et al.* [25] have reported the computer time for *ab initio* SCF calculation for the decavanadate ion $[\text{V}_{10}\text{O}_{28}]^{6-}$ to be 20,060 seconds on a Cray-2 computer. However, the time taken for the MESP calculation for 8035 points on a particular plane passing through the molecular framework is 1724 seconds. Scanning just a dozen of such planes would thus typically require 20,688 seconds! This example shows how *ab initio* computation of $V(\mathbf{r})$ could be more expensive than that of the wave function itself. Such a computational formidability restricts the use of *ab initio* MESP as a tool for the investigation of chemical properties and reactivities of large molecules. Towards an affirmative end, however, several ingenious techniques have been developed for faster computation of MESP. Various mathematical inequalities and numerical checks have been found useful for achieving an efficient computation of the MESP [26]. It can be seen from Eq. 2.5 that if a density

matrix element $P_{\mu\nu}$ is numerically close to zero, then the integrals involving the interaction of ϕ_{μ} and ϕ_{ν} need not be evaluated for any point on the grid. Thus for large molecules, even though $N(N+1)$ integrals are involved, most of them can be neglected depending on the value of $P_{\mu\nu}$ and the distance between the centres of the corresponding AOs.

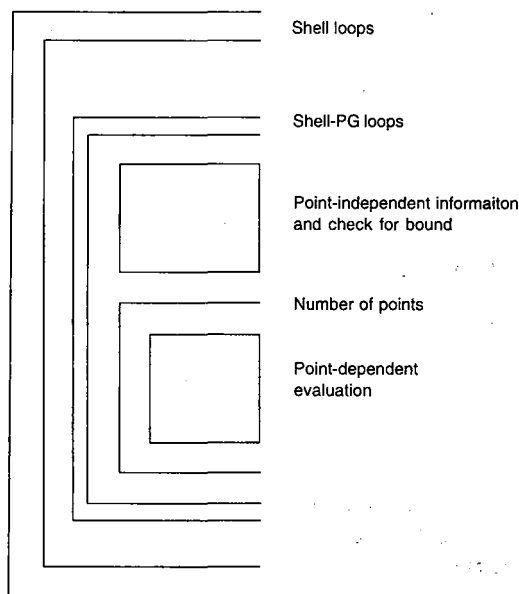


Fig. 2.3 Loop structure using shells for MESP evaluation.

The quantum mechanical evaluation of MESP can be understood from the algorithm shown schematically in Fig. 2.3 wherein the concept of shell [27] has been used (cf. Appendix D for an introduction to Gaussian basis sets). A shell is a set of mathematically related atomic orbitals. For instance, p_x , p_y and p_z orbitals on a given atom form a shell. Referring to Fig. 2.3, within the shell loops are the loops over primitive Gaussians. A part of this processing is independent of the point at which the MESP is to be computed, and it may be stored in appropriate arrays, if required. As seen above, many of the integrals are numerically very small (less than 10^{-12} , say) and are thrown out forever.

We have described here an algorithm for computing MESP on a sequential computer. However, with the development in computer technology, parallel and distributed architectures have gained popularity. A detailed review of these is beyond the scope of this monograph. However, it may be noted here in passing that the MESP evaluation can be very effectively implemented on parallel computers. In fact, it is one of the most embarrassingly parallel algorithms! Since the time required for MESP evaluation is almost independent of the position of the point in the given set, it is expected that, for a large number of points, the parallelization over points will give perfect load balancing (a term popularly used in parallel computing jargon [26]), independent of the basis set. The parallel algorithm developed by Gadre *et al.* [26], as expected, gives a linear performance with the number of processors used in the network. In this work, it was demonstrated that the use of bounds and parallelization leads to a performance (on a 32-node old-fashioned transputer-based parallel computer) better than that on a powerful CRAY, without using these ingenious techniques. The program UNIPROP [26] is quite efficient and, in addition to the evaluation of the MESP, it helps in locating and characterizing various critical points in the MESP distribution.

Since reliable HF-SCF or post-HF calculations (within the *ab initio* framework) are possible only for medium-sized molecules, the so-called fragmentation approach may be fruitfully used for large molecules. Within this approach, a large molecule is first divided into smaller overlapping parts which are later put together in order to simulate the parent molecule. These studies include the bond-fragment method due to Náráy-Szabó [28] that utilizes the transferable localized molecular orbitals mostly within semi-empirical procedures. The fragmentation approach has also been recently developed [29] for the *ab initio* computation of MESP. In this method, an approximate *ab initio* density matrix for a large molecule is obtained by 'patching' small fragments of the *ab initio* density matrices. Due care is to be taken at the boundaries, where large overlaps are ensured between the neighbouring fragments. The approximate density matrix thus obtained is used for $V(\mathbf{r})$ computation of the original supermolecule. This method, christened as *molecular tailoring approach*, has been found to be very efficient, and yields electrostatic properties that are very close to those obtained from the actual *ab initio* computation for the supermolecule. This approach has been successfully tested on polypeptides and a ten-membered ring of a zeolite cage [29]. For studying very large molecules, the corresponding density matrix may be obtained from semi-empirical methods [30], and $V(\mathbf{r})$ is conveniently calculated since *ab initio* calculations are prohibitively expensive for such systems. An introduction to semi-empirical methods is provided in Appendix E.

2.5 MESP from Semi-Empirical and other Approximate Methods

Giessner-Prettre and Pullman were among the early pioneers who investigated the possibility of using CNDO (complete neglect of differential overlap) wave functions [31] for the MESP computation. Within the ZDO framework, the MESP defined by Eq. 2.5 could be evaluated in many ways, depending on which of the following approximations are used in the semi-empirical procedures [32].

- i) Approximate the integral on the r.h.s. of Eq. 2.5, employing assumptions compatible to those made for evaluating two-electron integrals [33].
- ii) Assume that $\int \frac{\phi_\mu^*(\mathbf{r}')\phi_\nu(\mathbf{r}')d^3\mathbf{r}'}{|\mathbf{r}-\mathbf{r}'|} = 0$ if ϕ_μ and ϕ_ν are on different sites. The ϕ_μ 's are represented by STOs and the corresponding single-centre integrals are evaluated explicitly. The CPU time requirement in this case increases roughly proportional to the number of AOs.
- iii) A de-orthogonalization procedure $\mathbf{C}' = \mathbf{S}^{-1/2}\mathbf{C}$ [34] is implemented since the integrals in (ii) above do not identically vanish. Here \mathbf{C} and \mathbf{C}' stand for the original and transformed MO coefficient vectors and \mathbf{S} is the overlap matrix. The electronic contribution to MESP is then computed by employing expressions involving STOs.

It is found that although the method (iii) yields highly accurate results, the CPU time increases approximately as the square of the number of AOs involved. Apart from the CNDO procedure, other related semi-empirical methods [35] such as MNDO, AM1, PM3, etc. have also been tried out for $V(\mathbf{r})$ computations. Such an approach has been found to be very useful for studying large molecules, such as biomolecules.

Giessner-Prettre and Pullman [31], and more recently, Duben [36] have carried out a comparison of the MESP obtained from CNDO and INDO wave functions against their *ab initio* counterparts. They found that reliable results are obtained from the former only if ZDO approximation is relaxed by means of de-orthogonalization of the STO basis and if all the integrals are included in the MESP calculations. More recently, Luque *et al.* [37] have utilized GTO expansions of STO-based MOs within the MNDO approximation, with the built-in inherent assumption of the freezing of the inner shells, etc. The essential features of *ab initio* MESP are generally brought out by the MNDO-based one quite well.

More recently, Marynick [38] has reported a new approach for obtaining ESP-fitted atomic charges. The MESP obtained from MOs derived

from a semi-empirical method, named as PRDDO/M, is parametrized against the corresponding *ab initio* MP2/6-31G** one. This naturally results in an MESP that is in good agreement with its *ab initio* counterpart.

The MESP obtained within the framework of the density functional theory (DFT) is also generally found to be in good qualitative agreement with the corresponding HF-SCF one. DFT-based MESP [39, 40] has been recently employed for the determination of covalent radii. The suitability of the DFT method towards the calculation of electrostatic properties of molecules has recently been assessed by Soliva *et al.* [41, 42]. The ESP and related properties of molecules containing phosphorus, sulfur and chlorine atoms (which are more difficult to represent than those involving only first-row atoms) are found to be remarkably improved on including two sets of *d* orbitals on these atoms and *p* orbitals on the hydrogen atom [41]. Further, the calculations at the MP2 level have been found to be quite adequate for capturing most of the electron correlation effects [42]. It was later observed [41, 42] that DFT methods do not noticeably improve the MESP representation at the Hartree-Fock level. However, a more remarkable improvement was seen on employing hybrid non-local functionals (see Appendix F for a brief introduction to DFT). Since DFT is a computationally economical method, it can be gainfully employed for examining molecular electrostatics of larger systems. It is noteworthy that since 1990, the DFT-based methods have gained popularity for tackling large molecular systems.

2.6. Experimental Determination of Electrostatic Potentials

The experimental determination of MESP is made on crystalline samples. A crystal is composed of a large number of perfectly ordered unit cells. In a typical X-ray diffraction experiment, $\sim 10^{15}$ cells take part in the Bragg scattering [3, 4]. One may look at the charge density $\rho(\mathbf{r})$ of this 'giant' molecule as participating in this scattering process. As seen in Chapter 1, the electronic part of the MESP for this system is given by

$$V_e(\mathbf{r}) = \int \frac{\rho(\mathbf{r}')}{|\mathbf{r} - \mathbf{r}'|} d^3\mathbf{r}' \quad (2.6)$$

Introducing the transform

$$|\mathbf{r} - \mathbf{r}'|^{-1} = (2\pi^2)^{-1} \int e^{-i\mathbf{k} \cdot (\mathbf{r} - \mathbf{r}')} d^3\mathbf{k}/k^2 \quad (2.7)$$

in Eq. 2.6 yields

$$V_e(\mathbf{r}) = (2\pi^2)^{-1} \iint \rho(\mathbf{r}') e^{-i\mathbf{k}\cdot(\mathbf{r}-\mathbf{r}')} d^3r' d^3k/k^2 \quad (2.8)$$

Here \mathbf{k} is the scattering vector and $k = |\mathbf{k}|$. The integration over \mathbf{r}' can be readily implemented. This yields the molecular form factor, $f(\mathbf{k})$ which is defined as the Fourier transform of $\rho(\mathbf{r})$, viz.

$$f(\mathbf{k}) = \int \rho(\mathbf{r}') e^{i\mathbf{k}\cdot\mathbf{r}'} d^3r' \quad (2.9)$$

Using this definition, Eq. 2.8 reduces to

$$V_e(\mathbf{r}) = (2\pi^2)^{-1} \int f(\mathbf{k}) e^{-i\mathbf{k}\cdot\mathbf{r}} d^3k/k^2 \quad (2.10)$$

One may, at this point, employ the periodicity conditions for a crystal, viz. that both $\rho(\mathbf{r})$ and $V(\mathbf{r})$ are periodic [4] over the 'giant' molecule under consideration as the crystal is made up of exact replicas of the unit cell. Now, consider the general displacement vector \mathbf{r} . Due to the periodicity conditions, \mathbf{r} may be expressed as a displacement vector \mathbf{x} (which is now restricted only to the reference unit cell), to which a vector $\mathbf{u}_j = \mathbf{u}_{j_1, j_2, j_3}$ is added.

$$\mathbf{r} = \mathbf{x} + \mathbf{u}_{j_1, j_2, j_3} = \mathbf{x} + (j_1\mathbf{a} + j_2\mathbf{b} + j_3\mathbf{c})$$

Here, \mathbf{j} stands for the triplet of integers j_1, j_2 , and j_3 , and $\mathbf{a}, \mathbf{b}, \mathbf{c}$ are the translations of the unit cell along the a, b and c axes respectively. Thus

$$V_e(\mathbf{x}) = (2\pi^2)^{-1} \sum_j \int f(\mathbf{k}) e^{-i\mathbf{k}\cdot(\mathbf{u}_j + \mathbf{x})} d^3k/k^2 \quad (2.11)$$

This relation ensures that the experimentally obtained $V(\mathbf{r})$ is periodic, viz. $V(\mathbf{r}) = V(\mathbf{r} + \mathbf{u}_j)$. The sum in Eq. 2.11 is to be carried out over all the unit cells in the crystal. The expression 2.11 may be reduced further in terms of the Bragg vector, \mathbf{H} , which is simply a triplet of integers (h, k, l) with magnitude $|\mathbf{H}| = 2 \sin \theta / \lambda$, where λ is the wavelength of incident X-rays, and θ is the scattering angle. With this discretization, the integration in Eq. 2.11 may be reduced [3] to a sum

$$V_e(\mathbf{x}) = (4\pi\Omega)^{-1} \sum_H F_H e^{-2\pi i \mathbf{H}\cdot\mathbf{x}} / (\sin \theta / \lambda)^2 \quad (2.12)$$

where Ω is the volume of the corresponding unit cell.

It is noteworthy that the Fourier sum in Eq. 2.12 is quite similar to the expression for $\rho(\mathbf{x})$, in the direct experimental determination of the electron density [4] viz.

$$\rho(\mathbf{x}) = (4\pi\Omega)^{-1} \sum_H F_H e^{-2\pi i \mathbf{H} \cdot \mathbf{x}} \quad (2.13)$$

The only difference in Eqs. 2.12 and 2.13 is the 'weightage' of $(\sin\theta/\lambda)^2$ appearing only in the case of $V_c(\mathbf{x})$. Thus, an advantage of employing Eq. 2.12 is that it enables direct evaluation of $V_c(\mathbf{x})$ in a crystalline solid. There is no need of evaluating $\rho(\mathbf{x})$ first, followed by a numerical quadrature as indicated in Eq. 1.27. However, due to the similarity between Eqs. 2.12 and 2.13, it is clear that the experimental determination of $\rho(\mathbf{x})$ and $V_c(\mathbf{x})$ is plagued by essentially the same set of problems. The most significant one happens to be the so-called 'phase problem' [5]. The root cause of this problem is that the measurable quantity in an X-ray scattering experiment is $|F_H|$, viz. the structure factor amplitude. Thus, only the magnitude of F_H is known from the experimental data, not the phases. The phases are estimated exclusively via model calculations and are quite reliable only for the centrosymmetric cases [4].

Spackman and Stewart [4] have summarized the experimental results for several inorganic crystals, such as beryllium, silicon, quartz, corundum, etc. It has been found that, similar to the deformation density $[\Delta\rho(\mathbf{r})]$ maps often reported in crystallographic literature, it is convenient to report the deformation electrostatic potential, $\Delta V(\mathbf{r})$. These $\Delta V(\mathbf{r})$ maps agree well with the intuitive picture of charge build-up on chemical bonding. However, the $\Delta V(\mathbf{r})$ maps have not as yet become a standard weapon in a chemist's toolbox! The corresponding $\Delta\rho(\mathbf{r})$ and the Laplacian $\nabla^2\rho(\mathbf{r})$ maps have, on the other hand, become extremely popular for exploring the chemical bonding effects. MESP has been mapped from the Bragg diffraction data for a variety of molecules. One of the earlier measurements was reported by Stewart [6] for the N_2 crystal. Epstein and Swanton [7] computed the electric field gradients in imidazole at 103 K from X-ray diffraction data. Destro *et al.* [8] computed MESP maps of L-alanine from single-crystal X-ray data collected at 23 K. They also computed electric field gradients from the experimental scattering data. Downs and Swope [9(a)] have reported MESP calculated from the X-ray diffraction data for the mineral coesite, a framework silicate containing Si-O-Si groups. For this system it was found that MESP exhibits a minimum near a particular oxygen atom. This is consistent with the local features observed in the corresponding $\Delta\rho(\mathbf{r})$ and $\nabla^2\rho(\mathbf{r})$ maps. More recently, Espinosa *et al.* [9(b)] have

experimentally determined the MESP of L-arginine phosphate monohydrate and found a good agreement with its theoretical counterpart. This is significant since the electrostatic interactions dominate in hydrogen bond formation and hence the MESP is the scalar field worth considering for these investigations. In a similar spirit, Ghermani *et al.* [9(c)] have employed the experimental MESP for predicting the 'active site' in the case of 2,2-dimethyl-6,6'-diphenyl-4,4'-bipyrimidine towards its metallic complexation. Their predictions are in agreement with the structural studies on copper bipyrimidine complexes. Koritsanszky *et al.* [9d] have reported the experimental low temperature (120 K) MESP of $[\text{K}(\text{18C6})]^+ \text{N}_3^- \cdot \text{H}_2\text{O}$, a complex of 18-crown-6 (18C6). In summary, one may say that reliable experimental MESP maps are becoming available only now. Because of this, it may still take a few years before one finds them routinely in chemical literature. Having summarized the theoretical and experimental methods for $V(\mathbf{r})$ determination, we now briefly discuss graphics visualization of MESP.

2.7 MESP Visualization

It may be noted that the MESP is a three-dimensional quantity, unlike the molecular wave function, which is multi-dimensional in nature. This three-dimensional function can be visualized with the help of a computer wherein various colours can be assigned for representing the value of MESP. Since the MESP can assume both positive and negative values through zero (cf. Eq. 2.5), unlike $\rho(\mathbf{r})$ which attains only non-negative values, one expects that three-dimensional visualization of MESP will yield more detailed information than that furnished by $\rho(\mathbf{r})$ in the study of molecular recognition. With the advent of computer graphics techniques, the three-dimensional visualization of data has become an attractive tool in computational chemistry for interpreting the results obtained in the form of numbers. However, the visualization of $V(\mathbf{r})$ over a dauntingly large number of points covering the region of molecular framework needs a sophisticated approach.

2.7.1 Two-dimensional visualization

The MESP can be visualized on various planes with the help of contour lines or pixel plots. In a contour plot, different linestyle or colours may be used for a gradation of $V(\mathbf{r})$ values. In pixel plots, the points are given a colour code according to the MESP values on the grid, and intermediate points are assigned interpolated colours. One plane may be chosen at a time or various planes can be simultaneously displayed in conjunction, so as to get a glimpse of its three-dimensional structure. These planes can be plotted along with a ball-and-stick molecular model for getting a better 'feel' of

the scalar field. Several such two-dimensional plots are given in Plate 3. The planar MESP pixel plots for the decavanadate ion, $[\text{V}_{10}\text{O}_{28}]^{6-}$ (discussed earlier in Sec. 2.4), are depicted in Plates 3(b) to 3(d). The ball-and-stick model (side and top views) of the ion are shown in Plate 3(a) for reference. The red and green spheres (not drawn to scale) represent vanadium and oxygen atoms respectively. Plates 3(b) to 3(d) display the MESP pixel plots for the anion, with the red and blue colours representing positive and negative MESP regions respectively. It can be noticed that the ion is surrounded by a negative MESP sheath (see the discussion on molecular anions in Chapter 3). In fact, it is possible to locate the most basic oxygens in the cluster with the help of these planar cross-sections.

The 'flying carpets' of the MESP of the benzene molecule are depicted in Plate 4(a). These represent pseudo three-dimensional MESP plots on the planes parallel to the molecular plane. It may be noticed that the MESP minima of -0.026 a.u., shown in blue, are attained typically 1.8 \AA above (and below) the plane of the molecule. Shown in Plate 4(b) is the MESP pixel plot of the acetylene moiety, with the most negative value of -0.039 a.u. The yellowish-white contour of zero-MESP value is also noticeable. That the H end of the HF molecule approaches the most negative (blue) region, perpendicular to the bond axis of acetylene so as to form a $\pi\dots\text{H}$ bond can be clearly seen from this Plate.

2.7.2 Three-dimensional visualization

Three-dimensional (3D) views of MESP may be obtained using isovalued surfaces differing in colour and transparency. This can also be achieved with the help of 3D or stacked contours. The contours in parallel planes are plotted simultaneously so as to generate a 3D feel. Another way in which a 3D MESP structure can be studied is to plot the MESP on some predefined surface (e.g. a surface on which $\rho(r)$ is constant, van der Waals surface, minimal surface, covalency surface [40], etc.) of molecules using suitably chosen colour codes. Various facilities of computer graphics such as rotation, scaling, shifting, etc. may be employed for obtaining a better understanding of the picture. The MESP can also be visualized on a black-and-white monitor in a grey scale i.e., by using different densities of black-and-white pixels for the MESP values. It is always useful to visualize the molecule under consideration by a ball-and-stick representation along with $V(r)$ for reference. Several computer programs are available which are helpful in the computation of molecular properties and/or graphics visualization of scalar/vector fields (in particular, that of MESP) [43, 44]. These programs [45] include SPARTAN, HyperChem, PCModel, Molecular Editor, UNIVIS, POPROT, AVS etc., which run on various machines.

Several samples of three-dimensional visualization employing the UNIVIS [45(e)] package are presented in Plates 4 and 5. MESP's textured on the van der Waals envelopes of C_{60} and C_{70} fullerene molecules are shown in Plates 4(c) and (d) respectively. The blue regions correspond to pockets of electron localization. It may be seen that the exo bonds to the pentagons (five-membered rings) bear a more double-bond character, i.e., they have negative-valued MESP minima located over them. Plate 4(c) also brings out the fact that the 'inside' of C_{60} (bucky ball) is devoid of negative MESP values. An appropriately 'cut' surface is shown to facilitate such a view.

The negative MESP regions of the guanine and cytosine molecules are depicted in Plate 5(a). The isosurface on the left represents an MESP value of -0.05 a.u. for the guanine molecule and shows a continuous negative MESP region formed by the joining of the lone pair regions of nitrogen and oxygen atoms. The MESP isosurface for the same value, viz. -0.05 a.u., of the cytosine molecule is shown on the right.

An illustration of many features of a scalar field that can be brought out by a single picture may be seen for the benzene molecule as shown in Plate 5(b). It shows opaque as well as transparent MESP surfaces with values of -0.0296 and -0.0258 a.u. respectively. Further, it also depicts several planar pixel cuts superposed on the same figure.

Two different isosurfaces of the *n*-decane molecule are superimposed in Plate 5(c). The brown isosurface corresponds to an MESP value of 0.1 a.u., whereas the dark pink isosurface bears an MESP of -0.003 a.u. The surprising fact is that a chemically 'inert' molecule such as *n*-decane also has a substantial negative MESP region where a cation may bind or an electrophile would form a weak complex. This fact is also noticed from Plate 5(d) for the methane molecule, which exhibits two transparent MESP isosurfaces: a blue one (positive) and a brown one (negative). The minima along the C_3 axes are denoted by white dots.

We have seen in this Chapter how the MESP is obtained by experimental as well as theoretical methods and how it can be visualized in different ways. On the other hand, there are several rigorous general results regarding the atomic and molecular electrostatic potential, which could be proven analytically. These will be summarized in the following Chapter.

References

1. (a) For a comprehensive survey of theoretical and experimental methods of MESP evaluation, see *Chemical Applications of Atomic and Molecular Electrostatic Potentials*, Ed. P Polizer and D G Truhlar, Plenum, New York (1981). (b) For a more recent introduction to theory, experimental methods and applications of MESP, see *Molecular Electrostatic Potentials: Concepts and Applications*, Ed. J S Murray and K Sen, Elsevier, Amsterdam (1996).
2. R F Stewart, and B M Craven, *Biophys. J.* **65**, 998 (1993).
3. J Warwicker, D L Ollis, F M Richards and T A Steitz, *J. Mol. Biol.* **186**, 645 (1985).
4. (a) M A Spackman and R F Stewart, in *Chemical Applications of Atomic and Molecular Electrostatic Potentials*, Ed. P Politzer and D G Truhlar, Plenum, New York (1981). (a) R F Stewart and D Feil, *Acta Cryst.* **A36**, 503 (1980).
5. See, for example, (a) R F Stewart, *Acta Cryst.* **A32**, 565 (1976). (b) C K Johnson, *Acta Cryst.* **A25**, 187 (1969).
6. R F Stewart, *Chem. Phys. Letters* **65**, 335 (1979).
7. J Epstein and D J Swanton, *J. Chem. Phys.* **77**, 1048 (1982).
8. R Destro, R Bianchi and G Morosi, *J. Amer. Chem. Soc.* **93**, 4447 (1989).
9. (a) J W Downs and R J Swope, *J. Phys. Chem.* **96**, 4834 (1992); J W Downs, *J. Phys. Chem.* **99**, 6849 (1995). (b) E Espinosa, C Lecomte, N E Ghermani, J Devery, M-M Rohmer, M Bénard and E Molins, *J. Amer. Chem. Soc.* **118**, 2501 (1996), and references therein. (c) NE Ghermani, N Bouhmaid, C Lecomte, A L Papet and A Marsura, *J. Phys. Chem.* **98**, 6287 (1994). (d) T Koritsanszky, J Buschmann, P Luger, A Knöchel and M Patz, *J. Amer. Chem. Soc.* **116**, 6748 (1994).
10. A J Stone, *Chem. Phys. Letters* **83**, 233 (1981).
11. J R Rabinowitz, K Namboodiri and H Weinstein, *Intern. J. Quantum Chem.* **29**, 1697 (1987).
12. F Vigne-Maeder and P Claverie, *J. Chem. Phys.* **88**, 4934 (1988).
13. (a) J D Jackson, *Classical Electrodynamics*, Wiley, New York (1962) p. 99. (b) See, for a comprehensive review, J G Ángyán and C Chipot, *Intern. J. Quantum Chem.* **52**, 17 (1994).
14. (a) W Sokalski and R Poirier, *Chem. Phys. Letters* **98**, 86 (1983). (b) W Sokalski and A Sawaryn, *J. Chem. Phys.* **87**, 526 (1987). (c) A Sawaryn and W Sokalski, *Comput. Phys. Commun.* **52**, 397 (1989).
15. A J Stone and M Alderton, *Mol. Phys.* **56**, 1047 (1985) and references therein.
16. (a) A M Köster, C Kölle and K Jug, *J. Chem. Phys.* **99**, 1224 (1993). (b) K Jug and C Kölle, *Proc. Ind. Acad. Sci. (Chem. Sci.)* **99**, 3084 (1994).
17. A D Buckingham and P W Fowler, *Can. J. Chem.* **63**, 2018 (1985).
18. G Tasi, I Kiricsi and H Förster, *J. Comput. Chem.* **13**, 371 (1992).
19. (a) C Culot, M Dory, F Durant and D P Vercauteren, *Intern. J. Quantum Chem.* **46**, 211 (1993). (b) For an interesting work that discusses conformation-dependent point charges, cf. C A Reynolds, J W Essex and W G Richards, *J. Amer. Chem. Soc.* **114**, 9075 (1992).

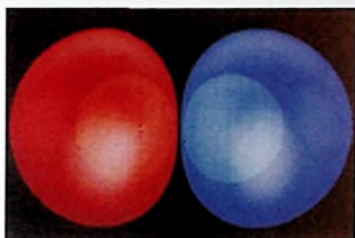
20. (a) C Chipot, J G Ángyán, G G Ferenczy and H A Scheraga, *J. Phys. Chem.* **97**, 6628 (1993). (b) C Chipot, B Maigret, J-L Rivail and H A Scheraga, *J. Phys. Chem.* **96**, 10276 (1992). (c) C Breneman and K Wiberg, *J. Comput. Chem.* **8**, 894 (1987). (d) G G Ferenczy, *J. Comput. Chem.* **12**, 913 (1991).
21. (a) GRID: C Chipot, Fortran Program performing charge fitting to molecular electrostatic potentials (Laboratoire de Chimie Theorique, University de Nancy, I-F-54506, Vandoeuvre-le's-Nancy, France, 1992). (b) MULFIT: G Ferenczy: Fortran Program performing charge fitting to multipole series (Chemical works of Gedeon Richter Ltd., H-1475, Budapest, P O Box-27, Hungary, 1992). (c) CHELP: L E Chirlian and M M Francl, *J. Comput. Chem.* **8**, 894 (1987). (d) CHELPG: C M Breneman and K B Wiberg, *J. Comput. Chem.* **11**, 361 (1990). (e) VESPA: B Beck, T Clark and R C Glen, *J. Comput. Chem.* **18**, 744 (1997) for a discussion ESP-driven charges from semi-empirical methods.
22. G G Hall and C M Smith, *Intern. J. Quantum Chem.* **42**, 1237 (1992) and references therein.
23. I H Shrivastava and S R Gadre, *Intern. J. Quantum Chem.* **49**, 397 (1994).
24. C G Mohan, C H Suresh and P C Mishra, *Proc. Indian Acad. Sci. (Chem. Sci.)* **108**, 469 (1996).
25. M-M Rohmer, R Ermenwein, M Ulmschneider, R Wiest and M Bénard, *Intern. J. Quantum Chem.* **40**, 723, (1991).
26. For the package UNIPROP by Gadre *et al.*, Department of Chemistry, University of Pune, see (a) S R Gadre, S Bapat and I H Shrivastava, *Comput. and Chem.* **15**, 203 (1991). (b) R N Shirsat, S V Bapat and S R Gadre, *Chem. Phys. Letters* **200**, 373 (1992). (c) S R Gadre, R N Shirsat, S V Bapat and A Taspaa, *Curr. Sci. (India)* **62**, 798 (1992).
27. M Dupis, J Rys and H F King, *J. Phys. Chem.* **65**, 111 (1976).
28. G Náray-Szabó, *Intern. J. Quantum Chem.* **16**, 265 (1979).
29. S R Gadre, R N Shirsat and A C Limaye, *J. Phys. Chem.* **98**, 6445 (1994).
30. J A Pople and D L Beveridge, *Approximate Molecular Orbital Theory*, McGraw-Hill, New York (1970).
31. C Giessner-Prettre and A Pullman, *Theoret. Chim. Acta (Berl.)* **25**, 83 (1972); *ibid* **37**, 335 (1974).
32. C A Reynolds, G G Ferenczy and W G Richards, *J. Mol. Struct. (Theochem)* **88**, 249 (1992).
33. J J P Stewart, *J. Comput. Aided Mol. Design* **4**, 1 (1990).
34. P-O Löwdin, *J. Chem. Phys.* **18**, 365 (1950).
35. M J S Dewar and W Thiel, *J. Amer. Chem. Soc.* **99**, 4899 (1977), M J S Dewar, E G Zoebisch, E F Healy and J J P Stewart, *J. Amer. Chem. Soc.* **107**, 3902 (1985), J J P Stewart, *J. Comput. Chem.* **10**, 20 (1989).
36. A J Duben, *Theoret. Chim. Acta (Berl.)* **59**, 81 (1981).
37. F J Luque, F Illás and M. Orozco, *J. Comput. Chem.* **11**, 416 (1990).
38. D S Marynick, *J. Comput. Chem.* **18**, 955 (1997).
39. J S Murray, J M Seminario, M C Concha and P Politzer, *Intern. J. Quantum Chem.* **44**, 113 (1992).

38 *Electrostatics of Atoms and Molecules*

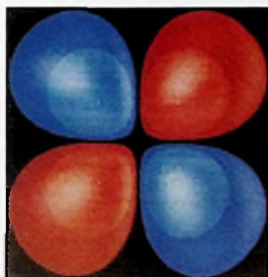
40. J J M Wiener, M E Grice, J S Murray and P Politzer, *J. Chem. Phys.* **104**, 5109 (1996).
41. R Soliva, F J Luque and M Orozco, *Theoret. Chem. Accts.* **98**, 42 (1997).
42. R Soliva, M Orozco and F J Luque, *J. Comput. Chem.* **18**, 980 (1997).
43. S R Gadre and A Taspas, *J. Mol. Graph.* **12**, 45 (1994).
44. (a) W A Sokalski and S F Sneddon, *J. Mol. Graph.* 74 (1991). (b) F Sanz, F Manaut, J Rodriguez, E Lozoya and E Lopez-de Brinas, *J. Comput. Aided Mol. Design* **7**, 337 (1993).
45. (a) SPARTAN: Wave function, Inc., 18401 Von Karman, Suite 310, Irvine CA 92715, U.S.A. (b) Hyper Chem: Autodesk, Inc., Scientific Modeling Division, 2320 Marinship Way, Sausalito CA 94965, U.S.A. (c) PCModel 4.41 for Macintosh; Serena Software, P O Box 3076 Bloomington, IN 47402, U.S.A. (d) Molecular Editor: Acad. Software Exch, 4141 State Street, Santa Barbara, Ca 93110, U.S.A. (e) UNIVIS: S R Gadre and coworkers, Department of Chemistry, University of Pune, Pune 411 007, INDIA. See, A Limaye, P V Inamdar, S M Dattawadkar and S R Gadre, *J. Mol. Graph.* **14**, 19 (1996). (f) POTROT: Kolossvary, Department of Analytical Chemistry, Technical University, Budapest (1987). (g) ACS Chemistry Viewer v2.0: (MSI, M A Burlington 1992).
Some of these packages are also available at a reasonable cost.



(a)

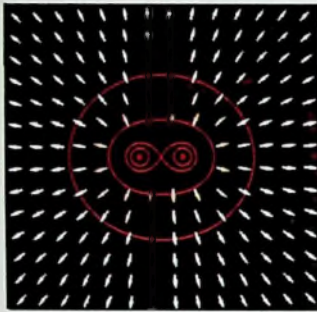


(b)

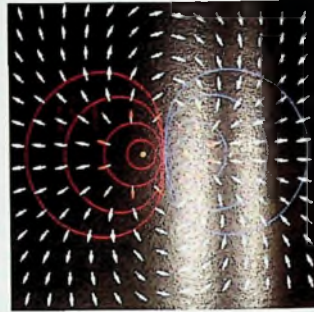


(c)

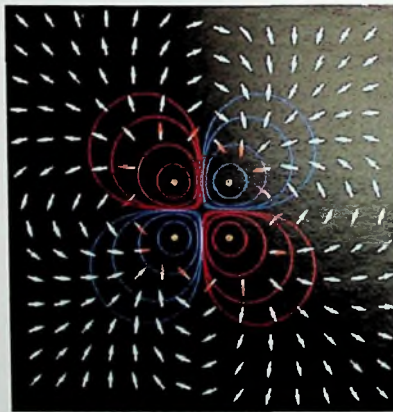
Plate 1 (a) Electrostatic potential due to two point charges (+1, +1) kept at a unit distance. The potential values for inner and outer isosurfaces are 1.0 and 0.5 a.u. respectively. **(b)** Electrostatic potential due to two point charges (+1, -1) kept at a unit distance. The potential values for the inner and outer red isosurfaces are 0.3 and 0.1. The corresponding values for the blue isosurfaces are -0.3 and -0.1 a.u. **(c)** Electrostatic potential generated by two pairs of equal and opposite unit charges kept at the corners of a square of unit length. The values of the potential for the outer and inner surfaces are ± 0.1 and ± 0.3 a.u. (blue: negative, red: positive).



(a)

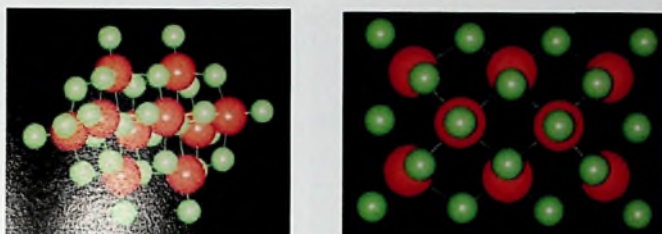


(b)



(c)

Plate 2 (a) Electrostatic potential contours of values 10.0, 3.0, 2.0, 1.5 and 0.5 a.u. due to two point charges kept at a unit distance. The magnitude of electric field (shown as vectors) is colour coded as: blue: 0 to 0.2; green: 0.2 to 0.4; yellow: > 0.4. (b) Electrostatic potential (blue: negative, red: positive) and field due to a dipole. The contour values are ± 10.0 , ± 1.0 , ± 0.3 , ± 0.1 and ± 0.05 a.u. The electric field values are coded as: blue: 0 to 0.1; green: 0.1 to 0.3; orange: >0.3. (c) Potential (blue: negative, red: positive) and field due to a quadrupole. The contour values are ± 10.0 , ± 1.0 , ± 0.3 , ± 0.1 and ± 0.05 a.u. The electric field is colour coded as: blue: 0 to 0.1; green: 0.1 to 0.3; orange: >0.3.



(a)

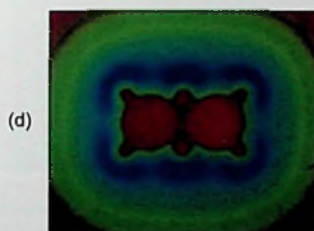
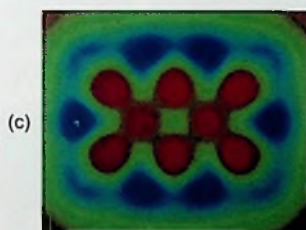
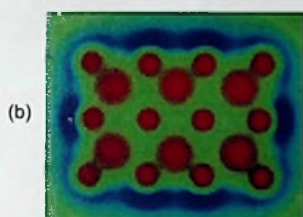
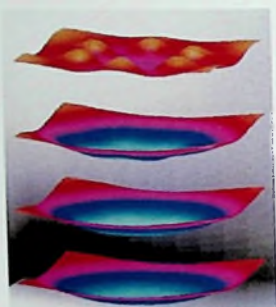


Plate 3 (a) Side and top view of the decavanadate ion ($V_{10}O_{28}^{6-}$). The vanadium and oxygen atoms are shown by red and green spheres respectively. The sizes of atoms are not to scale. (b, c, d) Two-dimensional MESP plots for the decavanadate ion through several planes, blue colour representing relatively more negative values.



(a)



(b)

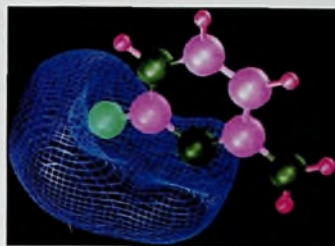
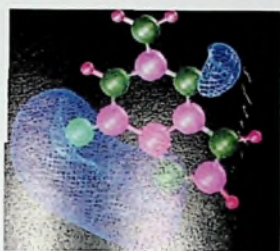


(c)

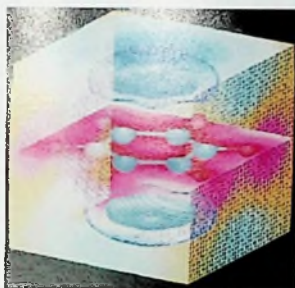


(d)

Plate 4 (a) Pseudo three-dimensional plots of MESP for the benzene molecule intercepted at various planes parallel to the molecular plane. The MESP values go from positive to negative for blue to yellow colour. (b) MESP pixel plot of the acetylene molecule; the light blue value corresponds to -0.039 a.u. approximately, and the deep red value stands for the positive MESP. Ball-and-stick model of the molecule as well as MESP contours are shown. The probable site for binding of the HF molecule, with the H end pointing towards the most negative MESP value of acetylene is also displayed. (c) MESP textured on the van der Waals envelope of C_{60} fullerene molecule. For visualizing the MESP inside, the bucky ball is cut into two parts. The red to blue colours show MESP ranging from positive to negative values. (d) MESP textured on the van der Waals envelope of C_{70} molecule. The blue colour corresponds to MESP value of -0.0027 a.u. The pink colour denotes positive values.



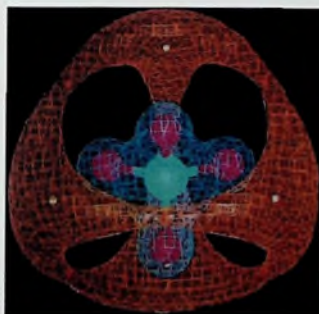
(a)



(b)

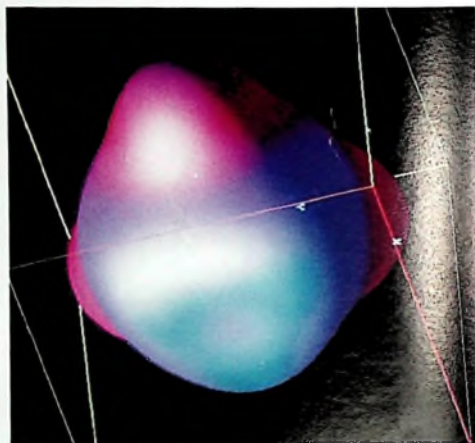


(c)



(d)

Plate 5 (a) MESP isosurface for guanine (left) and cytosine (right) molecules corresponding to the value of -0.05 a.u. along with the ball-and-stick models. (b) MESP isosurface for the benzene molecule corresponding to the value of -0.025 a.u.; superimposed on it are various planar sections along with the ball-and-stick model of the molecule. (c) Two MESP isosurfaces corresponding to the decane molecule. The light and dark pink surfaces correspond to MESP values of 0.1 and -0.003 a.u. respectively. (d) MESP isosurfaces of the methane molecule. The brown isosurface corresponds to MESP value of -0.0027 a.u. The white dots represent MESP minima.



(a)

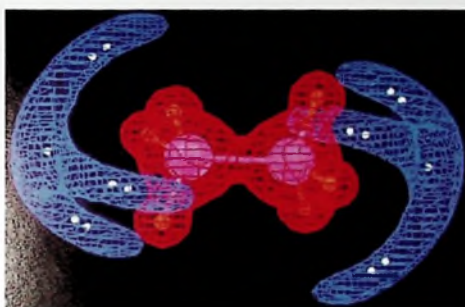


(b)

Plate 6 MESP minimal surfaces for (a) chlorate ion (b) phenolate ion; the red colour depicts most negative regions. (Please note that this convention is different from the one employed for other systems in this monograph).

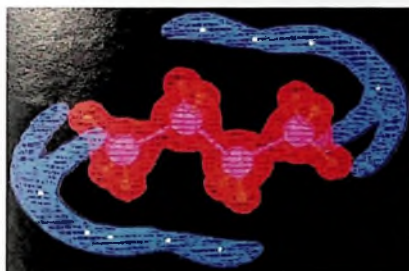


(a)

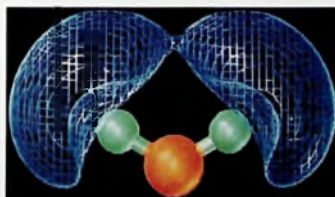


(b)

(c)



(d)



(e)

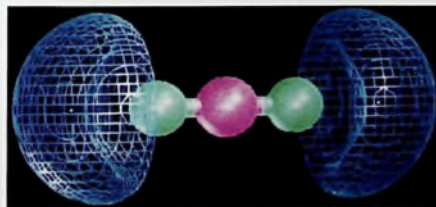


Plate 7 Three-dimensional plots showing MESP isosurfaces for (a) C_2H_4 (b) C_2H_6 (c) C_4H_{10} (d) SO_2 and (e) CO_2 molecules. The corresponding ball-and-stick models are also displayed. The CP's are shown by white dots. The isosurface values are: (a) -0.015 (b) and (c) red: 0.5 ; blue: -0.003 (d) -0.02 (e) -0.015 (all values in a.u.).

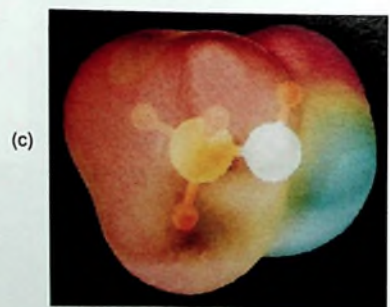
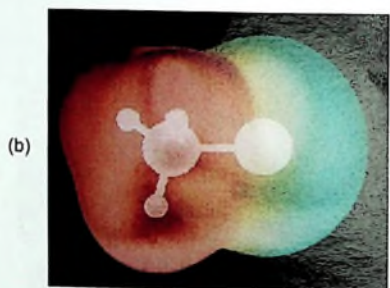
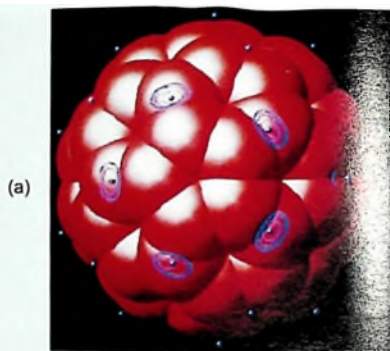
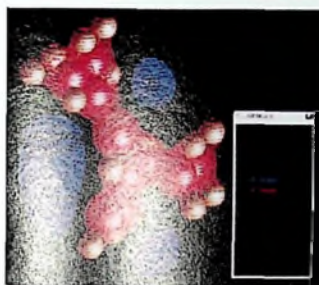
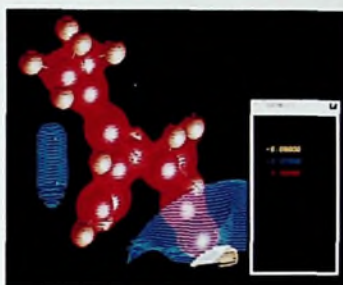


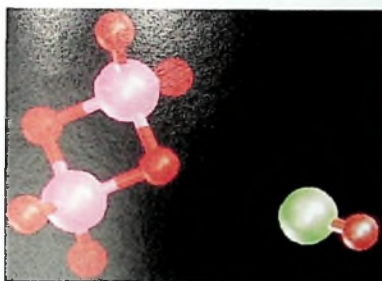
Plate 8 (a) MESP minima (blue dots) of exo bonds to the five-membered rings in C_{60} . Superposed on the van der Waals surface are the MESP contours representing MESP value of -0.001 a.u. MESP textured on molecular surface for (b) methyl chloride and (c) methanol molecules superimposed on ball-and-stick models. Blue and red colours denote negative and positive MESP's respectively.



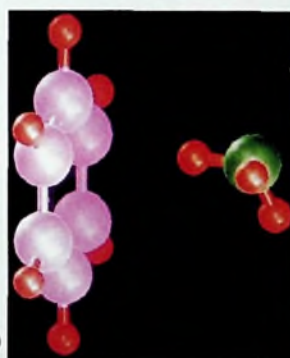
(a)



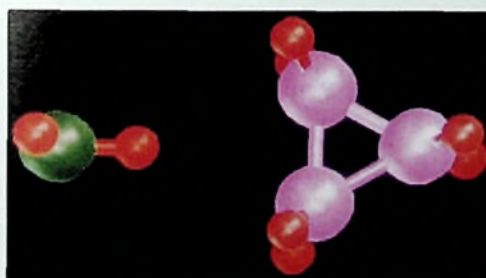
(b)



(c)

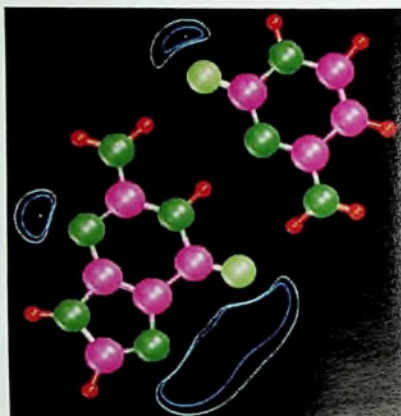


(d)

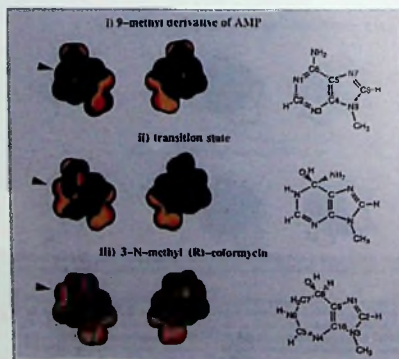


(e)

Plate 9 The MESP contours superimposed on the ball-and-stick models of (a) 7-isopropylidinenorbornene and (b) cyano derivative of 7-isopropylidinenorbornene. The MESP minima are shown by blue dots. The MESP values shown are in atomic units. Structures of some weakly bound complexes within the EPIC model. (c) $B_2H_6 \dots HF$ (d) $C_6H_6 \dots NH_3$ (e) $C_3H_6 \dots H_2O$.

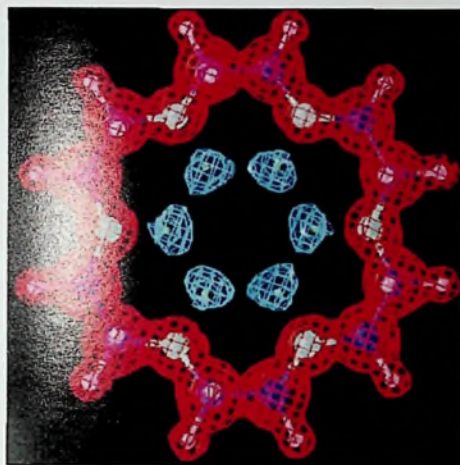


(a)

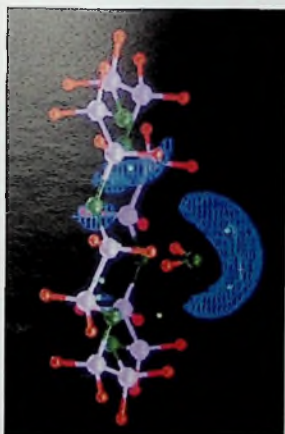


(b)

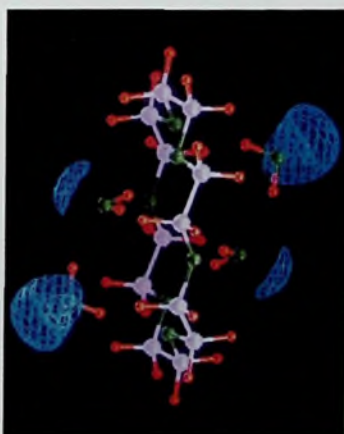
Plate 10 (a) *Ab initio* optimized structure of the guanine-cytosine (GC) complex. The green and blue contours correspond to MESP values of -0.060 and -0.075 a.u. **(b)** MESP surfaces for model substrate, transition state and transition state inhibitor, respectively, of the AMP deaminase reaction. The colour images on the left are front and rear views of (i) substrate (ii) transition state and (iii) transition state inhibitor. The colour spectrum from red to blue represents gradation from positive to negative potential. The structures on the right correspond to the orientations of the left-most molecular electrostatic surfaces. Reproduced with permission from Ref. [47(a)]. Copyright American Chemical Society (1996).



(a)

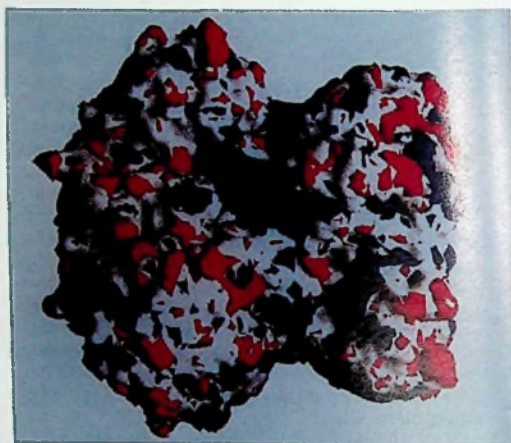


(b)

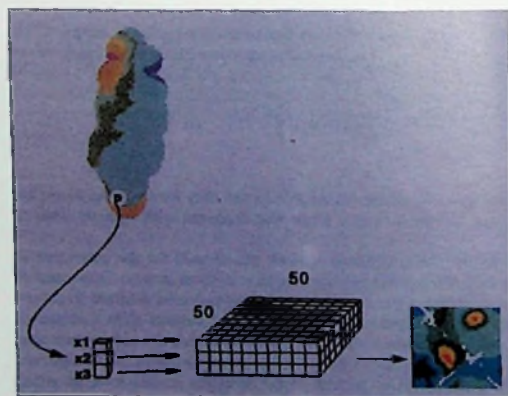


(c)

Plate 11 (a) Three-dimensional *ab initio* MESP (for *ab initio* optimized geometries) contours of 18C6; (red: 0.5 a.u.; blue -0.105 a.u.) (b) Structure of 18C6.H₂O with an MESP isosurface of value -0.1. (c) Structure of 18C6.4H₂O. Blue isosurface corresponds to MESP value of -0.09 a.u.



(a)



(b)

Plate 12 (a) Electrostatic potential textured on the molecular surfaces around MDH-CS fusion protein calculated at zero ionic strength. The blue and red surfaces correspond to potentials of + 1.5 kJ and -1.5 kJ respectively. Note the presence of a continuous positive MESP covering the area where the MDH and CS dimers meet. Reproduced with permission from Ref [50(a)]. Copyright *American Chemical Society* (1996). **(b)** The 3D model of corticosterone, parallel projection of the MESP onto the van der Waals surface of the molecule and the corresponding Kohonen map. Reproduced from Ref. [56], with permission from Wiley-VCH, Basel.

3

Some General Results Regarding Atomic and Molecular Electrostatic Potentials

3.1 Molecular Non-binding Theorems within Statistical Theories

An early semi-classical atomic model incorporating the electron density as a basic variable was proposed independently by Thomas [1] and Fermi [2]. In retrospect, this pioneering contribution, now known as the Thomas–Fermi (TF) theory, along with its numerous refined versions [1–4], happens to be historically the first one in which the electron density $\rho(\mathbf{r})$ played a key role, and there is no “wave function” defined within its regime. The general subject of the density functional theory (DFT) was formally born much later with the enunciation of the celebrated Hohenberg–Kohn theorems [5, 6] (Refer to Appendix F for an introduction to electron density and DFT). A peculiarity of the TF atom model in the context of the present monograph is that the electron density (within this model) at a site \mathbf{r} is related to the corresponding value of the electrostatic potential, $V(\mathbf{r})$.

Semi-classical phase space considerations are employed for deriving the TF atom model. A cell in phase space has a typical volume $d^3r \cdot d^3p$ of the order of $(2\pi)^3$ in a.u. according to the Heisenberg uncertainty relation. Each such cell may contain a maximum of two electrons, yielding

$$2 \int \frac{d^3r \cdot d^3p}{(2\pi)^3} = N \quad (3.1)$$

where N is the total number of electrons in an atom for which spherical symmetry is assumed. Noting that $\int \rho(\mathbf{r}) d^3r = N$, one may identify

$$\rho(\mathbf{r}) = 2 \int \frac{d^3p}{(2\pi)^3} \quad (3.2)$$

40 *Electrostatics of Atoms and Molecules*

The integral on the r.h.s. of Eq. 3.2 (for $0 < p < p_f$) is simply $p_f^3/6\pi^2$ where $p_f = p_f(r)$ is the Fermi momentum at r , yielding

$$\rho(r) = p_f^3(r)/6\pi^2 \quad (3.3)$$

Now, the maximum total energy an electron could have at a distance r from the nucleus is $(p_f^2(r)/2) - V(r)$. This should equal a negative constant ($-V_0$), since otherwise the electron would fly to infinity, i.e.,

$$(p_f^2(r)/2) = V(r) - V_0 \quad (3.4)$$

In conjunction with Eq. 3.3, this yields

$$\rho(r) = [2(V(r) - V_0)]^{3/2} / 3\pi^2 \quad (3.5)$$

For a neutral TF atom, as $r \rightarrow \infty$, both $\rho(r)$ and $V(r) \rightarrow 0$, implying $V_0 = 0$. Thus, the spherically symmetric atomic electron density $\rho(r)$ is described simply in terms of the corresponding electrostatic potential $V(r)$ (both expressed in a.u.) for a neutral TF atom by the following relation.

$$\rho(r) = 2^{3/2} V^{3/2}(r) / (3\pi^2) \quad (3.6)$$

Yet another universal connection, from classical electrostatics, between the atomic $\rho(r)$ and $V(r)$, is offered by the Poisson equation as detailed in Chapter 1. Equation 1.20, on conversion to atomic units ($4\pi\epsilon_0 = 1$) and realizing that the charge density there is negative, emerges as

$$\nabla^2 V(r) = 4\pi\rho(r) \quad (3.7)$$

Combining Eqs. 3.6 and 3.7, one obtains

$$\nabla^2 V(r) = \frac{2^{7/2} V^{3/2}(r)}{3\pi} \quad (3.8)$$

which is an interesting differential equation in terms of the atomic electrostatic potential. On substituting

$$V(r) = Z\phi(r) / r \quad (3.9)$$

followed by a change of variable $r = x(9\pi^2 / 2Z)^{1/3} / 4$ ($\sim 0.8853Z^{-1/3} x$), Eq. 3.8 assumes a compact universal form, viz.

$$\frac{d^2\phi}{dx^2} = \frac{\phi^{3/2}(x)}{x^{1/2}} \tag{3.10}$$

Equation 3.10 represents the standard form of the atomic TF equation. Noting that $\phi(x)$ is simply related to the corresponding ESP, viz. $V(r)$, the key role of the latter quantity within the TF model is evident. The nonlinear and 'stiff' differential Equation (3.10) for a neutral atom has a 'universal' solution. However, while it cannot be solved analytically exactly, highly accurate numerical solutions have been tabulated. The solution $\phi(x)$ must satisfy $\phi(0) = 1$ and it can be readily verified that the asymptotic solution is given by $\phi(x) \cong 144/x^3$. Further, on employing this solution, properties such as $\langle r^n \rangle$ expectation values etc. of such an atom also assume a universal form and can be readily computed.

How do molecules behave within the TF framework? This question of molecular binding [7–10] within the TF framework was first addressed by Sheldon [7]. He showed, employing a numerical computation, that the N_2 molecule is not bound within the TF framework. He also conjectured that this result may generally hold good within statistical theories. Teller gave a rigorous general proof to this effect [8]. This interesting proof, summarized below, is based on energetic considerations wherein a molecule-building process starting from an atom [8, 10] is envisioned.

Consider a neutral TF atom, to which a small localized positive charge $\xi(\mathbf{r})$ is added at a non-nuclear site \mathbf{r} . This is compensated by an equal, diffuse negative charge. Let the perturbation in the corresponding electrostatic potential be $\epsilon(\mathbf{r})$. It can be readily shown, for small $\epsilon(\mathbf{r})$, using Eq. 3.7, that

$$\nabla\epsilon(\mathbf{r}) = \frac{3}{2}V^{1/2}(\mathbf{r})\epsilon(\mathbf{r}) - \xi(\mathbf{r}) \tag{3.11}$$

It may be shown, following Teller [8], that $\epsilon(\mathbf{r}) \geq 0$ at all sites \mathbf{r} by *reductio ad absurdum*. Assume to the contrary, that ϵ changes sign in different regions. It is always possible to select a spatial region Ω , not containing $\xi(\mathbf{r})$, for which $\epsilon < 0$ inside the enclosing surface S and $\epsilon > 0$ outside, with ϵ vanishing on S . Further, $\nabla^2\epsilon(\mathbf{r}) = \frac{3}{2}V^{1/2}(\mathbf{r})\epsilon(\mathbf{r})$ for a region not containing $\xi(\mathbf{r})$. By invoking the divergence theorem, vide Appendix C, we have

42 Electrostatics of Atoms and Molecules

$$\int_{\Omega} \nabla^2 \varepsilon(\mathbf{r}) d^3r = \oint_S \nabla \varepsilon \cdot d\mathbf{S} = \frac{3}{2} \int_{\Omega} V^{1/2}(\mathbf{r}) \varepsilon(\mathbf{r}) d^3r \quad (3.12)$$

Since $\varepsilon(\mathbf{r}) < 0$ inside Ω and $V(\mathbf{r}) > 0$, the integral on the r.h.s. of Eq. 3.12 must be negative. However, since $\nabla \varepsilon(\mathbf{r})$ points outward at all points on the surface, the middle term in Eq. 3.12 should be positive, leading to a contradiction. Hence, being positive in the vicinity of $\xi(\mathbf{r})$, the perturbation in the ESP, $\varepsilon(\mathbf{r})$, should be positive throughout and vanish at infinity.

Now consider the molecule-building process envisioned by Teller [8], wherein the addition of an infinitesimally small positive charge at a fixed site is repeated. This charge is duly compensated at each stage by an equal, diffuse negative charge. This eventually builds up the molecule starting from an atom. As seen above, at each stage, the incremental ESP $\varepsilon(\mathbf{r})$ in this building-up process is positive, leading to

$$V(\mathbf{R})_{\text{molecule}} > V(\mathbf{R})_{\text{separated atoms}} \quad (3.13)$$

where the term on the l.h.s. of Eq. 3.13 denotes the ESP at any site \mathbf{R} in the molecule and the r.h.s. term stands for that due to separated atoms.

During this process, the total energy of the system also changes. This net change, δE , was shown by Teller to be

$$\delta E = \delta q \int \frac{d^3r [\rho_+(\mathbf{R}) - \rho(\mathbf{R})]}{|\mathbf{r} - \mathbf{R}|} = \delta q V(\mathbf{R}) \quad (3.14)$$

where $\rho_+(\mathbf{R})$ is nuclear (positive) charge density, and $\delta q = \int \xi(\mathbf{r}) d^3r$. This eventually yields $\delta E > 0$, thereby ruling out the existence of stable molecules within the TF theory.

Balázs [9] extended the validity of Teller's theorem, and proved a more general result, viz., no theory within which $\rho(\mathbf{r})$ is a function, exclusively of the electrostatic potential, $V(\mathbf{r})$ at the same location \mathbf{r} , can describe stable molecules. Balázs' proof of this general result is based on electrostatic *force* considerations, rather than the *energetic* ones employed by Teller. Balázs showed, by an elegant construction, that the force on the nucleus A in a homonuclear diatomic molecule AA' within such a model is directed in the outward direction. The force on the nucleus A is given by

$$\mathbf{F}_A = \int \rho_A(\mathbf{r}) \mathbf{E}(\mathbf{r}) d^3r \quad (3.15)$$

where \mathbf{E} denotes the molecular electrostatic field (MEF). Figure 3.1 depicts two surfaces S' (flat) and S (curved) enclosing a volume Ω around the nucleus A . The surface S , upon which \mathbf{E} vanishes identically, may be located at infinity. The force on A may be calculated by employing the Poisson equation

$$\rho_A(\mathbf{r}) = -(\nabla^2 V(\mathbf{r}) / 4\pi) + \rho(\mathbf{r}). \tag{3.16}$$

where $\rho(\mathbf{r})$ and $\rho_A(\mathbf{r})$ denote the electronic and nuclear charge distributions respectively, and $\mathbf{E} = -\nabla V$; the force on the nucleus A is given as (employing vector integral theorems discussed in Appendix C)

$$\begin{aligned} \mathbf{F}_A = & \oint_{S+S'} \{ \nabla V(\mathbf{r}) \cdot d\mathbf{S} [\nabla V(\mathbf{r})] / 4\pi \} - \oint_{S+S'} \frac{(\nabla V(\mathbf{r}))^2}{8\pi} d\mathbf{S} \\ & - \int_{\Omega} \rho(\mathbf{r}) \nabla V(\mathbf{r}) d^3r \end{aligned} \tag{3.17}$$

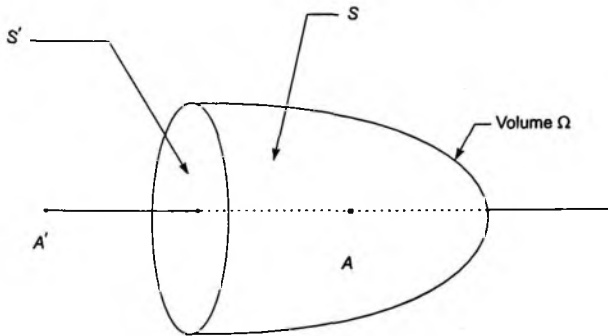


Fig. 3.1 Balázs' construction of curved (S) and flat (S') surfaces for a homonuclear diatomic molecule AA' . The surfaces enclose a volume Ω .

On the surface S , the field is zero and further, on S' , $\nabla V \cdot d\mathbf{S} = 0$. Hence, the first term on the r.h.s. of Eq. 3.17 as well as the S' contribution to the second term vanishes. It was shown by Balázs that the remaining terms individually, and hence upon addition, lead to a positive force on nucleus A . This means that whenever $\rho = f(V)$, the nuclei will fly apart, leading to no binding.

44 Electrostatics of Atoms and Molecules

It was further shown by Balázs [9] that these arguments can be readily generalized to heteronuclear systems as well. He subsequently demonstrated that the introduction of the so-called Weizsäcker term [9, 10] in the kinetic energy functional can, in fact, lead to molecular binding. It is of interest to note that the non-binding theorems discussed above employ MESP and MEF as key quantities. Yet another connection exists between MESP at the nuclei and the electronic energy of the corresponding molecular system, which is discussed in the following Section.

3.2 ESP at Nuclei and Electronic Energies of Atoms and Molecules

The MESP at a nucleus A of a molecule, viz. $V_{0,A}$ can be obtained by dropping out the nuclear contribution due to Z_A from the definition of MESP, via Eq. 1.27

$$V_{0,A} = \sum_{B \neq A} \frac{Z_B}{|\mathbf{R}_B - \mathbf{R}_A|} - \int \frac{\rho(\mathbf{r}') d^3 r'}{|\mathbf{r} - \mathbf{r}'|} \quad (3.18)$$

Employing the Hellmann–Feynman theorem, Politzer and Parr [11] derived *exact* formulae for atomic and molecular energies respectively in terms of electrostatic potential at nuclei. The atomic energy E_{at} for an atom with nuclear charge Z and N electrons is given as:

$$E_{\text{at}} = \frac{1}{2} Z V_0 - \frac{1}{2} \int_0^Z Z' (\partial V_0 / \partial Z') - V_0]_N dZ' \quad (3.19)$$

where V_0 is the electrostatic potential at the nucleus due to electrons, and for a single free atom it is given as

$$V_0 = - \int \frac{\rho(r) d^3 r}{r} \quad \text{and} \\ E_{\text{mol}} = \frac{1}{2} \sum_A Z_A V_{0,A} - \frac{1}{2} \sum_A \int_0^{Z_A} [Z'_A (\partial V_{0,A} / \partial Z'_A) - V_{0,A}]_{N_A} dZ'_A \quad (3.20)$$

An interesting feature of Eq. 3.20 is that the molecular energy appears there as a simple summation of atomic-like relation, viz. Eq. 3.19. It is noteworthy that within the TF theory, $E_{\text{at}} = 3ZV_0 / 7 \cong -0.7687 Z^{7/3}$ since

V_0 for this theory is $-1.794 Z^{4/3}$. Politzer proposed [12] a linear relation between the atomic V and ρ for the outer (valence) regions. However, he found that a TF-type relation (cf. Eq. 3.6) holds good for the inner (core) regions of atoms. Incidentally, Politzer and Parr used the position of the most outward minimum in the plot of radial density, $D(r) = 4\pi r^2 \rho(r)$ for defining the core–valence separation.

By extending the argument that E_{mol} is a sum of atomic-like terms, Politzer [13] proposed an approximation in which the TF energy relation is used, viz.

$$E_{\text{mol}} = \frac{3}{7} \sum Z_A V_{0,A} \quad (3.21)$$

It was found that Eq. 3.21 represents molecular energies fairly well, typical deviation from the corresponding Hartree–Fock energies (at equilibrium geometries) being less than 2%. Politzer [14] further proposed an improvement over Eq. 3.21 by incorporating an empirical parameter k_A for each atom, rather than simply importing the TF value of $3/7$, viz.

$$E_{\text{mol}} = \sum_A k_A Z_A V_{0,A} \quad (3.22)$$

Using such empirically chosen k_A values, it was found [14] that the total molecular energies are excellently reproduced by Eq. 3.22, typical errors being only 0.5%. From the above discussion, the utility of MESP values at the nuclear sites in providing simple approximation to atomic and molecular energies is quite clear.

Levy *et al.* [15] have discussed several interesting relations between electrostatic potentials at nuclei and correlation energies. Starting again with the Hellmann–Feynman theorem, the following relation for an atomic system may readily be derived:

$$\frac{\partial E(Z, N)}{\partial Z} = \langle \psi(Z, N) \left| \frac{\partial \mathbf{H}}{\partial Z} \right| \psi(Z, N) \rangle = - \int d^3 r r^{-1} \rho(r, Z, N) \quad (3.23)$$

Here, Z is the nuclear charge, \mathbf{H} is the corresponding Hamiltonian operator, N is the number of electrons of the atomic system, $E(Z, N)$ is the atomic energy, $\psi(Z, N)$ is the electronic wave function, and the r.h.s. of Eq. 3.23 represents the ESP at the nucleus. Levy *et al.* [15] invoked ingenious scaling arguments for deriving several rigorous bounds to the ESP value at an atomic nucleus. For example, for an arbitrary λ ,

$$E(Z') \leq 2\lambda E(Z) - \lambda^2 E(Z) - \lambda(Z' - Z) \int d^3 r r^{-1} \rho(r, Z) \quad (3.24)$$

Optimization of λ in this relation yields the following tight bound

$$E(Z') \leq \left\{ 2E(Z) - (Z' - Z) \int d^3 r r^{-1} \rho(r, Z) \right\}^2 / 4E(Z) \quad (3.25)$$

In relations 3.24 and 3.25, $E(Z')$ denotes the energy of an atomic system isoelectronic with the one with atomic number Z possessing N electrons. Employing such relations in conjunction with the total energies of He, Li^+ and H^- , Levy *et al.* [15] obtained the following (rather tight) upper and lower bounds for the ESP at the nucleus of the helium atom (with $Z = 2$ and using a.u.)

$$3.33 \leq \int d^3 r r^{-1} \rho(r, 2) \leq 3.39 \quad (3.26)$$

The corresponding actual ESP value is 3.38. It was also pointed out by them [15] that H^- turns out to be stable, by utilizing only the energy data of the He atom in Eq. 3.25, viz.

$$E(\text{H}^-) \leq -0.5087 \text{ a.u.} \quad (3.27)$$

However, we can go only thus far and no further! This treatment fails to predict the selective stability of other negative ions.

Another related concept is the electronegativity of an atom. In recent years a new definition of electronegativity χ has been proposed by Parr and co-workers [16] as: $\chi = -\mu = -(\partial E / \partial N)_z$, i.e. the electronegativity equals the negative value of the Lagrange multiplier μ in the following equation (cf. Appendix F)

$$\delta \{ E_v[\rho] - \mu \int \rho(\mathbf{r}) d^3 r \} = 0$$

In addition to the relationship between the energies of atoms and molecules to the electrostatic potential at their nuclei, Parr and co-workers [11, 16] have brought out a further connection between V_0 and μ (and hence the electronegativity χ) of an atom with atomic number Z containing N electrons as

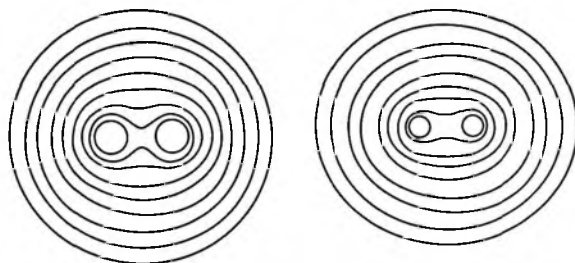
$$\left(\frac{\partial E}{\partial Z} \right)_{N=Z} = V_0 - \chi \quad (3.28)$$

Thus, electrostatic potential has interesting connections with the total electronic energy as well as a related energy derivative, viz. electronegativity, which is of great chemical interest.

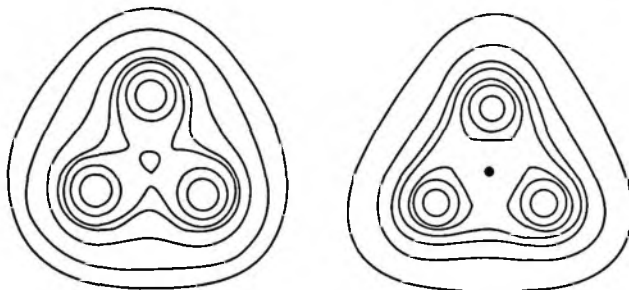
3.3 Similarities in Contour Maps of Molecular Electron Densities, Electrostatic Potentials and Bare-Nuclear Potentials [11–15]

The bare-nuclear potential (BNP) $V_{bn}(\mathbf{r})$, viz. only the nuclear contribution to the MESP, $V(\mathbf{r})$, is a fundamental entity. In terms of the Hohenberg–Kohn theorem [5], $V_{bn}(\mathbf{r})$ is identified with the external potential. This, in turn, fixes $\rho(\mathbf{r})$ for the ground state and, reciprocally, $\rho(\mathbf{r})$ fixes the external potential, $V_{bn}(\mathbf{r})$. Thus, heuristic considerations would imply a build-up of electron density in the regions where $V_{bn}(\mathbf{r})$ is higher. In this sense, Parr and Berk [19] have called $V_{bn}(\mathbf{r})$ a harbinger of the electron density $\rho(\mathbf{r})$. Similarity between $\rho(\mathbf{r})$ and $V_{bn}(\mathbf{r})$ was first noticed by Parr *et al.* [17] within a very simple local version of density functional theory for atoms wherein $\rho(\mathbf{r})$ turns out to be a *local function* of $V_{bn}(\mathbf{r})$. It is further noteworthy that for the spherically symmetric case of atoms, the contours of $V(\mathbf{r})$, $V_{bn}(\mathbf{r})$ and $\rho(\mathbf{r})$ are rather trivially identical. The relationship between $V_{bn}(\mathbf{r})$ and $\rho(\mathbf{r})$ was investigated topologically by Tal *et al.* [18] along the C_{2v} dissociative path of the water molecule. They showed that the structure diagrams of these two scalar fields are homeomorphic. They further conjectured that such a homeomorphism exists for any molecular system. The pictorial ‘similarity’ between the contour diagrams of these two scalar fields has been studied for B_2 [17], BeH, BH, B_2H_6 and H_2O [19]. Contours of BNP and MED are shown in Fig. 3.2, bringing out their visual similarity. Politzer and Zilles [20] and Gadre and Bendale [21] have subjected this hypothesis to more detailed scrutiny.

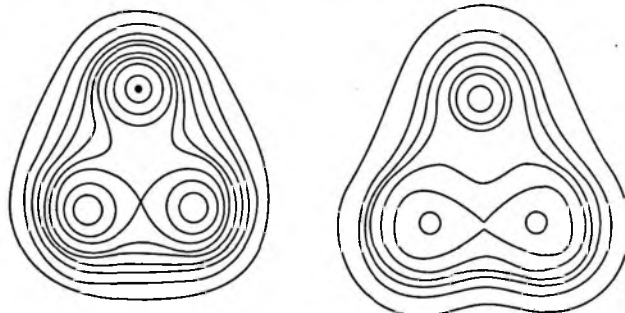
Politzer and Zilles [20] found that though the similarity between $V_{bn}(\mathbf{r})$ and $\rho(\mathbf{r})$ holds for many cases, it does not hold for molecules such as cubane and oxirane. They pointed out a fundamental difference between the *difference* quantities, $\Delta V_{bn}(\mathbf{r}) = V_{bn}^{mol}(\mathbf{r}) - \sum V_{bn}^{at}(\mathbf{r})$ and $\Delta\rho(\mathbf{r}) = \rho_{mol}(\mathbf{r}) - \sum \rho_{at}(\mathbf{r})$. Note that $\Delta V_{bn}(\mathbf{r})$ is identically zero whereas $\Delta\rho(\mathbf{r})$ is *not*, due to electron reorganization on bonding. Intrigued by the findings of Politzer and Zilles [20], and prompted by the simple TF-like prediction that contours of $\rho(\mathbf{r})$ and $V(\mathbf{r})$ are alike, Gadre and Bendale [21] examined the cases of cyclopropane, oxirane and diazirine molecules. It was found by them that the contours of these two scalar fields appear to be strikingly similar over the ring region. They also pointed out that probing the similarity in the outside regions would be useful (cf. Chapter 2), whereby it turns out that $V_{bn}(\mathbf{r})$, and $\rho(\mathbf{r})$ behave quite differently.



(a) H_2 : The successive BNP values (left): 0.75, 0.85, 0.98, 1.15, 1.4, 1.7, 2.2, 2.8 and 4.0. The MED values (right): 0.002, 0.004, 0.01, 0.02, 0.05, 0.09, 0.15, 0.25, and 0.32.



(b) C_3H_6 (Cyclopropane): The BNP values (left): 7.0, 8.0, 9.0, 10.0, 12.0, 12.82, 15.0 and 22.0. The MED values (right): 0.02, 0.08, 0.15, 0.2 and 0.27.



(c) CH_2N_2 (Diazirine): The BNP values (left): 8.0, 9.0, 10.0, 11.0, 12.0, 13.0, 15.0, 18.0 and 30.0. The MED values (right): 0.04, 0.08, 0.1, 0.15, 0.2, 0.3, 0.5 and 10.0.

Fig. 3.2 Contours of BNP (left) and MED (right) at HF/6-31G** level for some simple molecules. The successive contour values for the BNP and the MED given here are from outermost regions to centres of atoms and are given in a.u.

3.4 Maximal and Minimal Characteristics of Atomic and Molecular Electrostatic Potentials

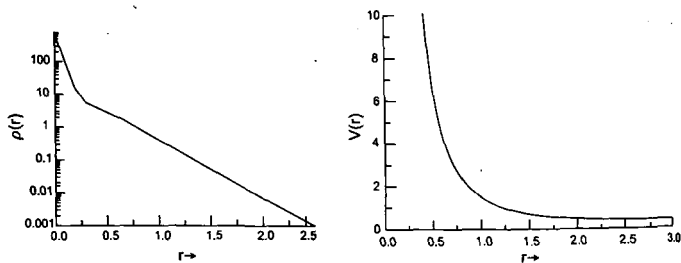
Weinstein *et al.* [22] rigorously proved the non-existence of finite valued maxima in atomic ESPs. Their proof is simple and should indeed form a part of any introductory course on electrostatics. Consider the Poisson equation at all points except at the nuclear site, for a spherical atomic system viz. $\nabla^2 V(r) = 4\pi\rho(r)$. On transcription to spherical polar co-ordinates, as discussed in Appendix C, and exploiting spherical symmetry, one obtains

$$\frac{d^2V(r)}{dr^2} + \frac{2}{r} \frac{dV(r)}{dr} = 4\pi\rho(r) \quad (3.29)$$

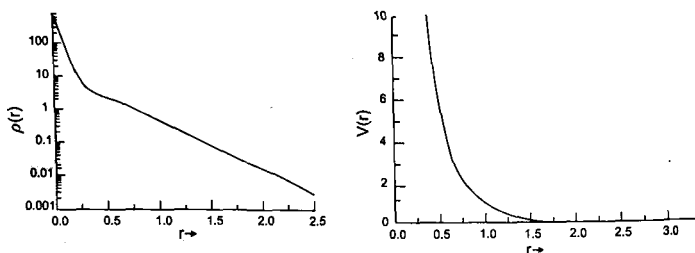
The necessary and sufficient conditions for the existence of a maximum in $V(r)$ are: $dV(r)/dr = 0$ and $d^2V(r)/dr^2 < 0$. However, this leads to a contradiction, since the l.h.s. of Eq. 3.29 is negative where a maximum in $V(r)$ exists. The r.h.s., on the other hand, is always non-negative. Thus, no non-nuclear maximum exists for a spherically symmetric one-centre system. A similar result holds for atomic cations as well. In Fig. 3.3 are presented the Hartree–Fock level ESP, $V(r)$ and ED, $\rho(r)$ plots for three isoelectronic atomic systems, Na^+ , Ne and F^- . The first two systems do not lead to any local minimum in MESP. However, F^- shows a negative-valued minimum, which will be discussed in the following Section. On the other hand, all the MED plots turn out to be monotonic. Weinstein *et al.* [22] were actually investigating the monotonic behaviour of spherically averaged ground state atomic electron densities in this work: a deceptively simple-looking problem, which has so far eluded a rigorous solution!

The lack of non-nuclear maxima in three-dimensional (molecules or solid) MESP distributions is a non-trivial extension [23, 24] of the above result. The necessary and sufficient conditions for a (*nondegenerate*) maximum at point P in $V(r)$ are as follows. The first partial derivatives $\frac{\partial V}{\partial x}$, $\frac{\partial V}{\partial y}$ and $\frac{\partial V}{\partial z}$ should all identically vanish at the point P . Further, all the three eigenvalues ($\lambda_1, \lambda_2, \lambda_3$) of the corresponding Hessian matrix \mathbf{H} must be strictly negative (cf. Appendix G for an introduction to topography). Note that \mathbf{H} is a real symmetric (and therefore Hermitian) matrix. Hence, \mathbf{H} can be diagonalized by an appropriate unitary transformation. As stated above, for the point P to be a nondegenerate maximum, all the eigenvalues of \mathbf{H} should be strictly negative [23, 24]. However, as in the atomic case,

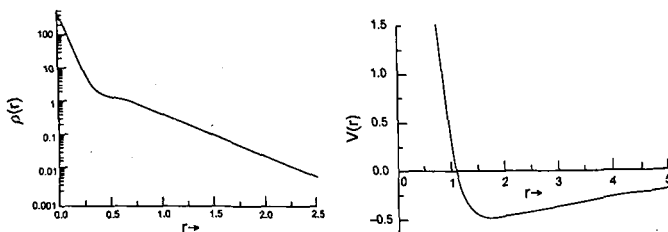
50 *Electrostatics of Atoms and Molecules*



(a) $\rho(r)$ on log scale vs r for the Na^+ ion. (a) $V(r)$ vs r for the Na^+ ion.



(b) $\rho(r)$ on log scale vs r for the Ne atom. (b) $V(r)$ vs r for the Ne atom.



(c) $\rho(r)$ on log scale vs r for the F^- ion. (c) $V(r)$ vs r for the F^- ion.

Fig. 3.3 Plot of $\rho(r)$ on log scale (left) and $V(r)$ (right) against r for a few atomic systems: (a) Na^+ , (b) Ne and (c) F^- , ions respectively. Atomic units are used throughout.

this leads to a contradiction at a non-nuclear site \mathbf{r} , since the Poisson equation demands that

$$\nabla^2 V(\mathbf{r}) = (\lambda_1 + \lambda_2 + \lambda_3) = 4\pi\rho(\mathbf{r})$$

with $\rho(\mathbf{r}) \geq 0$ at all \mathbf{r} . The extension to degenerate maxima [23, 24] (one or two of the eigenvalues are zero, and the remaining are negative) is also straightforward. Thus, the three-dimensional MESP distribution of a molecule or solid *cannot* exhibit non-nuclear maxima. The MED topography [25] (cf. Appendix F) is also similar in this respect, barring non-nuclear maxima shown by some molecules. This prompts one to look into the topographical features of MESP, which indeed turn out to be interesting (see Section 3.6), owing to its inherently rich structure.

Arguing on similar lines, it can be readily shown that no maxima or minima exist within $V_{bn}(\mathbf{r})$. Employing the Laplace equation at non-nuclear sites, viz. $\nabla^2 V_{bn}(\mathbf{r}) = 0$, and the necessary condition for a non-degenerate maximum or minimum ($\nabla^2 V_{bn}(\mathbf{r}) < 0$ and > 0 respectively), leads to a contradiction. Thus, the topography of $V_{bn}(\mathbf{r})$ is expected to be quite poor as compared to that of $V(\mathbf{r})$. In the vicinity of the nuclear framework, however, these two distributions may exhibit striking similarity as discussed earlier in Section 3.3.

A generalization of this result throws light on a serious drawback of all point charge models, i.e. no point charge model is capable of properly representing minima in the corresponding MESP. The so-called MESP-driven charges (cf. Chapter 2), popular in the literature for molecular interaction studies, indeed lead to a reasonably good numerical fit of MESP in the exterior regions of molecules. However, they miss out an extremely significant topographical characteristic—they fail to show any minima!

It indeed turns out that the MESP topography of molecules is generally richer than that of the MED and BNP. Such studies have been extremely rewarding in unearthing the structure and reactivity features of molecules. These are presented in Section 3.6, and their chemical applications are discussed in Chapter 4.

3.5 Atomic and Molecular Anions

We have seen in Section 3.4 that no non-nuclear maxima exist in the ESP of atoms and molecules. However, this does not rule out the existence of MESP minima for these systems as has been demonstrated for the F^- ion in Section 3.4. In particular, the question of negative valued ESP minima for atomic anions was investigated by Sen and Politzer [26, 27]. They proved the

52 Electrostatics of Atoms and Molecules

following general result for these systems. Consider the $V(r)$ of an atomic anion X^{q-} . It attains large positive values close to the nucleus. However, at large r , due to Coulomb's law, $V(r)$ should die out as $-q/r$. For intermediate values, $V(r)$ (cf. Fig. 3.3(c)) due to its continuity and smoothness, must attain a negative valued *minimum* at, $r = r_m$, say. We may now recall Gauss' theorem (cf. Chapter 1), viz.

$$\oint \nabla V \cdot d\mathbf{S} = \int \nabla^2 V d^3 r \quad (3.30)$$

On choosing the surface S as that of a sphere with the nucleus as its centre and radius r_m , the l.h.s. = 0. The r.h.s., in conjunction with Poisson's equation, yields the net charge inside the surface S as

$$\int \nabla^2 V d^3 r = 0 \quad (3.31)$$

which means that the sphere with radius r_m encloses a *net zero charge*. In other words, it can be imagined that the entire charge carried by the anion, viz. $-q$, is 'sitting' outside this sphere. Using this logic, Sen and Politzer [27] proposed r_m as a measure of the radius of monoatomic anions. They found that the agreement of r_m values with the anionic radii reported in the literature is qualitatively good. However, they also observed that the halide ions, F^- , Cl^- , Br^- and I^- generally turn out to be somewhat smaller than the respective crystal radii.

In this respect, the treatment of polyatomic anions is far more interesting. The so-called 'thermochemical' or 'crystal' radii so popular in the chemical literature represent only a spherical average of some kind. In fact, thermochemical radii do not necessarily refer to the spatial extent of polyatomic anions. They are actually fit-parameters for reproducing experimental values of lattice energies. The inadequacy in the treatment of sites of polyatomic anions has been recognized in the literature. For instance, Huheey [28] has remarked that "In many cases, the fact that the ions (such as CO_3^{2-} , CNS^- , $CH_3CO_2^-$ etc.) are markedly non-spherical, limits the use of these radii". Another example of desirability of a non-spherical anion may be seen for the intuitive pictures [29] of CN^- and OH^- ions in NaCN and $Ca(OH)_2$ crystals respectively shown in the standard treatise on structural inorganic chemistry by Wells. The subject of anisotropy in ionic interactions is also currently being discussed. In particular, the statements regarding near-sphericity of NH_4^+ and CN^- ions, as far as interactions are concerned, are of interest [29]. Thus a general treatment of sizes, shapes and anisotropies of molecular anions is of great utility.

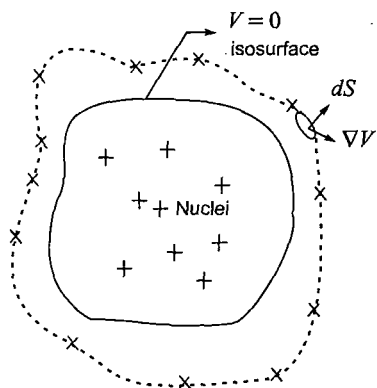


Fig. 3.4(a) A schematic representation of MESP surface described by $\nabla V(\mathbf{r}) \cdot d\mathbf{S} = 0$. Nuclear framework is shown by positive signs covered by negative sheath of potential. The CPs lying on the surface are denoted as 'x'. The outward normal is $d\mathbf{S}$ and the gradient vector is $\nabla V(\mathbf{r})$.

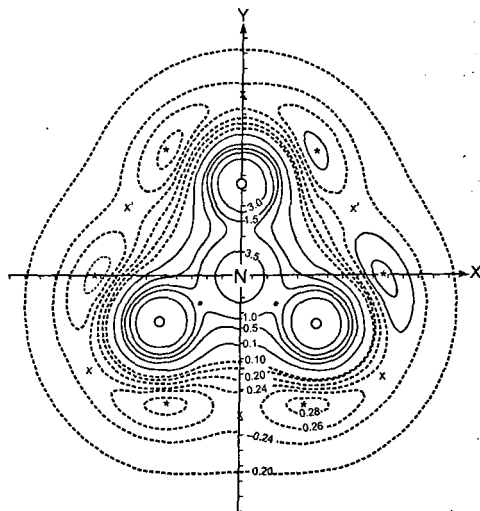


Fig. 3.4(b) MESP contour maps for the nitrate (NO_3^-) ion in the molecular plane. CPs are marked as x, x', * and *. This figure is reproduced with permission from Ref. 30. Copyright (1991) American Institute of Physics.

Such a clearcut, rigorous definition has been offered by Pathak and Gadre [24] in terms of a generalization of the earlier work by Sen and Politzer [26]. Their theorem for polyatomic anions ensures the existence of a 'minimal' surface constructed from rays emanating outward from nuclei of the species. Such a surface satisfies the condition, $\nabla V \cdot d\mathbf{S} = 0$ at points on it and hence, by Gauss' theorem, the net charge on the anion resides outside this surface. Further, the MESP values at all points on this surface and outside are negative. Consequently, the atomic and molecular anions would appear as though they are wearing a sheath (or jacket) of negative MESP around them in all directions! This surface could be taken as a reference for obtaining sizes, shapes and anisotropies of interactions of the anion concerned [30–32]. The two-dimensional projection of such a surface is shown schematically in Fig. 3.4(a). A two-dimensional MESP contour plot for the nitrate ion (NO_3^-) is depicted in Fig. 3.4(b). The minimal surface for this ion is seen to pass through the negative valued CPs shown in the figure. The extent of the anion in various directions could be averaged out and compared with the respective thermochemical radius. The agreement has, in general, been found to be fairly good [30]. The 'minimal' surface with the MESP textured on it offers a good electrostatic picture of the anion [31, 32]. Two such pictures are shown in Plate 6. Plate 6(a) shows the MESP minimal surface for the chlorate ion. The red colour represents a more negative value of MESP and the blue one represents the lesser negative region of the MESP. It can be seen qualitatively from this graphic that near the oxygen atoms, the MESP is more negative. Plate 6(b) shows the corresponding minimal surface for the phenolate ion. Here also, the MESP near the oxygen atom is qualitatively more negative.

We have seen above, how the MESP-based considerations provide a rigorous treatment of anionic sizes and shapes. In a similar spirit, Politzer *et al.* [33] have suggested a search of the point r where $V(r) = -\mu$ for an atom. Using the Mulliken electronegativity definition, $\chi = (I + A) / 2$, and the earlier discussed definition (cf. Section 3.2) $\chi = -\mu$, the covalent radius r is defined such that $V(r) = (I + A) / 2$, where I and A are the ionization potential and electron affinity of the atom. More recently [33(b)], the covalent radii have been defined in terms of the distances of the respective nuclei from the $(3, -1)$ saddles of the MESP distributions.

Thus, the MESP is found to be a convenient quantity for defining anionic and covalent radii. Due to the lack of distinctive topographical features in the case of cations, it has so far not been possible to define cationic radii in terms of the MESP. This is still an open problem.

3.6 Topography of Molecular Electrostatic Potentials

Several such investigations on MESP have been reported by Gadre *et al.* [23, 24, 35, 36]. These studies parallel the pioneering works of Bader and co-workers on the MED topography. There are some similarities between the topographical features of the MESP and MED of a given molecule, and there are several differences as well. For example, the MED shows a maximum at nuclear sites, where the MESP also displays a (pseudo) maximum. As seen in Section 3.4, the MESP *cannot* exhibit a non-nuclear maximum. However, there are a few cases where the MED shows such a feature [37]. These examples include molecules such as Li_2 , C_2 , Si_2 etc. in their ground states. A contour diagram bringing out such a feature for Li_2 has been presented in Appendix F.

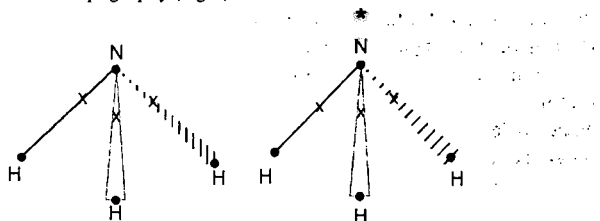
An important similarity in the topography of the MESP and the MED is the existence of a $(3, -1)$ saddle point (at which both the scalar fields possess positive values). However, the electron density is a positive semi-definite function, whereas the MESP can attain negative values also. Due to this significant difference, the MESP of many neutral molecules



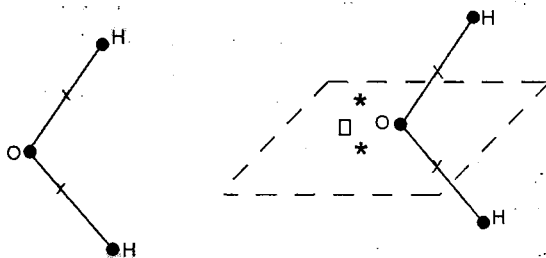
(a) H_2 : The MED (left) shows two nuclear maxima and a $(3, -1)$ bond saddle. The MESP (right) displays two additional (degenerate) minima on the perpendicular bisector of the H-H axis.



(b) N_2 : The MED (left) exhibits only two nuclear maxima and a $(3, -1)$ bond saddle. An additional feature of two (nondegenerate) minima on the bond axis is seen in the MESP topography (right).



(c) NH_3 : This molecule exhibits four nuclear maxima and three $(3, -1)$ bond saddles for both the MESP and the MED. A 'lone pair' minimum is shown only by the MESP (right) on the C_3 axis.



(d) H_2O : Both the MED and the MESP have a common feature of three nuclear maxima and two $(3, -1)$ bond saddles. The MESP (right) exclusively shows two 'lone pair' minima and a connecting $(3, +1)$ saddle.

Fig. 3.5 A schematic representation of comparative MED (left) and MESP (right) topographies of some small molecules (distances not shown to scale). *, x, □ and * denote, respectively, a maximum, $(3, -1)$ saddle, $(3, +1)$ saddle, and a minimum (degenerate or nondegenerate).

exhibits negative-valued minima as well as $(3, +1)$ saddles. These features are conspicuous by their absence in the respective MED distributions. Figure 3.5 displays schematically the essential topographical features of the MED and the MESP distributions of some small molecules, viz. H_2 , N_2 , NH_3 and H_2O . These features are obtained from the corresponding Hartree–Fock calculations at the 6–31G** level. It has been verified that this level is normally adequate for a qualitative and semi-quantitative description of the topography. The molecular geometries and positions of the CPs are not accurately shown on a quantitative scale.

It may be noticed from Figs. 3.5(a) and (b) that the electron localizations as indicated by the MESP minima are perpendicular and along the internuclear axis for the hydrogen and nitrogen molecules. The MED fails to bring out these features. Similarly, the 'lone pair' along the C_3 axis in the ammonia molecule appears in the form of a negative-valued MESP minimum. Also the chemist's description of 'rabbit ears' of the water molecule is clearly borne out by the corresponding MESP topography. The π bond in ethylene is similarly brought out in terms of MESP minima. However, the electron density itself shows no maximum in this region. In fact, the electron density very rarely displays non-nuclear maxima [34]. Recourse has to be taken to the Laplacian of the electron density, viz. $\nabla^2\rho(\mathbf{r})$ [25] or to the so-called electron localization function [35(b)] for unearthing such features of electron localizations. It may sound surprising that the MESP

can probe the patterns of electron localizations in the MED much better [36, 37] than the MED itself does! Cyclopropane is an unusual system supposedly endowed with a π character. The topography of the MED fails to bring out this feature except for the $(3, -1)$ C–C bond CP being about 0.1 \AA outside the ring: a feature predicted by the Coulson–Moffitt ‘banana bond’ model [25(d)]. However, the MESP topography brings out these features rather vividly, as depicted in Fig. 3.6. These include three MESP minima each along the C_2 axis, about 2.1 \AA away from the C–C bond midpoint! These are, in turn, connected by three negative-valued $(3, +1)$ saddles lying in the ring plane along the H–C–H angle bisector (cf. Fig. 3.6). A ring CP, with a positive value, is seen for both the distributions.

The MESP-topographical picture of the benzene molecule (cf. Fig. 3.7) appears like a hamburger! Firstly, there are several positive-valued CPs in the ring plane. Secondly, six minima appear on each side of the ring, approximately 1.725 \AA away from the ring plane. These are joined by six $(3, +1)$ saddles, lying in a plane about 0.01 \AA away. These CPs are topped by a negative-valued $(3, -1)$ saddle which is placed very close to the plane of the $(3, +1)$ saddles. Thus, the MESP distribution of the benzene molecule is rather flat, the most negative part being located around 1.73 \AA from the molecular plane. It may be conjectured that this plays a significant role in the stacking of benzene molecules.

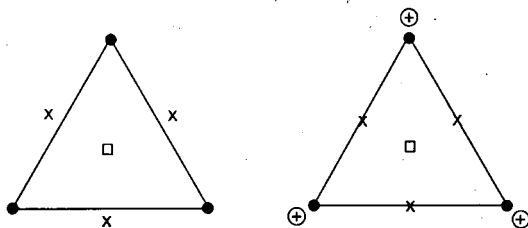


Fig. 3.6 Schematic representation of the topography of the MED (left) and the MESP (right) of the cyclopropane molecule (hydrogen atoms not shown) in the plane of the ring. • and × denote nuclear maximum and $(3, -1)$ bond saddles respectively. □ stands for the $(3, +1)$ ring saddle, ⊕ represents a negative-valued $(3, +1)$ MESP saddle point and * denotes a negative-valued MESP minimum (distances not to scale).

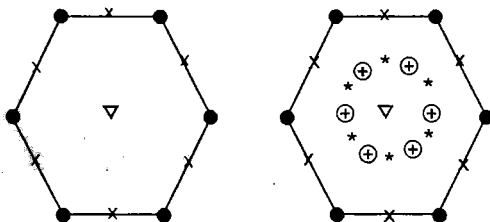


Fig. 3.7 A top view of the schematic MED (left) and MESP (right) topography of the benzene molecule (distances not according to scale and hydrogen atoms not shown). Nuclear maxima and $(3, -1)$ bond saddles are marked as \bullet and \times respectively. The $(3, +1)$ MED ring saddle is shown as ∇ . Six negative-valued MESP minima ($*$) and $(3, +1)$ saddles (\oplus) are approximately 1.725 and 1.734 Å respectively from the ring plane. The MESP topography is capped by a negative valued saddle (∇) close to the plane of six $(3, +1)$ saddles (\oplus).

There is a further interesting feature shown exclusively by the MESP and not by the MED as depicted in Fig. 3.8. Schematically shown here are the degenerate $(2, +2)$ ring CPs in the MESP topography of HF and HCl (essentially due to $C_{\infty v}$ symmetry). As expected, the diameter of the ring for HCl is larger than that for HF. Further, the value of (degenerate) minimum for HF is deeper (-0.054 a.u.) as compared to the one for HCl (-0.045 a.u.). Not all linear molecules HX are endowed with this unusual characteristic. The topography of HCN just shows a minimum localized on the bond axis (cf. Fig. 3.8). This may have repercussions on the way the acidic protons of an approaching species form a complex with the electron-rich F, Cl and N ends of the above molecules. The approach to HF and HCl is expected to be lateral whereas HCN may be attacked in a rather head-on fashion! The MESP of acetylene also exhibits this degenerate ring of CPs. The MESP values corresponding to the degenerate rings in HF, HCl and C_2H_2 are respectively -0.054 , -0.022 and -0.030 a.u. The MESP minimum for HCN is much deeper, viz. -0.078 a.u. The respective radii of the rings are 1.01, 1.78 and 1.48 Å. No known molecule is as yet known to possess the degenerate ring of MED CPs.

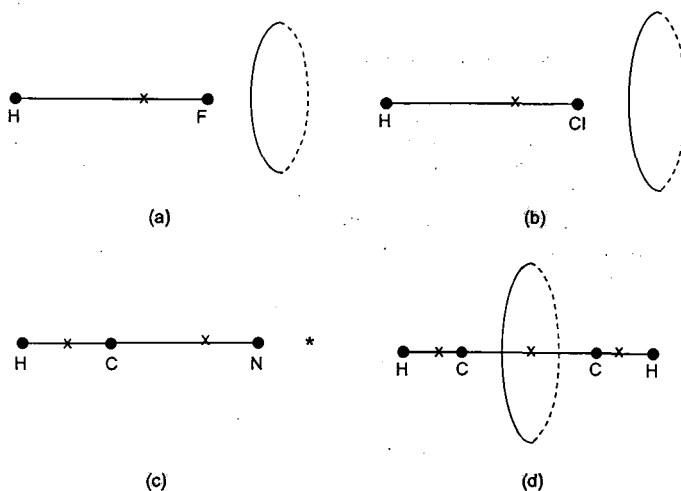


Fig. 3.8 A schematic representation of MESP topography of (a) HF (b) HCl (c) HCN and (d) C_2H_2 molecules. *, • and × denote, respectively, minima, nuclear maxima and (3, -1) bond saddles. Also marked are degenerate ring CPs.

MESP topographical studies vividly bring out negative-valued CPs for molecules as exemplified by ethane, butane, ethylene, sulfur dioxide and carbon dioxide in Plate 7. In fact, four minima for methane, each located on a C_3 axis, have already been presented in Plate 5(d).

Colour-coded isosurfaces of MESP value -0.015 (blue) are shown for the ethylene molecule in Plate 7(a). Two MESP minima corresponding to the π bond in ethylene are shown by white dots. Similar to the case of the methane molecule discussed earlier, other saturated hydrocarbons are also endowed with negative MESP regions with the corresponding critical points. In Plate 7(b) and (c) are shown two isosurfaces each (red: 0.5 a.u. and blue: -0.003 a.u.) for ethane and *n*-butane. Several CPs surrounding the molecule are displayed as white dots. The most negative regions are potent sites for binding of a metal ion, or attack by an electrophile or the hydrogen end of an approaching HX moiety, etc.

The blue coloured isosurfaces for SO_2 and CO_2 (with MESP values of -0.02 and -0.015 a.u.) are displayed in Plates 7(d) and (e) respectively. The corresponding CPs are also shown in these figures. All the negative

valued CPs for SO₂ lie in the plane of the molecule with no negative region surrounding the sulfur atom. Similarly the negative MESP regions in CO₂ are concentrated on the internuclear axis, quite away from the oxygen atoms. In C₆₀, the MESP displays minima exclusively over the bonds 'exo-' to the five-membered rings (cf. Plate 8(a)). Plate 8(a) presents a space-fill model of the C₆₀ fullerene molecule with van der Waals radii. The MESP contours of value -0.001 a.u. are shown with blue colour. The corresponding MESP minima can be seen with blue dots which show that only exo bonds to the five-membered ring exhibit double bond character. As remarked earlier, these patterns are of great utility for predicting sites of interaction of such molecules with the approaching electrophilic species.

Very accurate experimental methods are now [38] available for probing such interactions. However, no semi-quantitative guidelines for the sites and energetics of weak interactions are, as yet, available. This aspect will be discussed in Chapter 4, along with detailed applications of the MESP to a variety of chemical problems.

References

1. L H Thomas, *Proc. Camb. Phil. Soc.* **23**, 542 (1926).
2. E Fermi, *Z. Phys.* **48**, 73 (1928).
3. P Gombàs, *Die Statistische Theorie des Atoms und Ihre Anwendungen*, Springer (1949).
4. For a lucid description of the Thomas-Fermi and related theories, see N H March, *Self-Consistent Fields in Atoms*, Pergamon (1975); L Landau and E Lifshitz, *Quantum Mechanics*, Pergamon, New York (1976), p. 259.
5. P Hohenberg and W Kohn, *Phys. Rev.* **136**, B864 (1964).
6. R G Parr and W Yang, *Density Functional Theory of Atoms and Molecules*, Oxford, New York (1989).
7. J W Sheldon, *Phys. Rev.* **99**, 1291 (1955).
8. E Teller, *Rev. Mod. Phys.* **34**, 627 (1962).
9. N L Balázs, *Phys. Rev.* **156**, 42 (1967).
10. For a review, see S R Gadre and R K Pathak, in *Adv. Quantum Chem.* **22**, 211, Ed. P-O Löwdin, Academic, New York (1991).
11. P Politzer and R G Parr, *J. Chem. Phys.* **61**, 4258 (1974). See P Politzer in *Chemical Applications of Atomic and Molecular Electrostatic Potentials*, Ed. P Politzer and D G Truhlar, Plenum, New York (1980) p. 7.
12. (a) P Politzer, *J. Chem. Phys.* **72**, 3027 (1980). (b) P Politzer and R G Parr, *J. Chem. Phys.* **64**, 4634 (1976).
13. P Politzer, *J. Chem. Phys.* **64**, 4239 (1976).
14. P Politzer, *J. Chem. Phys.* **70**, 1067 (1979).

15. M Levy, S C Clement and Y Tal in *Chemical Applications of Atomic and Molecular Electrostatic Potentials*, Ed. P Politzer and D G Truhlar, Plenum, New York (1980) p. 29 and references therein.
16. (a) R G Parr, R A Donnelly, M Levy and W E Palke, *J. Chem. Phys.* **68**, 3801 (1978). (b) R A Donnelly and R G Parr, *J. Chem. Phys.* **69**, 4431 (1978).
17. R G Parr, S R Gadre and L J Bartolotti, *Proc. Natl. Acad. Sci. (U.S.A.)* **76**, 2522 (1979).
18. Y Tal, R F W Bader and J Erkkku, *Phys. Rev.* **A21**, 1 (1979).
19. R G Parr and A Berk, in *Chemical Applications of Atomic and Molecular Electrostatic Potentials*, Ed. P Politzer and D G Truhlar, Plenum, New York (1981) p. 51–62.
20. P Politzer and B Zilles, *Croatica Chim. Acta* **57**, 1055 (1984).
21. S R Gadre and R D Bendale, *Chem. Phys. Letters* **130**, 515 (1986).
22. H Weinstein, P Politzer and S Srebrenik, *Theoret. Chim. Acta (Berl.)* **38**, 159 (1975) have given the first proof of monotonicity of atomic MESP.
23. S R Gadre and R K Pathak, *Proc. Ind. Acad. Sci. (Chem. Sci.)* **102**, 18 (1990).
24. (a) R K Pathak and S R Gadre, *J. Chem. Phys.* **93**, 1770 (1990). (b) For a further discussion, cf. H Silberbach, *J. Chem. Phys.* **94**, 8638 (1991), (c) S R Gadre, S A Kulkarni and R K Pathak, *J. Chem. Phys.* **94**, 8639 (1991).
25. See, for a comprehensive treatment, (a) R F W Bader, *Acc. Chem. Res.* **8**, 34 (1975). (b) R F W Bader, *Atoms in Molecules: A Quantum Theory*, Clarendon, Oxford (1990). (c) R F W Bader, *Chem. Rev.* **91**, 893 (1991). (d) C A Coulson and W E Moffitt, *Philos. Mag.* **40**, 1 (1949).
26. K D Sen and P Politzer, *J. Chem. Phys.* **90**, 4370 (1989).
27. K D Sen and P Politzer, *J. Chem. Phys.* **91**, 5123 (1989).
28. J Huheey, *Inorganic Chemistry*, Third edition, Harper, Cambridge (1983) p. 77–78.
29. A F Wells, *Structural Inorganic Chemistry*, Fourth Edition, Clarendon, Oxford (1975); see p. 521 and 751 for intuitive pictures of the cyanide and hydroxide anions in NaCN and Ca(OH)₂ crystals.
30. For an earlier discussion on sizes of anions, based on two-dimensional contour maps, refer to S R Gadre and I H Shrivastava, *J. Chem. Phys.* **94**, 4384 (1991).
31. For three-dimensional visualization of polyatomic anions, see S R Gadre, C Kölmel, M Ehrig and R Ahlrichs, *Z. Naturforsch.* **A48**, 137 (1993).
32. S R Gadre, C Kölmel and I H Shrivastava, *Inorg. Chem.* **31**, 2281 (1992).
33. (a) P Politzer, R G Parr and D R Murphy, *J. Chem. Phys.* **79**, 3859 (1983). (b) M K Harbola, R G Parr and C Lee, *J. Chem. Phys.* **94**, 6055 (1991).
34. A D Becke and K E Edgecombe, *J. Phys. Chem.* **92**, 5397 (1990).
35. S R Gadre, S A Kulkarni and I H Shrivastava, *J. Chem. Phys.* **96**, 5253 (1992).

62 *Electrostatics of Atoms and Molecules*

36. S A Kulkarni and S R Gadre, *J. Mol. Struct. (THEOCHEM)* **361**, 83 (1996).
37. (a) W L Cao, C Gatti, P J McDougall and R F W Bader, *Chem. Phys. Letters* **141**, 386 (1987). (b) J. Cioslowski, *J. Phys. Chem.* **94**, 5496 (1990). (c) K B Wiberg, R F W Bader and C D H Lau, *J. Amer. Chem. Soc.* **109**, 985 (1987).
38. For a review of experimental and theoretical studies on weakly bound complexes, see, (a) A C Legon and D J Millen, *Chem. Soc. Rev.* **16**, 467 (1987). (b) P Hobza and R Zahradnik, *Chem. Rev.* **88**, 871 (1988).

4

Applications of Molecular Electrostatic Potential

4.1 *Introduction*

The earlier Chapters of this monograph have introduced the MESP as an important tool for the investigation of molecular structure and reactivity. Earlier [1, 2] pioneering applications have focused on locating the sites of electrophilic attack, viz. the negative-valued regions or minima that appear in the MESP maps. In this connection, we have seen several examples highlighting the regions of large electron localizations in Chapters 2 and 3 of the present monograph. However, work due to Sjoberg and Politzer [3] has shown that MESP can be employed for the prediction of the site of a nucleophilic attack as well. This makes MESP a versatile tool for probing molecular reactivity engendering numerous applications to chemistry. A variety of applications are found in organic chemistry, pharmacology, biology, chemistry of explosives, drug designing, etc. wherein MESP has been used as a parameter to study the structure–activity relationship (SAR). This Chapter presents some of the typical applications of MESP involving these aspects. It may be pointed out that the MESP applications are found in extremely diverse areas such as biology, molecular biophysics, all branches of chemistry, etc. We shall present a few typical test cases with a note that the coverage here, like the proverbial tip of the iceberg, is just indicative, and not a very deep and detailed one. Some typical applications reported in the literature during 1996–1998 are included here to bring out the flavour of the applied aspects of molecular electrostatics.

4.2 *MESP as a Reactivity Parameter in Chemistry*

As seen earlier, MESP is the potential generated by the molecular charge distribution as experienced by a positive point charge. The deepest minimum in the MESP distribution can generally be taken as the most favourable position for an approaching positive charge. The minima in the MESP indicate

localization of electron density and can be treated as potent sites of electrophilic attack (by a positively charged or electron deficient species) in organic chemistry. Pullman [1(b)] has presented a lucid account of earlier work on the sites of protonation in terms of the most negative MESP regions in guanine and related molecules. These form a part of the early success story of MESP applications to chemistry. For example, in guanine, which is a base in naturally occurring DNA, the MESP map shows that there are two probable sites of electrophilic attack associated with N_3 and N_7 . The local minimum near N_7 (marked as G_5 in Fig. 4.1) is found to be deeper than that around N_3 (G_8 in Fig. 4.1) indicating that N_7 is preferentially protonated or alkylated. The experimental results [4] confirm this observation. The negative-valued MESP isosurfaces for guanine and cytosine molecules have already been displayed in Plate 5(a). Figure 4.1 shows schematic diagrams [1(c)] of these molecules with all the negative-valued CPs (in plane of the molecule) around these two molecules. The minima and saddles are shown by * and + respectively (the CPs are labelled as G_1, G_2, \dots, G_8 for guanine and C_1, C_2, \dots, C_7 for cytosine molecule). The CPs G_6, G_7 and C_6, C_7 respectively denote (numerically small) negative-valued MESP CPs above and below the NH_2 plane. Such a depiction of isosurfaces and CPs brings out the sites of electrophilic attack as well as the lock-and-key features of these two DNA bases and helps explain the base-pair formation (see Section 4.3 for a description of G...C complex).

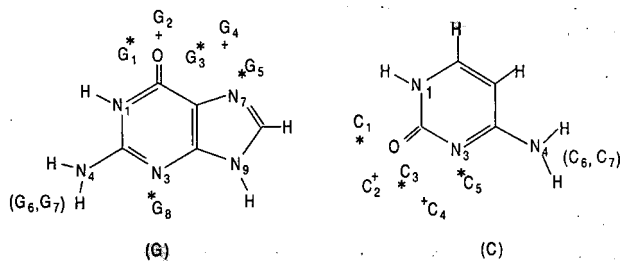


Fig. 4.1 Schematic diagrams of guanine (G) and cytosine (C) molecules. The MESP minima and saddles are shown by * and + respectively.

Since the non-nuclear maxima do not occur in $V(\mathbf{r})$ distribution (as seen in Section 3.4), the positive regions in the MESP maps are not found useful for exploring the regions favourable for the nucleophilic attack. For this purpose, it is convenient to employ [3] MESP textured on some

surfaces viz. van der Waals or isodensity surfaces (normally a surface with $\rho(r) = 0.001$ or 0.002 a.u. is used). This may be seen from the simple example of S_N2 replacement of group X by Y (Fig. 4.2) in aliphatic systems. It is well-known that this replacement occurs through the inversion of configuration.

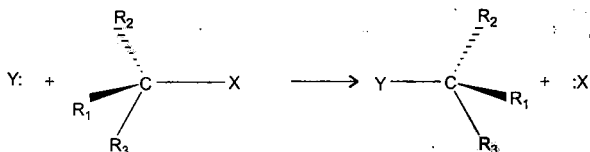


Fig. 4.2 Schematic diagram showing nucleophilic attack in a typical S_N2 reaction.

For a given nucleophile Y., this is known to be more facile for methyl chloride than for methanol. This experimental result may be explained with the help of the plots of MESP evaluated on the above-mentioned isodensity surfaces for these molecules. Politzer and co-workers (see Ref. [3] and later related works) have presented several illustrations of nucleophilic attack. We illustrate here such textured surfaces for CH_3OH and CH_3Cl (cf. Plates 8(b) and (c)) respectively visualized using the indigenously developed UNIVIS package (cf. Ref. [45(e)] in Chapter 2). These plots show that the potential is more positive on the methyl side in CH_3Cl than in CH_3OH , bringing out the above-mentioned feature of ease of nucleophilic attack on CH_3Cl .

MESP is also found to be a useful tool in the interpretation and design of regioselectivity [5, 6]. This is clearly brought out by the example of π -facial distereoselection for electrophilic addition to 7-methylene- and 7-isopropylidene-norbornene and the corresponding norbornenes. The electrophilic π -facial selection either syn or anti to the substituent (cf. Fig. 4.3) is controlled by the nature and type of substituent. Mehta *et al.* [6] have studied this π -facial distereoselection for electrophilic addition to the above systems. In 7-isopropylidene-norbornenes [6], a remarkable feature of MESP is seen to occur. The two $\text{C}=\text{C}$ moieties in Fig. 4.3 are not in direct conjugation, but show a through-space conjugation because of the geometry of the molecule (cf. Plate 9). This effect may be taken as a realization of what is termed in organic chemistry literature as homoconjugation. This (through-space) homoconjugation can be visualized from Plates 9(a) and (b). Plate 9(a) presents the three-dimensional contour map of MESP along with a ball-and-stick model for 7-isopropylidene-norbornene and Plate 9(b) displays

a cyano derivative of 7-isopropylidene-norbornene, wherein the MESP minima are shown by blue dots. The negative-valued region common to both the double bonds on the anti side to the cyano groups gives a visual picture of homoconjugation. Thus it may be predicted that the anti attack would be favoured in the case presented in Plate 9(a) due to electrostatic swamping. In the cyano-substituted case, the orbital-based Cieplack model [7] would take over and prefer an approach from the syn side.

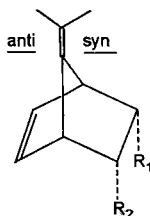


Fig. 4.3 Schematic representation of 7-isopropylidene-norbornene showing syn and anti sides with respect to the substituents.

The cation- π binding interaction is found to be an important guiding force for molecular recognition in biological receptors. This aspect can be treated as an electrophilic interaction of the cation with the aromatic rings. Here too MESP comes in as a handy tool for exploring cation- π interaction without resorting to a full *ab initio* quantum mechanical calculation. This has been shown by Mecozzi *et al.* [8(a)] with the study of MESP calculated on isodensity surface ($\rho(r) = 0.002$) at 6-31G** level for a series of aromatic systems forming cation- π complexes with a non-polarizable cation such as Na⁺. Mecozzi *et al.* found, for a series of 11 derivatives of benzene, an excellent correlation between the SCF binding energies and MESP at the optimized binding position of the Na⁺ in the complex. In a similar spirit, Cubero, Luque and Orozco [8(c), (d)], on exploring the role of polarization correction to the MESP, found that polarization is a large contributor to cation- π interactions. They defined a generalized molecular interaction potential, incorporating polarization (GMIP_p) which has been found to be a very fast and effective tool for the prediction of binding of cation to aromatic compounds. More recently, Gadre and Pingale [8(e)] have successfully employed the polarization-corrected MESP for predicting cation binding sites of saturated hydrocarbons.

4.3 Electrostatics-Based Models for Intermolecular Interactions

The van der Waals (vdW) complexes, in general, and weakly bonded species such as π -bonded or hydrogen-bonded complexes, in particular, have been a subject of detailed recent theoretical and experimental investigations [9–16]. These complexes are encountered in many branches of chemical, biological and atmospheric sciences. A variety of theoretical models, in which electrostatics plays a dominant role, have been developed for understanding these weak intermolecular interactions. Four of such models, viz. those due to Legon and Millen [9], Buckingham and Fowler [17, 18], Dykstra [20] and Alhambra *et al.* [21], will be briefly discussed here.

Legon and Millen [9] rules allow a prediction of geometries of B...HX complexes in the gas phase. Here, B is a molecule possessing non-bonding or π -bonding electron pairs, and X may be an electronegative atom or group such as F, Cl, CN, etc. The rules are as follows.

- (i) The molecular axis of HX coincides with the axis of the non-bonding electron pair of molecule B.
- (ii) For the cases where B contains only π -electron pairs, the H-X axis intersects the π -bond axis and is perpendicular to the plane of symmetry of the π -bond.

Rule (i) overrides (ii) when B possesses both non-bonding and π -bonding pairs. These rules have been found to be quite successful for a qualitative prediction of geometries of weak molecular complexes. However, it is not clear how the positions of these electron pairs can be located. Further, these rules are not directly applicable to complexes wherein there are no 'obvious' non-bonding or π -bonding electron pairs, e.g. CH₄, C₂H₆, B₂H₆ etc.

Buckingham and Fowler (B-F) [17, 18] have developed an electrostatic interaction model for the structure predictions of vdW complexes. In this celebrated model, each molecule is treated as a set of atomic hard spheres wherein atoms are assigned the corresponding vdW radii. The electrostatic interaction energy is obtained using distributed multipole moments (DMM) in which the multipoles are placed at the atom centres of the embedded molecule (cf. Chapters 1 and 2). The multipoles used here are determined by DMM analysis [19] of the respective SCF charge densities. The orientational electrostatic interaction energy is minimized by rolling one molecule on the other. The structures of complexes thus obtained are generally found [18] to be in very good agreement with the respective experimental ones. However, the B-F model fails to correctly predict the

structures of the complexes such as $\text{H}_2\text{O}\dots\text{CO}_2$, $\text{H}_2\text{O}\dots\text{N}_2\text{O}$ and $\text{NH}_3\dots\text{CO}_2$. Also, it is not very successful for those cases in which the shapes are not well-described by hard spheres ($\text{CO}_2\dots\text{H}_2\text{O}$ and $\text{ClF}\dots\text{HF}$) and when there is a delicate balance between electrostatic and other interactions (e.g. $\text{H}_2\text{O}\dots\text{HF}$, $\text{H}_2\text{O}\dots\text{HCCH}$, $\text{CO}_2\dots\text{HF}$, etc.). Further, the B-F model has not been tried out for HX complexes with CH_4 , C_2H_6 , C_3H_6 , etc., since it is felt that, due to the weak electrostatic effects involved, it would fail for these systems [22].

Alhambra *et al.* [21] have recently proposed a new method for representing interactions between solutes and water. Here, the water molecule is represented as three point charges viz. -0.834 , 0.417 and 0.417 a.u. In this model, the orientation of water molecule is optimized at various values of geometrical parameters defining the relative orientation of the two species so as to give minimum interaction energy. The geometries thus obtained agree quite well with their full HF-SCF counterparts. Alhambra *et al.* [21] employed this model for studying the solvation of several molecules. They reported isopotential maps for water...water interactions and also studied benzene...water and DNA bases...water interaction energies. This approach still remains to be further tested for other weak interactions. However, it seems promising, due to the enormous saving in the computational efforts involved.

Dykstra [20, 23, 24] has devised the 'molecular mechanics for clusters' (MMC) model wherein 6-12 potentials are used for the non-electrical part. The charge fields are represented by central multipoles for small molecules and distributed ones for larger molecules. The MMC model [24] thus has considerable electrostatic inputs and is reasonably successful in predicting structural features and potential well-depths of the weak complexes.

A shortcoming of all the above models is that they offer *no prior insights* on the location and strengths of active sites in molecules. Keeping this in mind, Gadre *et al.* [25(a)-(c)] have proposed an alternate and complementary approach for qualitatively predicting the structural aspects of such complexes. In this model, christened by them as the electrostatic potential for intermolecular complexation (EPIC), a connection between the MESP topography and energetics of weak molecular interactions has been made. Based on the MESP topography of the interacting molecules the potent site around which the interacting species would like to anchor is determined. The systems of bi-molecular complexes studied by Gadre *et al.* [25(a)-(c)] are of the type B...HX. Here, molecule B is called as *lock* and molecules studied as B are CH_4 , C_2H_4 , C_2H_2 , C_3H_6 , HCHO , C_6H_6 , and B_2H_6 . The molecule HX is named as *key* where X = F, Cl or CN. Further, molecules

like H_2O and NH_3 are also taken as keys. Schematic pictures of EPIC-optimized geometries of some of these complexes are given in Plate 9. Plates 9(c), (d) and (e) respectively depict ball-and-stick representations of $\text{NH}_3\text{B}_2\text{H}_6\cdots\text{HF}$, $\text{C}_3\text{H}_6\cdots\text{H}_2\text{O}$ and $\text{C}_6\text{H}_6\cdots\text{NH}_3$ complexes. It is seen from Plate 9(c) that HF can bind to the B_2H_6 molecule through its F end, corresponding to a local minimum energy within the EPIC framework. The structure of the $\text{C}_3\text{H}_6\cdots\text{H}_2\text{O}$ complex (Plate 9(d)) has the O–H bond almost along the perpendicular bisector of the ring C–C bond. The complex between benzene and ammonia is shown in Plate 9(e) with one of the N–H bonds tilted towards the negative MESP region over the benzene ring. The geometries and the interaction energies of these weakly bound complexes agree quite well with their experimental counterparts.

The merit of the EPIC model is that it does attempt at offering 'primitive patterns of understanding' by recognizing 'active' sites in electrostatic interactions. The strength of this topography-based approach lies in its simplicity and use of exclusively electrostatics-based information, viz. the MESP and MESP-driven charges of the interacting species.

A few more examples [25(a), (b)] illustrating the utility of the EPIC model are described below. In Plate 5(a) we have seen the MESP isosurfaces for the DNA bases guanine and cytosine. Also seen in Fig. 4.1 are the negative-valued CPs which provide likely sites of interaction. How guanine and cytosine lock into each other due to electrostatic complementarity is seen from Plate 10(a), which depicts the structure of the G...C complex obtained by EPIC model is subjected to a subsequent *ab initio* optimization. The negative-valued MESP contours of the G...C pair are also superposed on the corresponding ball-and-stick model.

The role of co-operative electrostatics for understanding the successive hydration patterns of a molecule can be investigated by employing the EPIC model. The 18-crown-6 (18C6) molecule in its D_{3d} conformation has been used as a test molecule [25(b), (c)] for these studies. Plate 11(a) shows two sets of 3D contours, viz. -0.105 (blue) and 0.5 (red) for 18C6. The first incoming water molecule is hence expected to position itself so that two hydrogens anchor around two minima (blue) of 18C6. In fact, the two hydrogens cannot bind to the two neighbouring islands seen in Plate 11(a), but to a minimum and the next-near neighbour. The structure in Plate 11(b) shows an enhanced oxygen lone pair of this water molecule to which the second incoming water molecule is bound. In this figure the isosurfaces corresponding to MESP value of -0.1 a.u. are shown, the largest one being around the water lone pair. The remaining lone pair minima of 18C6 are depicted with green dots. On further hydration, one obtains an interesting structure [25(b), (c)] of $18\text{C}6.4\text{H}_2\text{O}$ with four isosurfaces of MESP value

-0.09 a.u. (cf. Plate 11(c)). It is noteworthy that only the lone pairs of water molecules are seen, the MESP minima corresponding to the ether oxygens being conspicuous by their absence.

Electrostatics has also been employed for exploring the interaction of a molecule with a crystal surface. For example, Chacon-Taylor and McCarthy [25(d)] have recently employed classical electrostatic potential for describing adsorbate-surface interaction. The MESP of the (001) surface of MgO crystal was computed by using periodic Hartree-Fock method. The interaction energy of this crystal with a few prototype molecules, viz. H_2O , HCl and NH_3 was calculated. For this purpose, the electric potential, the field, and the field gradient of the MgO cluster were fitted as a function of position over the surface. The interaction of this with the electric multipoles of the adsorbate molecule was minimized by translations and rotations of the latter. A short-range repulsion term of the form r^{-12} was also included. Thus electrostatic modelling seems to be an efficient and reliable tool for studying adsorbate-surface interactions. Further testing and applications of such studies seem to be rewarding.

4.4 High-Energy Molecules

High-energy molecules is a respectable name generally used for explosives and other related species! Explosives are found extremely useful not only in wartime but also for peaceful applications. The study of structure-property relationship of these molecules helps in identification of factors that determine the sensitivity of such molecules towards the action of chemical agents, heat, shock and impact. A better understanding of these factors could lead to the design and synthesis of chemical systems yielding high performance and improved stability [26]. The MESP has been extensively employed, in addition to the other molecular properties such as bond orders, intramolecular hydrogen bonding, dipole moment etc., for studying the behaviour of high-energy materials at the molecular level [27].

The nitroaromatic compounds (class of explosives) detonate on shock or impact. There is evidence to show that the rupture of the C-NO₂ bond is a key step in the decomposition of the nitroamines [27]. In this respect Murray *et al.* [28] have studied a series of polynitroaromatics, at the *ab initio* HF-SCF level, employing the respective crystallographic geometries. In this work, they obtained a linear correlation between the impact sensitivity and the corresponding largest value of electrostatic potential (evaluated using Mulliken charges on C and N atoms) at the midpoint of C-NO₂ bonds (V_{mid}). Based on these investigations, they have suggested that the C-NO₂ bond endowed with the largest V_{mid} is the one

which makes polynitroaromatics shock-sensitive. This theoretical conjecture is generally in line with the corresponding experimental results of impact or shock-sensitivity. In retrospect, this work is a rather *ad hoc* treatment which seems to work rather surprisingly! Further, in a more rigorous study, Politzer and Murray [29] have used the MESP textured on the molecular surface for their investigations. They employed the average deviation of MESP (π) on the molecular surface as a parameter for this purpose, where

$$\pi = \sum_{i=1}^n \frac{|V(r_i) - \bar{V}_s|}{n} \quad (4.1)$$

(here \bar{V}_s is the mean MESP on the surface and i is the number of points). The surface maximum, $V_{s,\max}$ was also computed. An excellent correlation was found between the shock sensitivity (S) with π and $V_{s,\max}$, in terms of a relation $S = \alpha[\pi^2 \cdot V_{s,\max}]^{-1} + \beta\pi^2 + \gamma$ with parameters α , β and γ . A linear correlation coefficient of about 0.99 was obtained. They found that the dissociation energies are related to the MESP maxima on the molecular surface above the bond regions ($V_{s,\max}$). They have also concluded that these $V_{s,\max}$ (C-NO₂) values reflect inversely the strengths of the C-NO₂ bonds. The effect of various substituents on nitroaromatics has been studied, and the NH₂ group is noticed to have a stabilizing influence on nitroaromatics [30]. This can be seen in terms of the strength of the C-NO₂ bonds. The hydroxyl group, on the other hand, destabilizes the nitroaromatics [31]. The degree of activation or deactivation of aromatic rings towards the electrophilic attack, upon substitution of NH₂ or NO₂ groups has been monitored via MESP. This examination leads to the conclusion that the build-up of positive potential above the C-NO₂ bond in nitroaromatics serves as an initial site for the nucleophilic attack [27].

Köster *et al.* [32] have recently studied the MESP of the ammonium nitrate (NH₄⁺ NO₃⁻) system along the collision course. The collision between NH₄⁺ ion and NO₃⁻ ion is assumed to take place immediately after the impact of shock in the explosive. The MESP has been evaluated using DFT and *ab initio* molecular dynamics methodology employing Newton's equations. With the help of these dynamical MESP plots, a pictorial representation of the reaction is offered. It is seen from these pictures that the first step of the reaction is the polarization of nitrate ion by the ammonium ion, followed by the actual reaction leading to formation of ammonia resulting from the abstraction of a proton from the ammonium ion by the nitrate ion. The collision also produces ·OH and ·NO₂ radicals which come together to form HNO₃.

4.5 MESP Applications to Catalysis

4.5.1 Zeolites, oxides and related materials

Electrostatics is useful for describing the behaviour of a variety of catalysts including zeolites and enzymes, which are macromolecules. Zeolites are an important class of catalysts that influence gas phase reactions through interaction with the reacting partners. Zeolites are open-framework rigid structures composed of highly polar SiO_4 and AlO_4 tetrahedra bearing the net negative charge that is compensated by the metal cations. These tetrahedra are connected by sharing their corners to form one-, two- and three-dimensional channels throughout the crystal. The resulting system of channels thus formed allows zeolites to efficiently function as molecular sieves and provides large surface area for its selective activity in adsorption catalysis [33]. Zeolites have been demonstrated to act as ion exchangers, adsorbents and catalysts [34]. These properties of zeolites are mainly determined by the dimensions of their internal pore systems. Strong electrostatic fields are conjectured to exist in the zeolite cages which can polarize the adsorbate molecule or create very strong acid sites [35]. The MESP has been used as an important tool in the study of zeolite catalytic activity for the last few years [33, 36–39]. This scalar field brings out the locations of favourable and unfavourable interactions between adsorbed species and zeolite lattice. The minima in the MESP distribution are treated as favourable places for positively charged particles, such as Na^+ ion, to reside. Such points are normally found near the oxygen atoms and hence the oxygens may be assumed to be involved in the zeolite catalysis through weak Lewis basicity [40]. Since the quantum mechanical calculations are not feasible for these systems due to their large size, various approximations are used. A part of the zeolite structure is studied by terminating the framework by a hydrogen or a hydroxyl group [40]. In this connection, the fragmentation method discussed in Chapter 2 seems to be very promising for investigating such large systems since *ab initio* quality calculations are thereby possible for larger frameworks.

Theoretical studies on various zeolite frameworks have shown that the proton affinity of the bridging hydroxyl group is affected by MESP changes at the acid sites [33, 38, 39]. MESP computations of the acidity and the vibrational frequency sequence of skeletal OH groups in fujasite supports the conclusions derived from experiments [36]. These results indicate that a high MEF value inside the zeolite cavity, emerging mostly from long-range contributions [40], is an essential factor for their reactivity. The location and orientation of organic molecules inside a pore of zeolites can also be predicted by such a study. These predictions of the location and

orientation of molecules inside the zeolite cage by MESP calculation may be used as an alternative to the expensive quantum mechanical geometry optimizations in a theoretical study of the cleavage and formation of bonds in these cages. For instance, the exact orientation of pyrrole and acetaldehyde molecules inside the supercage of fujasite obtained by quantum mechanical docking method and that obtained by proper fitting of MESP of the host and guest, have shown a perfect match [40(b)]. The mechanism of the reaction can also be derived from the polarity shown by MESP maps.

Furthermore, catalytic properties of crystal surfaces of various oxides have also been studied with the help of MESP. For example, McCarthy and Hess [41(a)] were able to predict adsorption sites of Cl_2 on the MgO (001) surface by inspecting the corresponding MESP features and concluded that the interaction is dominated by electrostatics. Polyoxometallates have been of immense interest to chemists for several decades [41(b)–(d)]. Some of the often-encountered structures are the Lindquist $\{(\text{M}_6\text{O}_{19})^{n-}\}$ and the α -Keggin ion $\{(\text{XM}_{12}\text{O}_{40})^{m-}\}$ where X is P, As, Si, Cu, Fe or Co, and M is a transition metal such as V, Mo, etc. The approach of the cations to the outer oxygen atoms of such ions can be readily predicted by employing the corresponding MESP maps. The MESP features could be used for studying the positioning and energetics of neutral guest molecules such as acetonitrile, benzonitrile or water within the hosts [41(c)]. The concept of 'electronically inverse hosts' [41(d)] (an alternate name for lock-and-key!) has emerged from these studies.

4.5.2 Enzyme catalysis

Enzyme catalysis is found to work through three main factors, viz. entropy, general acid-base catalysis and electrostatics [42]. In this monograph, emphasis is given only on the electrostatic contributions to the enzymatic acceleration of reactions. It has long been known that proteins provide strong electrostatic potential in their interior as well as around them [43]. Hence the catalytic activity of enzymes (a class of proteins) can be described in terms of their MESP distributions. The computation of MESP for enzymes, however, needs to take into account the varying dielectric constants due to bulk water. Computational methods have been developed to take into account the role of water as a solvent and reproduce protein MESP to a sufficient accuracy comparable to the experiments. This offers new insights into protein electrostatics and its role in the catalytic activity [43]. For a charged substrate, the long-range electrostatic effects may be important. For instance, in the encounter of triose phosphate isomerase with glyceraldehyde phosphate, the protein MESP orients the substrate in the best position for binding even

at a relatively large distance, increasing the diffusion-controlled rate constants [44(a)]. Furthermore, MESP distributions have been employed for searching for similarity among a series of compounds [44(b)].

In a recent biological application, two physiologically equivalent proteins, viz. cytochrome c6 and plastocyanin were compared on the basis of their MESPs [44(c)]. The importance of electrostatic interactions in RNA aminoglycosides binding has been highlighted in a recent work due to Wang and Tor [44(d)]. Conroy *et al.* [44(e)] have demonstrated the utility of electrostatic considerations for designing a new class of inhibitors for cysteine proteases. Warshel and Levitt [45] have reported computational results on lysozyme, which lead to the conclusion that in enzymatic mechanisms where the polarity of the transition state is higher than that of ground state, the major source of catalytic rate acceleration is the electrostatic stabilization of the transition state by protein dipoles. This conclusion is further supported by work due to Naray-Szabo in which similar studies for serine protease and xylose isomerase have been reported [46].

Reliable information on enzymatic transition state structures in enzyme-catalyzed reactions is now becoming available experimentally. Molecular similarity measures, based on MESP-textured vdW surfaces were applied by Bagdassarian *et al.* [47(a)] for studying the similarity of substrates and inhibitors with the enzyme-stabilized transition states. It was found, for enzymes like AMP deaminase, adenosine deaminase and AMP nucleosidase, that transition state inhibitors are qualitatively more similar to the transition states than are the substrates. Plate 10(b) reproduced from Ref. 47(a) clearly highlights this fact for the AMP deaminase reaction. It was hence concluded by the authors [47(a)] that this method may be useful in the logical design of transition state inhibitors.

Electrostatic complementarity considerations have been applied by Merz and Banci [47(b)] for considering the patterns observed in small anion binding to human carbonic anhydrase-II (HCAII). From their study the authors concluded that HCAII controls the preferred resonance structure of the ion by electrostatic complementarity. The MESP and MEF maps of an enzyme provide useful information about favourable sites of electrostatic and hydrophobic interactions. The positive and negative regions of MESP indicate favourable interactions with negative and positive substrate sites respectively, whereas low and high values of MEF determine hydrophobic and hydrophilic regions inclined to associate with substrate sites of same nature [48]. Such electrostatic complementarity between the binding of Lys-15 side chain of bovine pancreatic trypsin inhibitor (BPTI) to the specificity pocket of trypsin has been pictorially illustrated using MESP textured on vdW surface by Naray-Szabo *et al.* [49].

The diffusion of the oxaloacetate ion between the active sites of two enzymes viz. malate dehydrogenase (MDH) and citrate synthase (CS) of the citric acid cycle was considered by Elcock and McCammon [50(a)]. It was found that a continuous region of positive electrostatic potential exists in the area where the MDH and CS meet. A graphical visualization of this is brought out in Plate 12(a), showing a large blue region (positive potential) between the species. Thus, the diffusion of a substrate with a charge of -2 quite naturally turns out to be highly efficient in this region. This is a classic example of electrostatic channelling in a biological context. The importance of electrostatic interactions along a protein-folding pathway has been pointed out by Oliveberg and Fresht [50(b)]. They considered the passage of barnase from the denatured state to the native state through the folding intermediate (followed by a major transition state). It was found that dominant electrostatic interactions are present in the major transition state. These interactions resemble those in the native state, highlighting their significance for protein folding.

In addition to the applications to enzyme catalysis discussed above, MESP has also been utilised as a supportive tool for the quantitative understanding of electron transfer processes in enzymatic reactions and enzyme modelling studies. For this purpose, the package GRASP has been extensively used for the computation and visualization of MESP on the molecular surfaces in the current literature [51].

4.6 *Structure-Property and Structure-Activity Relationships*

Structure-property as well as structure-activity relationships (SAR) are based on the assumption that molecules with similar structures possess similar properties/activity. Quantitative SAR (QSAR) [52] is a highly active research field that has been applied to the problems of toxicity, hydrophobicity, partition coefficients, carcinogenesis, etc. The MESP is employed as a basic quantity in many such treatments.

The activity in these areas essentially started in 1935 with the pioneering contributions of Hammett [53]. The Hammett constant, σ , has now become an inseparable part of organic chemistry literature. For example, positive values of σ represent electron withdrawal by the substituent from an aromatic ring. Negative values of σ denote electron donation by the substituent. Despite its usefulness, the Hammett treatment suffers from certain drawbacks. One of them is the additivity assumption for the parameter σ in the case of multiply-substituted aromatics. In this connection, it is of interest to note that MESP has been gainfully employed for probing

the subtle electronic perturbations of the benzene ring caused by substituents attached to it [54]. Good correlation of MESP minima (V_{\min}) over the aromatic ring was found with the corresponding σ values on a study of 45 doubly substituted benzenes. A simple additive model to obtain V_{\min} for triply substituted benzenes exclusively from the corresponding singly and doubly substituted V_{\min} values was also successfully tested out by Suresh and Gadre [54].

The so-called Kohonen network has been applied [56] to the SAR. In this technique, a condensed two-dimensional representation of a three-dimensional MESP-textured molecular surface is obtained. An example from Ref. 56 is reproduced in Plate 12(b) for illustrating the Kohonen map (KM) of corticosterone. This map brings out the relation between the 3D MESP-textured vdW surface with the corresponding KM. In Plate 12(b), the sites 1, 3 and 4 denote negative potential regions whereas the region marked 2 is a positive one. Due to the reduction in dimensionality from 3 to 2, the KMs represent reduced information regarding a molecule, which can be readily saved and retrieved from a computer. Such 2D maps can help devise better strategies for drug design [56].

The oil-water partition coefficient, P , is a widely used measure of the so-called hydrophobicity in chemistry. Sasaki *et al.* [55] presented arguments supporting the importance of surface tension, electrostatics and charge transfer in determining $\log(P)$. They recommended the use of the electrostatic surface potential obtained from *ab initio* calculations for obtaining $\log(P)$ values from the molecular charge density distribution.

Politzer *et al.* have more recently [57-59] developed a method called general interaction properties function (GIPF) based on the properties of potential evaluated on the $\rho(\mathbf{r}) = 0.001$ a.u. molecular surface. The GIPF method is based on a conjecture that a molecular property Q may be expressed as a function f of the parameters of molecular surface potential, i.e.

$$Q = f[A, V_{S,\max}, V_{S,\min}, \pi, \sigma^2, \gamma] \quad (4.2)$$

Here, A denotes the area of the molecular surface and $V_{S,\max}$ and $V_{S,\min}$ are maximum and minimum values of MESP on the surface, respectively. Further, π is given by Eq. 4.1, while σ^2 and γ are defined as

$$\sigma_{\pm}^2 = \sum [V^{\pm}(\mathbf{r}_i) - \bar{V}_{s,\pm}]^2 / n_{\pm}; \quad \sigma^2 = \sigma_+^2 + \sigma_-^2$$

and $\gamma = \sigma_+^2 \sigma_-^2 / (\sigma^2)^2$ (4.3)

Here V_{s+} and V_{s-} denote the positive and negative MESP values on the surface respectively at n_+ and n_- points with $n = n_+ + n_-$, being the total number of points on the surface. Several GIPF relationships have been successfully modelled by Politzer and co-workers. These include diverse molecular properties such as the boiling point, heat of vaporization, critical temperature, pressure and volume, and partition coefficient—just to mention a few [58].

MESP has also been used as a tool in predicting lattice energies of ionic crystals. Politzer and Murray [59] have given equations for lattice energies of ionic crystals in terms of the minimum value of MESP, $V_{s,\min}$, on isodensity surface ($\rho(r) = 0.001$), the area (A) of the isodensity surface and the average negative potential on the surface. For instance, the lattice energy (LE) equation for NH_4^+ compounds is given as

$$\text{LE} = -287.8Q - 0.6246 V_{s,\min} - 1.72 \times 10^{-7} [A \times (\bar{V}_s)]^2 - 199.4$$

where Q is the charge on the anion, the MESP values are in kcal/mol and area A in \AA^2 . This equation is found to yield LE values in good agreement with the experimental ones with a standard deviation of 7 kcal/mol.

The work done in Politzer's group on GIPF method has later been expanded and developed into a package MOLSURF [57] by Sjöberg. The descriptors available in this package include hydrogen bonding, charge transfer, polarity, etc.

4.7 Treatments Based on Poisson–Boltzmann Equation

As seen in the earlier Sections, electrostatic interactions play a vital role in a variety of biological processes including the interactions of charged macromolecules such as nucleic acids and proteins in solvents. Such systems cannot be studied at the microscopic level since interactions of a large number of solvent molecules (with the macromolecules as solute) are to be considered in addition to the effect of free ions present in the solvent. Hence such systems need a classical/macrosopic approach. In this approach, the Poisson–Boltzmann (PB) equation based on a continuum description of the dielectric properties of the solvent and the macromolecules is solved. The basic idea here is to employ a simplified electrostatic treatment within the continuum models since molecules are not treated explicitly therein. Such an approach was suggested by Tanford and Kirkwood [60(a)] long

ago by replacing the amino acid group by point charges fixed on a protein surface. This was later modified by Shire *et al.* [60(b)] who employed the extent of exposure of the exterior group to the solvent for attenuating the electrostatic interaction. Suitable measures [60(c)–(e)] of dielectric constants are needed for such an approach. This model has been recognized as an important qualitative paradigm and quantitative tool [60(f)] in structural biology, biochemistry, etc. The PB equation is given as

$$\nabla[\varepsilon(\mathbf{r})\nabla\cdot\phi(\mathbf{r})] - \varepsilon(\mathbf{r})k(\mathbf{r})^2 \sinh(\phi(\mathbf{r})) + \frac{4\pi\rho^f(\mathbf{r})}{kT} = 0 \quad (4.4)$$

where $\phi(\mathbf{r})$ is the electrostatic potential, $\varepsilon(\mathbf{r})$ is the dielectric constant and $\rho^f(\mathbf{r})$ is the fixed charge density. In the second term in the PB equation, $k(\mathbf{r})$ involves ionic strength of the bulk solution, and $k(\mathbf{r}) = 0$ when mobile ions are absent in the system. It can be seen that under these conditions, the PB equation reduces to the Poisson equation. For polar molecules in aqueous medium, two values of dielectric constants are used. Though the analytical solutions of the Poisson equation are available only for simple geometric objects like spheres, cylinders, planes, etc., numerical solutions to the PB equation make it possible to use the shape of the solute in atomic detail, keeping the simplified continuum description of the solvent. Within this model, an appropriate molecular surface is defined, inside which $\varepsilon(\mathbf{r})$ is given a low value (2–4) and for regions outside this surface, $\varepsilon(\mathbf{r})$ is assigned the value for water (~80). The charge distribution of the macromolecule is represented by point charges at nuclear sites. The molecular surface is defined, and in the second iterative step wherein the initial guess to the solution is refined successively, $\phi(\mathbf{r})$ is obtained.

The $\phi(\mathbf{r})$ can be evaluated for macromolecules in solutions of arbitrary ionic strength using the DELPHI [61] program. For a given molecular surface, a protein molecule generates a unique $\phi(\mathbf{r})$ which is a dimensionless electrostatic potential given in the units of kT/q (k = Boltzmann constant, T = absolute temperature and q is the charge on the proton). This $\phi(\mathbf{r})$ for the protein is normally used in structural biology for visual representation using GRASP [62]. The graphical visualization of electrostatic properties of macromolecular structures is creating a significant impact on the field of structural biology. An application [60(b)] of this technique is demonstrated for studying the driving force and directionality of electron transfer in *Rhodospseudomonas viridis* reaction centres. More recently, Gavryushov and Zielenkiewicz [60(h)] have carried out a comparison of the Poisson–Boltzmann and the Biogolyubov–Born–Green–Yvon Equations.

4.8 Biological and Medicinal Chemistry

In the earlier Sections of this Chapter, we have seen that the MESP and allied entities have been widely employed in the study of the quantitative structure–activity relationship (QSAR) of biomolecules and drugs in medicinal chemistry [63–65]. Electrostatics of molecules provides a highly informative means of characterizing the essential electronic features of drugs and their stereoelectronic complementarity with the receptor site. Since the receptor recognizes the stereoelectronic effects [66] and not the atoms, studies of two- and three-dimensional MESP and its gradient plots have become a popular tool for characterizing pharmacologically active molecules from an electronic point of view. Graphical representations of this property of biologically active molecules are widely available in the current literature. These three-dimensional MESP plots are employed to examine a given property within a chemical series and propose a compound with improved features or to investigate the interpretative abilities of some MESP-related parameters for determining a certain aspect of the intermolecular interactions involved. An example of this is given by a study of a series of nucleoside-hydrolase inhibitors [66(b)]. The similarity of the MESP surface of a proposed inhibitor with that of its experimentally determined transition state structure is found to be in good correlation with its binding pattern. This observation along with other reactivity parameters has led to the synthesis of new and stronger inhibitors. The dynamic effects are neglected in the rigid body approximation and the association between host (lock) and guest (key) is considered as the fitting [67] of a key into its lock. Among the steric, hydrophobic and electrostatic interactions [68(a)] which are to be considered in such a molecular ‘fit’, the electrostatic effects predominate wherever the ionic and polar interactions between the host and the guest molecules are dominant. The MESP features of several drug molecules vis-à-vis the complementarity features with the respective receptor sites have been probed in recent years [68(b)–(d)]. It can be seen from various studies on drug activity, that a major role is played by an aromatic ring usually present in the structure. The negative-valued MESP region on the aromatic ring generally accounts for the reactivity towards electrophilic reagents [69]. The aromatic moiety of the drug might be involved in a stacking type of interaction with another aromatic ring located at the receptor site. In the stacking complexes of the nucleic acid bases, for example, the electrostatic component is not necessarily a dominant term of the interaction energy, yet it has a decisive effect on the mutual orientation of the aromatic rings.

Tayar *et al.* [66(a)] have reported an MESP-based study for a series of β -adrenolytic and β -adrenergic agents belonging to three general classes viz. phenylethanolamines (PEAs), aryloxy propanolamines (AOPAs) and oxime ethers. These β -adrenoceptors are known to play an important role in the regulation of the autonomic nervous system. On the basis of specificities and activities, these receptors are subdivided into β_1 and β_2 subtypes. In this work, Tayar *et al.* [66(a)] have identified some of the stereoelectronic features responsible for β_1/β_2 selectivity of the drug in terms of the corresponding MESP features. This model study which shows common MESP features in PEAs, AOPAs and oxime ethers, leads to a proposed general model for β -adrenoceptor ligands.

With the help of crystallographic structure and STO-3G MESP calculations, Collin *et al.* [70] have shown that the stereoelectronic features of zetidoline are similar to those of other Na^+ -dependent D2 receptor antagonists viz. orthoparamides and indolones. Based on these stereoelectronic similarities, they have also postulated that orthoparamides, indolones and zetidoline will show identical mechanism of action at the molecular level. In recent years, an approach christened as comparative molecular field analysis (CoMFA) [71(a), (b)], utilizing the steric electrostatic potential fields has been applied to biologically active compounds. In this method, a series of compounds with similar biological activity are theoretically composed. The alignment of these structures is then carried out by a suitable algorithm employing the data based on the above fields. Similar ideas have been employed [71(c)] within a method called DYLOMMS (dynamic lattice oriented molecular modelling systems). DYLOMMS was used to model several derivatives of GABA uptake inhibitors [71(d)].

In summary, the applications of MESP are found in physics, chemistry, biology, as well as their interfaces. Many of these applications stem from the lock-and-key analogy formulated by the famous organic chemist Emil Fischer [67] over a hundred years ago. The MESP distribution along with its topographical features, seems to offer the mechanism for investigating these complementarity features.

An attempt has been made in this monograph to provide an introduction to various fascinating aspects of this interesting scalar field in pure as well as applied areas. It is hoped that the flavour of the subject has reached the reader!

References

1. (a) E Sorocco and J Tomasi, in *Adv. Quantum Chem.* **11**, 116 Ed. P-O Löwdin, Academic, New York (1978). (b) For an inspiring review on MESP applications to biology, reference may be made to B Pullman, *Intern. J. Quantum Chem. Quantum Biology Symp.* **17**, 81 (1990). (c) For the MESP topographical features of DNA bases and base pairs, cf. S R Gadre and S S Pundlik, *J. Phys. Chem.* **B101**, 3298 (1997); S S Pundlik and S R Gadre, *J. Phys. Chem.* **B101**, 9657 (1997).
2. See, for an earlier review, P Politzer and D G Truhlar (Eds.), *Chemical applications of Atomic and Molecular Electrostatic Potential*, Plenum, New York (1981).
3. P Sjöberg and P Politzer, *J. Phys. Chem.* **94**, 3959 (1990).
4. R Bonaccorsi, E Sorocco, J Tomasi and A Pullman, *Theoret. Chim. Acta (Berlin)* **36**, 339 (1975).
5. H B Broughton, S M Green and H S Rzepa, *J. Chem. Soc. Chem. Commun.* 998 (1992).
6. G Mehta, G Gunasekaran, S R Gadre, R N Shirsat, B Ganguly and J Chandrasekhar, *J. Org. Chem.* **59**, 1953 (1994).
7. (a) A S Cieplack, *J. Amer. Chem. Soc.* **103**, 4540 (1981). (b) A S Cieplack, B D Tait and C R Johnson, *J. Amer. Chem. Soc.* **111**, 8447 (1989).
8. (a) S Mecozzi, A P West and D A Dougherty, *Proc. Natl. Acad. Sci. (U.S.A.)* **93**, 10566 (1996). (b) D A. Dougherty, *Science*, **271**, 163 (1996). (c) E Cubero, F J Luque and M Orozco, *Proc. Natl. Acad. Sci. (U.S.A.)* **95**, 5976 (1998). (d) F J Luque and M Orozco, *J. Comp. Chem.* **19**, 866 (1998). (e) S R Gadre and S S Pingale, *J. Amer. Chem. Soc.* **120**, 7056 (1998).
9. For a comprehensive summary of properties of weakly bonded complexes, see the excellent review by A C Legon and D J Millen, *Chem. Soc. Rev.* **16**, 467 (1987).
10. G A Jeffrey and W Saenger, *Hydrogen Bonding in Biological Structures*, Springer, New York (1991).
11. P Schuster, G Zundel and C Sandorfy, *The Hydrogen Bond*, North-Holland, New York (1976).
12. W G Read, E J Campbell and G Henderson, *J. Chem. Phys.* **78**, 3501 (1983).
13. A M Andrews, KW Hillig, II and R L Kuczkowski, *J. Amer. Chem. Soc.* **114**, 6765 (1992).
14. Z Mielke, K G Tokhadze, Z Latajka and E Ratajczak, *J. Phys. Chem.* **100**, 539 (1996).
15. L W Buxton, P D Aldrich, J A Shea, A C Legon and W H Flygare, *J. Chem. Phys.* **75**, 2681 (1981).
16. G A Worth and R C Wade, *J. Phys. Chem.* **99**, 17473 (1995). See also M Levitt and M F Perutz, *J. Mol. Biol.* **201**, 751 (1988).
17. A D Buckingham and P W Fowler, *Can. J. Chem.* **63**, 2018 (1985).
18. A D Buckingham and P W Fowler, *J. Chem. Phys.* **79**, 6426 (1983).

82 *Electrostatics of Atoms and Molecules*

19. A J Stone, *Chem. Phys. Letters* **83**, 233 (1981).
20. C E Dykstra, *J. Amer. Chem. Soc.* **111**, 6168 (1989).
21. C Alhambra, F J Luque and M Orozco, *J. Phys. Chem.* **99**, 3084 (1995).
22. A J Stone, private communication to the authors (December 1995).
23. C E Dykstra, *J. Phys. Chem.* **94**, 6948 (1990); *J. Phys. Chem.* **94**, 180 (1990).
24. C E Dykstra, *Chem. Rev.* **93**, 2339 (1993).
25. (a) S R Gadre, P K Bhadane, S S Pundlik and S S Pingale, in *Molecular Electrostatic Potentials: Concepts and Applications*, Ed. J S Murray and K Sen, Elsevier, Amsterdam (1996). (b) S R Gadre, and S S Pingale, *Curr. Sci. (India)*, **75**, 1162 (1998). (c) S S Pingale, S R Gadre, and L J Bartolotti, *J. Phys. Chem.* **A102**, 9987 (1998). (d) M R Chacon-Taylor and M I McCarthy, *J. Phys. Chem.* **100**, 7610 (1996).
26. J Stals, C G Barradough and A S Buchanan, *Trans. Farad. Soc.* **65**, 904 (1969); M K Orloff, P A Mullen and F C Rauch, *J. Phys. Chem.* **74**, 2189 (1970); Z Iqbal, S Bulusu and J R Autera, *J. Chem. Phys.* **60**, 221 (1974); R J Doyle and J E Capana, *J. Phys. Chem.* **89**, 4251 (1985); T Urbanski, *Chemistry and Technology of Explosives*, Vol. 4, Pergamon, New York (1984).
27. P Politzer, L N Domelsmith and P Sjoberg, *Chem. Phys. Letters* **92**, 366 (1982); P Politzer, L Abrahmsen and P Sjoberg, *J. Amer. Chem. Soc.* **106**, 855 (1984); P Politzer, P R Laurence, L Abrahmsen, B A Zilles and P Sjoberg, *Chem. Phys. Letters* **111**, 75 (1984); J Sharma and F J Owens, *Chem. Phys. Letters* **61**, 280 (1979).
28. J S Murray, P Lane, P Politzer and P R Bolduc, *Chem. Phys. Letters* **168**, 135 (1990).
29. P Politzer and J S Murray, *J. Mol. Struct.* **376**, 419 (1996).
30. A Delpuech and J Cherville, *Propellants and Explosives* **3**, 169 (1990).
31. P Politzer, J M Seminario and P R Bolduc, *Chem. Phys. Letters* **158**, 463 (1989).
32. A M Köster, M Leboeuf and D R Salahub, in *Molecular Electrostatic Potentials: Concepts and Applications*, Ed. J S Murray and K Sen, Elsevier, Amsterdam (1991).
33. J C White and A C Hess, *J. Phys. Chem.* **97**, 6398 (1993).
34. D W Breck, *Zeolite Molecular Sieves*, Wiley, New York (1974).
35. E Preuss, G Linden and M Neuckest, *J. Phys. Chem.* **89**, 2955 (1985).
36. G G Ferenczy and J G Ángyán, *J. Chem. Soc. Faraday Trans.* **86**, 3461 (1990).
37. W Sankaraman, K B Yoon, T Yabe and J K Kochi, *J. Amer. Chem. Soc.* **113**, 1419 (1991).
38. H V Brand, L A Curtiss and L E Iton, *J. Phys. Chem.* **96**, 7725 (1992).
39. S J Cook, A K Chakraborty, A T Bell and D N Theodorou, *J. Phys. Chem.* **97**, 6679 (1993).
40. (a) J B Nicholas and A C Hess, *J. Amer. Chem. Soc.* **116**, 5428 (1994). (b) R Vetrivel, R C Deka, A Chatterjee, M Kubo, E Broclawik and A Miyamoto in *Molecular Electrostatic Potentials: Concepts and Applications*, Ed. J S Murray and K Sen, Elsevier, Amsterdam (1996).
41. (a) M I McCarthy and A C Hess, *J. Chem. Phys.* **96**, 6010 (1992). (b) See, for an exhaustive review, M-M Rohmer, M Bénard, J-P Blaudeau, J-M Maestre and

- J M Poblet, *Coord. Chem. Rev.* **180**, 1019 (1998). (c) W G Klemperer, T A Marquart and O M Yaghi, *Angew. Chem. Int. Ed. Engl.* **31**, 49 (1992) and references therein. (d) A Müller, H Reuter and S Dillinger, *Angew. Chem. Int. Ed. Engl.* **34**, 2328 (1995).
42. D M Hess and P A Kollman, *J. Amer. Chem. Soc.* **98**, 3335 (1976).
43. A Warshel, *Computer Modelling of Chemical Reaction in Enzymes and Solutions*, Wiley, New York (1991).
44. (a) B A Luty, R C Wade, J D Madura, M E Davis, J M Briggs and J A McCammon, *J. Phys. Chem.* **97**, 233 (1993). (b) D J Wild and P Willett, *J. Chem. Inf. Comp. Sci.* **36**, 159 (1996), D A Thorne, D J Wild, P Willett and P M Wright, *J. Chem. Inf. Comp. Sci.* **36**, 900 (1996). (c) G M Ullmann, M Hauswald, A Jensen, N M Kostic and E W Knapp, *Biochemistry* **36** 16187 (1997). (d) H Wang and Y Tor, *J. Amer. Chem. Soc.* **119**, 8734 (1997). (e) J L Conroy, T C Sanders and C T Seto, *J. Amer. Chem. Soc.* **119**, 4288 (1997).
45. A Warshel and M Levitt, *J. Mol. Biol.* **103**, 227 (1976).
46. G Náray-Szabó, *J. Mol. Recogn.* **6**, 205 (1994); see also G Náray-Szabó and G G Ferenczy, *Chem. Rev.* **95**, 829 (1995).
47. (a) C K Bagdassarian, V L Schramm and S D Schwartz, *J. Amer. Chem. Soc.* **118**, 8825 (1996). (b) K M Merz, Jr. and L Banci, *J. Phys. Chem.* **100**, 17414 (1996).
48. G Náray-Szabó, M Fuxreiter and A Warshel, *Computational Aspects of Biochemical Reactivity* Eds. G Náray-Szabó and A Warshel, Kluwer, Amsterdam (1997).
49. G Náray-Szabó, G Toth, G G Ferenczy and G Csonka, *Intern. J. Quantum Chem. Quantum Biol. Symp.* **21**, 227 (1994).
50. (a) A H Elcock and J A McCammon, *Biochemistry* **35**, 12652 (1996). (b) M Oliveberg and A R Fersht, *Biochemistry* **35**, 2726 (1996).
51. A Pacheco, J T Hazzard, G Tollin and J H Enemark, *J. Biol. Inorg. Chem.* **4**, 390 (1999); P M Matias, L M Saraiva, C M Soares, A V Coelho, J. LeGall and M A Carrondo, *J. Biol. Inorg. Chem.* **4**, 478 (1999).
52. See, for example, C Hansch and A Leo, *Exploring QSAR: Fundamentals and Applications in Chemistry and Biology*, American Chemical Society, Washington, D.C. (1995).
53. L P Hammett, *Chem. Rev.* **17**, 125 (1935); see also L P Hammett, *Physical Organic Chemistry*, McGraw Hill, New York (1970).
54. C H Suresh and S R Gadre, *J. Amer. Chem. Soc.* **120**, 7049 (1998).
55. Y Sasaki, H Kubodera, T Matusakai and H Umeyama, *Pharmacobio-Dyn.* **14**, 207 (1991).
56. S Anzali, G Barnickel, M Krug, M Wagener and J Gasteiger in *Computer-assisted Lead Fitting and Optimization*, Ed. H v d Waterbeemd, B Testa and G Folkers, Wiley-VCH, Basel (1997).
57. P Sjöberg in *Computer-assisted Lead Finding and Optimization*, Ed. H.v.d. Waterbeemd, B Testa and G Folkers, Wiley-VCH, Basel (1997). The package MOLSURF is marketed by Quemist AB, Hertig Carls alle 29, S-69141 Karlskoga, Sweden.

58. See, for example, J S Murray, T Brinck and P Politzer, *Chem. Phys.* **204**, 289 (1996); P Politzer, J S Murray and P Flodmark, *J. Phys. Chem.* **97**, 729 (1996); J S Murray, K Paulsen and P Politzer, *Proc. Acad. Sci. (Chem. Sci.)* **106**, 267 (1994) and references therein.
59. P Politzer and J S Murray, *J. Phys. Chem.* **A102**, 1018 (1998).
60. (a) C Tanford and J G Kirkwood, *J. Amer. Chem. Soc.* **79**, 533 (1957). (b) S J Shire, G I H Hanania and F R N Gurd, *Biochemistry* **13**, 2967 (1974). (c) B R Gelin and M Karplus, *Biochemistry* **18**, 1256 (1979). (d) B E Conway, T O Bockris and I A Ammar, *Trans. Faraday Soc.* **47**, 756 (1951). (e) See for details, G Náray-Szabó, in *Molecular Electrostatic Potentials: Concepts and Applications*, Ed. J S Murray and K Sen, Elsevier, Amsterdam (1996). (f) B Honig and A Nicholls, *Science* **268**, 1144 (1995). (g) M R Gunner, A Nicholls, and B Honig, *J. Phys. Chem.* **100**, 4277 (1996). (h) S Gavryushov and P Zielenkiewicz, *J. Phys. Chem.* **B101**, 10903 (1997).
61. (a) A Nicholls and B Honig, *J. Comput. Chem.* **12**, 435 (1991); M K Gilson, K A Sharp, B H Honig, *ibid.* **9**, 327 (1988). (b) For an excellent review of molecular modelling and simulations, see B Jayaram, *Proc. Ind. Sci. Acad. (Chem. Sci.)* **A64**, 179 (1998). (c) A comprehensive review of DNA modelling in aqueous solutions is provided by B Jayaram and D L Beveridge, *Annu. Rev. Biophys. Biomol. Str.* **25**, 367 (1996).
62. A Nicholls, K A Sharp and B H Honig, *Proteins* **11**, 327 (1988).
63. P Politzer and J S Murray, in K B Lipkowitz and D B Boyd, Eds. *Reviews of Computational Chemistry*, Vol.2 VCH, New York (1991).
64. P M Dean, *Molecular Foundation of Drug-Receptor Interaction*, Cambridge University Press, Cambridge (1989).
65. M K Shukla and P C Mishra, *J. Mol. Struct. (Theochem.)* **340**, 159 (1995).
66. (a) N El Tayar, P A Carrupt, H v d Waterbeemd and B Testa, *J. Med. Chem.* **31**, 2072 (1988). (b) J I Ehrlich and V L Schramm, *Biochemistry* **33**, 8890 (1994).
67. E Fischer, *Ber. Deutsch Chem. Ges.* **27**, 2984 (1894).
68. (a) G Náray-Szabó, *J. Mol. Recogn.* **6**, 205 (1993). (b) S Guha, D Majumdar and A K Bhattacharjee, *J. Mol. Str. (Theochem.)* **88**, 61 (1992). (c) A Kumar, A K Bhattacharjee and P C Mishra, *Intern. J. Quantum Chem.* **43**, 579 (1992). (d) A K Bhattacharjee, S S Pundlik and S R Gadre, *Cancer Investigation* **15**, 531 (1997).
69. D Kocjan, M Hodoscek and D Hadzi, *J. Med. Chem.* **29**, 1418 (1986).
70. S Collin, G Evrard, D P Vercauteren, F Durant, P A Carrupt, H v D Waterbeemd and B Testa, *J. Med. Chem.* **32**, 38 (1989).
71. (a) R D Cremer III, DE Paterson and J D Bunce, *J. Amer. Chem. Soc.* **110**, 5959 (1988). (b) See for summary C M Breneman and M Martinon in *Molecular Electrostatic Potentials: Concepts and Applications*, Ed. J S Murray and K Sen, Elsevier, Amsterdam (1996). (c) M Wise in *QSAR and Strategies in the design of Biomolecular Compounds*, Ed. J K Seydel, VCH, Weinheim (1985). (d) M Wise in *Molecular Graphics and Drug Design*, Ed. A S V Burgen, G C K Robert and M S Tute, Elsevier, New York (1986).

Appendix A

Some Biographical Notes on Pioneering Contributors to Electrostatics

William Gilbert (1540–1603) born at Colchester, England was a physicist and court physician in-ordinary to Queen Elizabeth I. He was primarily interested in magnetism, but conducted some studies on electrification by friction. He named the substances capable of being electrified as *electrics*, and he is considered to have coined the word *electricity*. Gilbert showed that the attractive power of amber is not unique to that substance: it is also shown by a large class of other bodies such as glass, sulfur, sealing wax, etc.

Niccolo Cabeo (1585–1650) an Italian Ferrara Jesuit, discovered around 1640 that two ‘electrics’ could repel each other. Cabeo as well as some other Jesuits attempted to bring the works on magnetism within the framework of Aristotelian philosophy. However, Cabeo seems to have frequently insisted on the desirability of following experience in scientific endeavours.

Otto von Guericke (1602–1686) was born in an old Magdelburg family. Designing the water barometer and performing the famous Magdelburg hemisphere experiments are his most noted contributions. He constructed an electrical machine made of a rotating sulfur sphere which yielded electrical potential high enough to generate phosphorescent light, and, occasionally, small sparks.

Stephen Gray (1696–1736) was an experimenter of whom little is known except that he was a pensioner of the London Charter House. He reported to the Royal Society his findings in 1729 (actually published in 1731) that the ability to produce the amber effect could be transmitted by some substances (e.g. metals) called conductors. He showed that the charge resides only on the outer surface of conductors, by electrifying two cubes, one solid and the other hollow.

Charles-Francois Du Fay (1698–1739) was a Superintendent of Gardens to the King of France. He observed two kinds of electricity in 1773: *vitreous*, the one found on glass rubbed with silk, and *resinous*, found on amber rubbed with fur. He also clearly recognized and distinguished conductors and insulators.

Benjamin Franklin (1706–1790) was an American statesman, philosopher and scientist. His contributions to electrostatics include studies on lightning and the invention of the lightning rod. He gave the labels *positive*

and *negative* respectively to the charges earlier identified as *vitreous* and *resinous* by Du Fay.

R G Boscovitch (1711–1787) a Croatian Jesuit, was the first exponent of Newton's ideas in Italy. He replaced material particles by fixed centres of force. Boscovitch also invented a force function to show the variation of forces with distance, a work referred later by Faraday.

Henry Cavendish (1731–1810) entered a seminary in 1742 and later attended Cambridge University without getting a degree. He determined the density and mass of the earth by a method now popularly known as the Cavendish experiment. His electrical studies were extensive: he proposed the inverse power law and freely used the concept of potential in his experiments on conductors.

Joseph Priestley (1733–1804) was the oldest of six children of a cloth dresser. Known as one of the discoverers of oxygen, he performed many original experiments with gases. He believed that human progress would be the natural result of political and religious freedom and of the applications of science. In 1767, Priestley published *The History and Present State of Electricity* summarizing the knowledge of electricity upto that time. The inverse square law was anticipated by him with his observation that an electrified hollow sphere contained no charge inside. He also contributed to political theory and religion.

Charles Augustin de Coulomb (1736–1806) was a French physicist, who developed the famous inverse square law, later named after him, around 1785. This is considered an offshoot of his attempt to investigate the law of electrical repulsions as stated by Joseph Priestley. To this end, he invented a sensitive apparatus to measure the electrical forces. He later spent nine years in the West Indies as a military engineer and returned to France with impaired health.

Luigi Aloisius Galvani (1737–1798) born in Bologna, Italy, occupied from 1775 a Chair of anatomy there. He reported in 1791 the so-called 'animal electricity', discovered accidentally by observing the convulsion of a frog's leg when two ends of it were connected to two different metals.

Alessandro Guiseppe Antonio Anastasio Volta (1745–1827) born at Como, Italy, was a professor of natural philosophy in the University of Pavia, Italy. He substituted cloth soaked with salt water for the animal tissue and by using stacks of metal discs, was able to demonstrate in 1800 the conversion of chemical energy into electrical energy. This eventually led to devices for electricity production.

Pierre Simon Laplace (1749–1827) the son of a Normandy farmer, took up several academic and administrative positions. Celestial Mechanics and the Theory of Probability are regarded as his two great works. His chief contribution to potential theory is what is now known as the Laplace equation, viz. $\nabla^2 V = 0$, though the equation had already been written by Euler in 1752 in a hydrodynamical context. Well-known is the anecdote in which Laplace replied to a query by Napoleon of why God was not mentioned in his works: “Sir, I did not require that hypothesis”.

Karl Friedrich Gauss (1777–1855) was born in the German city of Brunswick. The Duke of Brunswick recognised this child prodigy and took charge of his education. His *Allgemeine Lehrsätze* dealt with the theory of forces of inverse-square type. This marked the formal beginning of potential theory. Among his other noted contributions are the prediction of the position of an asteroid named Ceres, and the construction of a 17-sided polygon with only a compass and ruler. The formal proof of the fundamental theorem of algebra is his other pioneering contribution.

Simeon Denis Poisson (1781–1840) was a very productive mathematician as indicated by the frequency with which his name appears in textbooks. The Poisson Equation (1812) in potential theory was the result of his discovery that Laplace’s equation for the gravitational case holds only at the points where no mass is located.

Michael Faraday (1791–1867) was born in Newington, Surrey, England, to a blacksmith, and worked as an errand boy and bookbinder to George Ribau, a bookseller. He was appointed assistant to Sir Humphry Davy at the Royal Institution. He developed into a distinguished physicist and chemist, whose experimental investigations covered several electrical, magnetic, optical and chemical phenomena. He developed the concept of an electric field, on the lines of the earlier studies by Boscovitch.

George Green (1793–1841) who was a self-taught miller’s son from Nottingham, England, followed with great care the new discoveries in electricity around 1825. He produced *An Essay on the Application of Mathematical Analysis to Theories of Electricity and Magnetism* in 1828. A relation connecting line and surface integrals (closely related to the one by Stokes) is called Green’s theorem.

George Gabriel Stokes (1819–1903) contributed to the mathematical theory of partial differential equations encountered in mathematical physics. Stokes’ theorem relates the line integral of a vector function \mathbf{V} to the corresponding surface integral of $\nabla \times \mathbf{V}$ (see Appendix C).

James Clerk Maxwell (1831–1879) born in Edinburgh, grew up as a countryman at the house built by his father at Glenlair. At the age of 10, he was taken to live with his aunt at Edinburgh and schooled at the Edinburgh Academy. Maxwell performed an experiment similar to the one performed by Cavendish in 1772. He formulated the fundamental electromagnetic equations in his pioneering paper, *A Dynamical Theory of the Electromagnetic Field*. His other significant contributions include the theory of the primary colours and the kinetic theory of gases.

References

1. E Whittaker, *A History of the Theories of Aether and Electricity*, Thomas Nelson, New York (1951).
2. D J Struik, *A Concise History of Mathematics*, Vol 2, Dover, New York (1948).
3. G B Arfken, D F Griffins, D V Kelly and J Priest, *University Physics*, Academic, New York (1984).
4. D Halliday and R Resnick, *Fundamentals of Physics*, John Wiley, New York (1981).
5. *The New Encyclopaedia Britannica*, Fifteenth Edition, Encyclopaedia Britannica Inc., William Benton, Chicago (1974).
6. R A R Tricer, *The Contributions of Faraday and Maxwell to Electrical Science*, Pergamon, New York (1966).
7. O Glaser, *Amer. J. Roentgenol. Radium Therapy*, 180 (1933).

Appendix B

B.1 A List of Some Useful Fundamental Derived Physico-Chemical Constants*
(rounded to three digits after the decimal point).

Quantity	Symbol	Numerical Value & Units (SI)
Speed of light in vacuum	c	$2.998 \times 10^8 \text{ m s}^{-1}$
Fine structure constant	α	7.297×10^{-3}
Elementary charge	e	$1.602 \times 10^{-19} \text{ C}$
Planck's constant	h	$6.627 \times 10^{-34} \text{ Js}$
Avogadro's constant	N_A	$6.022 \times 10^{23} \text{ mol}^{-1}$
Atomic mass unit	amu	$1.667 \times 10^{-27} \text{ kg}$
Electron rest mass	m_e	$9.110 \times 10^{-31} \text{ kg}$
Proton rest mass	m_p	$1.673 \times 10^{-27} \text{ kg}$
Neutron rest mass	m_n	$1.675 \times 10^{-27} \text{ kg}$
Electronic charge to mass ratio	(e/m_e)	$1.759 \times 10^{11} \text{ C kg}^{-1}$
Rydberg's constant	R_∞	$1.097 \times 10^7 \text{ m}^{-1}$
Bohr radius	a_0	$5.292 \times 10^{-11} \text{ m}$
Bohr magneton ($e \hbar / 2m_e$)	μ_B	$9.274 \times 10^{-24} \text{ J T}^{-1}$
Electron magnetic moment	μ_e	$9.285 \times 10^{-24} \text{ J T}^{-1}$
Proton magnetic moment	μ_p	$1.411 \times 10^{-26} \text{ J T}^{-1}$
Nuclear magneton ($e \hbar / 2m_p$)	μ_N	$5.051 \times 10^{-26} \text{ J T}^{-1}$
Compton wavelength		
electron ($h/m_e c$)	λ_e	$2.426 \times 10^{-12} \text{ m}$
proton ($h/m_p c$)	λ_p	$1.321 \times 10^{-15} \text{ m}$
Boltzmann constant	k_B	$1.381 \times 10^{-23} \text{ J K}^{-1}$
Gravitational constant	G	$6.672 \times 10^{-11} \text{ m}^3 \text{ kg}^{-1} \text{ s}^{-2}$
Electron volt	eV	$1.602 \times 10^{-19} \text{ J}$
Permeability of free space	μ_0	$4\pi \times 10^{-7} \text{ Js}^2 \text{ C}^{-2} \text{ m}^{-1}$
Permittivity of free space	ϵ_0	$8.854 \times 10^{-12} \text{ C}^2 \text{ N}^{-1} \text{ m}^{-2}$
Electron rest energy	$m_e c^2$	0.511 MeV
Faraday's constant	F	$9.649 \times 10^4 \text{ C mol}^{-1}$
Universal gas constant	R	$8.314 \text{ J mol}^{-1} \text{ K}^{-1}$
Molar volume of ideal gas at STP	V_m	$0.224 \times 10^3 \text{ dm}^3 \text{ mol}^{-1}$

* C – Coulomb, J – Joule, T – Tesla, K – Kelvin.

90 Electrostatics of Atoms and Molecules

B.2 Atomic Units and their Conversion to SI Units (rounded to three digits after the decimal point).

Unit (Description/Name, symbol)	Value in SI units
Mass (electron rest mass, m_e)	9.105×10^{-31} kg
Charge (electronic charge, e)	1.602×10^{-19} C
Angular momentum ($\hbar/2\pi$)	1.055×10^{-34} J s
Energy (Hartree)*	4.360×10^{-18} J
Length (first Bohr radius, a_0)	5.292×10^{-11} m
Linear momentum	1.993×10^{-24} kg m s ⁻¹
Time	2.419×10^{-17} s
Electric dipole moment* ($e \cdot a_0$)	8.478×10^{-30} C m
Probability density (a_0^{-3})	6.748×10^{30} m ⁻³
Electron density ($e \cdot a_0^{-3}$)	1.081×10^{12} C m ⁻³
Quadrupole moment ($e \cdot a_0^2$)	4.487×10^{-40} C m ²
Electric polarizability (a_0^3)	1.482×10^{-31} m ³
Electrostatic potential ($e \cdot a_0^{-1}$)	3.028×10^{-9} C m ⁻¹

*1 a.u. of energy = 1 Hartree = 27.212 eV = 627.509 kcal mol⁻¹ \cong 2626.03 kJ mol⁻¹.

*1 a.u. of dipole moment \cong 2.542 Debye.

Appendix C

Introduction to Vectors

Physical properties that require specification of magnitude as well as direction and whose components follow appropriate co-ordinate transformation rules are called vectors. Some examples of vector quantities are force, velocity, momentum, etc. The vector functions describing these properties over a region of space are called vector fields. The velocity distribution in a stream of water is an example of a vector field. On the other hand, a scalar quantity, needing no description of the direction, associated with each point in a region of space defines a scalar field. The temperature distribution in a stream of water is a scalar field. In what follows, a brief introduction to vectors is provided.

A three-dimensional vector may be defined in terms of components along three mutually perpendicular axes. For example, as seen from Fig. C.1, the vector \mathbf{A} is resolved in cartesian components as $\mathbf{A} = A_x \mathbf{i} + A_y \mathbf{j} + A_z \mathbf{k}$. Here, \mathbf{i} , \mathbf{j} and \mathbf{k} are unit vectors in three mutually perpendicular cartesian directions. The magnitude of the vector \mathbf{A} is given by

$$|\mathbf{A}| = (A_x^2 + A_y^2 + A_z^2)^{1/2}$$

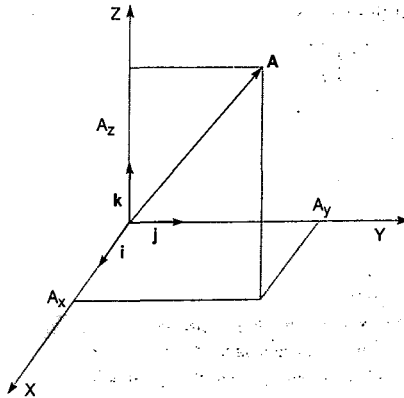


Fig. C.1 Resolution of vector \mathbf{A} into its cartesian components. Here, \mathbf{i} , \mathbf{j} , \mathbf{k} are unit vectors along the x , y and z directions respectively.

92 *Electrostatics of Atoms and Molecules*

The sum and difference of two vectors **A** and **B** are defined in terms of their respective components, viz.

$$\mathbf{A} \pm \mathbf{B} = (A_x \pm B_x)\mathbf{i} + (A_y \pm B_y)\mathbf{j} + (A_z \pm B_z)\mathbf{k}$$

When a vector **A** is multiplied by a scalar constant *c*, the resultant vector is: $c\mathbf{A} = cA_x\mathbf{i} + cA_y\mathbf{j} + cA_z\mathbf{k}$. The multiplication of two vectors is defined in two distinct ways viz. scalar and vector products. The scalar or dot product is defined as

$$\mathbf{A} \cdot \mathbf{B} = |\mathbf{A}||\mathbf{B}|\cos\theta$$

Here, θ is the angle between the two vectors. From the definition of dot product, it follows that $\mathbf{i} \cdot \mathbf{i} = \mathbf{j} \cdot \mathbf{j} = \mathbf{k} \cdot \mathbf{k} = 1$ and $\mathbf{i} \cdot \mathbf{j} = \mathbf{j} \cdot \mathbf{k} = \mathbf{k} \cdot \mathbf{i} = 0$ and hence

$$\mathbf{A} \cdot \mathbf{B} = A_x B_x + A_y B_y + A_z B_z$$

The dot product of two vectors is thus a scalar quantity. The vector or cross product of two vectors **A** and **B** is a vector **C** whose direction is perpendicular to the plane containing **A** and **B** and its magnitude is given by

$$|\mathbf{C}| = |\mathbf{A} \times \mathbf{B}| = |\mathbf{A}||\mathbf{B}|\sin\theta$$

The direction of **C** is given by the right-hand screw rule. The geometrical representation of the vector product of **A** and **B** is given in Fig. C.2.

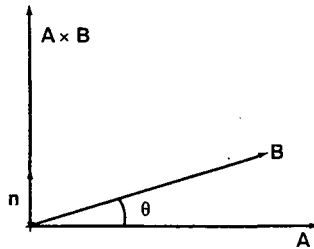


Fig. C.2 Geometrical representation of the vector product of two vectors **A** and **B**. Consider a rotation of a right-handed screw from **A** to **B**. The vector $\mathbf{A} \times \mathbf{B}$ points in the direction of the movement of the screw head and is perpendicular to both **A** and **B**.

It is clear from the definition of the vector product that $\mathbf{i} \times \mathbf{i} = \mathbf{j} \times \mathbf{j} = \mathbf{k} \times \mathbf{k} = 0$. Further, $\mathbf{i} \times \mathbf{j} = -(\mathbf{j} \times \mathbf{i}) = \mathbf{k}$ etc. The cross product of two vectors can be

given conveniently in terms of an appropriately defined determinant.

$$\mathbf{A} \times \mathbf{B} = \begin{vmatrix} \mathbf{i} & \mathbf{j} & \mathbf{k} \\ A_x & A_y & A_z \\ B_x & B_y & B_z \end{vmatrix}$$

Two kinds of products involving three vectors may be defined.

- (i) Triple scalar product $\mathbf{A} \cdot \mathbf{B} \times \mathbf{C}$: It can be expressed as the determinant

$$\mathbf{A} \cdot (\mathbf{B} \times \mathbf{C}) = \begin{vmatrix} A_x & A_y & A_z \\ B_x & B_y & B_z \\ C_x & C_y & C_z \end{vmatrix}$$

Geometrically, $\mathbf{A} \cdot (\mathbf{B} \times \mathbf{C})$ represents the volume of an appropriately defined parallelepiped with the vectors \mathbf{A} , \mathbf{B} and \mathbf{C} as edges as shown in Fig. C.3. Cyclic permutations of \mathbf{A} , \mathbf{B} and \mathbf{C} yield identical volumes as may be intuitively expected i.e., $\mathbf{A} \cdot (\mathbf{B} \times \mathbf{C}) = \mathbf{B} \cdot (\mathbf{C} \times \mathbf{A}) = \mathbf{C} \cdot (\mathbf{A} \times \mathbf{B})$, where A_x, A_y, A_z are the cartesian components of the vector \mathbf{A} , etc.

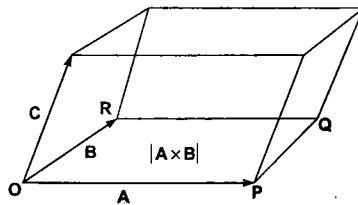


Fig. C.3 A parallelepiped with \mathbf{A} , \mathbf{B} , \mathbf{C} as the three sides. The area of the parallelogram $OPQR$ is $|\mathbf{A} \times \mathbf{B}|$.

- (ii) Triple vector product $\mathbf{A} \times (\mathbf{B} \times \mathbf{C})$: It can be seen that $\mathbf{B} \times \mathbf{C}$ is perpendicular to both \mathbf{B} and \mathbf{C} . The cross product of \mathbf{A} with $\mathbf{B} \times \mathbf{C}$ also lies perpendicular to $\mathbf{B} \times \mathbf{C}$. Hence, it must lie in the plane of \mathbf{B} and \mathbf{C} . Using the above definitions of vector and scalar products, it can be shown that $\mathbf{A} \times (\mathbf{B} \times \mathbf{C}) = (\mathbf{A} \cdot \mathbf{C})\mathbf{B} - (\mathbf{A} \cdot \mathbf{B})\mathbf{C}$. It may be noted that $(\mathbf{A} \times \mathbf{B}) \times \mathbf{C}$ is distinct from $\mathbf{A} \times (\mathbf{B} \times \mathbf{C})$. It is evident that products of the types such as $\mathbf{A} \times (\mathbf{B} \cdot \mathbf{C})$ and $\mathbf{A} \cdot (\mathbf{B} \cdot \mathbf{C})$ are not defined.

The rate of change with respect to a space co-ordinate of a vector or a scalar field is obtained with the help of a vector operator ∇ (del) defined as $\nabla = \mathbf{i} \frac{\partial}{\partial x} + \mathbf{j} \frac{\partial}{\partial y} + \mathbf{k} \frac{\partial}{\partial z}$. The space derivative of a scalar quantity is called its gradient. The dot and the cross products of ∇ operator with a vector function are called the divergence and curl respectively. These will be introduced later in this Section. The gradient of a scalar function f is defined by $\mathbf{A} = \text{grad } f = \nabla f = \mathbf{i} \frac{\partial f}{\partial x} + \mathbf{j} \frac{\partial f}{\partial y} + \mathbf{k} \frac{\partial f}{\partial z}$.

As an example, consider the gradient of a function, $1/|\mathbf{r}-\mathbf{r}'|$ which is of specific interest in electrostatics.

$$\begin{aligned} \nabla \left(\frac{1}{|\mathbf{r}-\mathbf{r}'|} \right) &= \sum_x \mathbf{i} \frac{\partial}{\partial x} \left\{ \frac{1}{(x-x')^2 + (y-y')^2 + (z-z')^2} \right\}^{1/2} \\ &= -\frac{\sum_x \mathbf{i}(x-x')}{|\mathbf{r}-\mathbf{r}'|^3} \\ &= -\frac{(\mathbf{r}-\mathbf{r}')}{|\mathbf{r}-\mathbf{r}'|^3} \end{aligned}$$

The summations in the above equations are to be taken with respect to y and z as well. Now consider $(\nabla f \cdot d\mathbf{r})$ where $d\mathbf{r}$ is a differential vector displacement $d\mathbf{r} = dx \mathbf{i} + dy \mathbf{j} + dz \mathbf{k}$.

$$\nabla f \cdot d\mathbf{r} = \frac{\partial f}{\partial x} dx + \frac{\partial f}{\partial y} dy + \frac{\partial f}{\partial z} dz$$

The r.h.s. of the above equation may be identified with the total differential, df . Hence, $df = \nabla f \cdot d\mathbf{r}$. An isosurface S of the function f is displayed in Fig. C.4(a). Consider a differential vector displacement $d\mathbf{r}$ tangential to the surface S on which f is constant. By definition, $df = \nabla f \cdot d\mathbf{r} = 0$ at any point on the isosurface of the scalar function f . Since $d\mathbf{r}$ is tangential to S , by the definition of dot product of vectors, ∇f is normal to it. Thus, the gradient of a function f is normal to the isosurface of f .

Similarly (cf. Fig. C. 4(b)), it may be noted that $df = \nabla f \cdot d\mathbf{r}$ is maximum when ∇f and $d\mathbf{r}$ point in the same direction. Thus, the gradient of a scalar function is a vector pointing in the direction of maximum rate of change of that function.

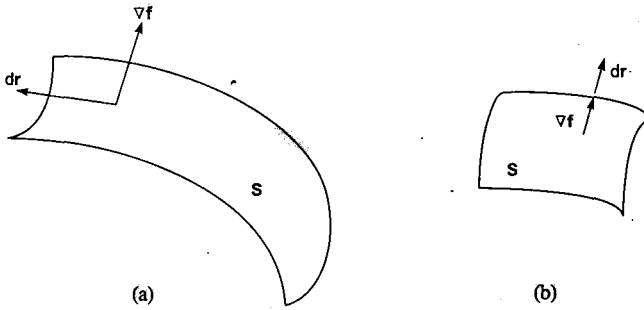


Fig. C.4 (a) S is an isosurface of a scalar function f with dr denoting the tangent to S . The gradient, ∇f is perpendicular to S . (b) The maximum value of ∇f occurs when ∇f and dr point in the same direction.

Now consider the dot product of the operator ∇ with a vector field \mathbf{A} , viz.

$$\nabla \cdot \mathbf{A} = \frac{\partial A_x}{\partial x} + \frac{\partial A_y}{\partial y} + \frac{\partial A_z}{\partial z}$$

where A_x , A_y , and A_z are the components of \mathbf{A} . The quantity $\nabla \cdot \mathbf{A}$ is called the *divergence* of \mathbf{A} . The physical meaning of divergence $\nabla \cdot \mathbf{A}$ is clear with the example of a fluid flowing through a unit area (normal to the flow direction) per unit time. If \mathbf{A} denotes the velocity vector field associated with the fluid then $\nabla \cdot \mathbf{A}$ is the net outward flow per unit volume. If $\nabla \cdot \mathbf{A} = 0$ at all points in space, the field \mathbf{A} is called solenoidal. It means, in the above example, that there is no net outward/inward flow of the fluid denoting incompressibility of the fluid.

The combination $\nabla \times \mathbf{A}$ is called the *curl* of \mathbf{A} . It can be expressed in determinant form as

$$\nabla \times \mathbf{A} = \begin{vmatrix} i & j & k \\ \frac{\partial}{\partial x} & \frac{\partial}{\partial y} & \frac{\partial}{\partial z} \\ A_x & A_y & A_z \end{vmatrix}$$

A vector field satisfying $\nabla \times \mathbf{A} = 0$ is termed *irrotational*. If $\mathbf{A} = \nabla\phi$, where

ϕ is a scalar function, then it can be readily seen that $\nabla \times \mathbf{A} = 0$. In fact, $\nabla \times \mathbf{A} = 0$ states the necessary and sufficient condition for $\mathbf{A} = \nabla \phi$ to be valid, and ϕ is called the potential of the vector function \mathbf{A} . Several interesting and useful relations can be derived for combinations of gradient, divergence and curl. Some of these are summarized below [3]. Here f and \mathbf{A} denote scalar and vector functions respectively.

$$(i) \quad \nabla \cdot (\nabla f) = \nabla^2 f$$

$\nabla \cdot \nabla$ is usually denoted as ∇^2 , and is called as the Laplacian operator, and

its operation on f yields $\nabla^2 f = \frac{\partial^2 f}{\partial x^2} + \frac{\partial^2 f}{\partial y^2} + \frac{\partial^2 f}{\partial z^2}$. $\nabla^2 f$ is called the

Laplacian of scalar field f .

$$(ii) \quad \nabla \times (\nabla f) = \begin{vmatrix} \mathbf{i} & \mathbf{j} & \mathbf{k} \\ \frac{\partial}{\partial x} & \frac{\partial}{\partial y} & \frac{\partial}{\partial z} \\ \frac{\partial f}{\partial x} & \frac{\partial f}{\partial y} & \frac{\partial f}{\partial z} \end{vmatrix} = 0$$

for a continuous function f , whose second partial derivatives are defined.

$$(iii) \quad \nabla \cdot (f\mathbf{A}) = (\nabla f) \cdot \mathbf{A} + f(\nabla \cdot \mathbf{A})$$

$$(iv) \quad \nabla \times (f\mathbf{A}) = (\nabla f) \times \mathbf{A} + f(\nabla \times \mathbf{A})$$

$$(v) \quad \nabla \cdot (\nabla \times \mathbf{A}) = 0$$

$$(vi) \quad \nabla \times (\nabla \times \mathbf{A}) = \nabla(\nabla \cdot \mathbf{A}) - \nabla^2 \mathbf{A}$$

$$(vii) \quad (\nabla \cdot \nabla)\mathbf{A} = \nabla^2 \mathbf{A}$$

It is sometimes found useful to express the gradient, curl and Laplacian in co-ordinate systems other than Cartesian. Two such systems are depicted in Figs. C.5 and C.6 (cylindrical and spherical polar systems respectively). In the cylindrical system, the position of a point P is specified as (ρ, φ, z) and the three corresponding unit vectors are denoted by (ρ_1, φ_1, z_1) as shown in Fig. C.5. Similarly, the point P is denoted as (r, θ, φ) and the respective unit vectors are labelled as r_1, θ_1 and φ_1 and in spherical polar co-ordinate system (cf. Fig. C.6). The transformations of the various entities in these two systems are given in Table C.1.

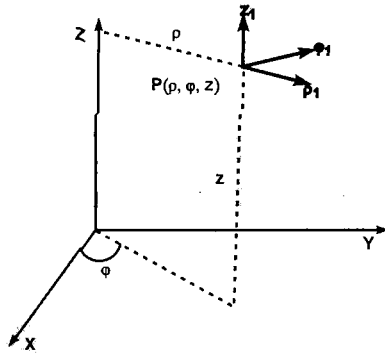


Fig. C.5 A representation of cylindrical co-ordinate system. The cylindrical co-ordinates of the point P are (ρ, φ, z) and the unit vectors are denoted by ρ_1, φ_1 and z_1 respectively.

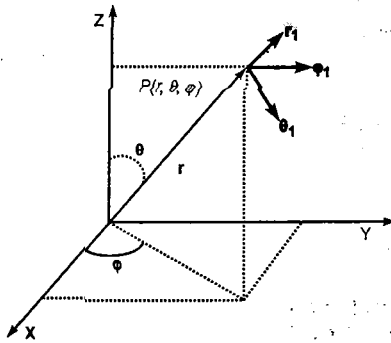


Fig. C.6 A representation of spherical polar system of co-ordinates. Point P is specified by (r, θ, φ) and the unit vectors are shown as $(r_1, \theta_1, \varphi_1)$.

Table C.1 The volume element, gradient, divergence and Laplacian in cylindrical and spherical polar co-ordinates.

Entity	Cylindrical co-ordinates	Spherical polar co-ordinates
dV	$\rho d\rho d\varphi dz$	$r^2 \sin\theta dr d\theta d\varphi$
∇f	$\frac{\partial f}{\partial \rho} \rho_1 + \frac{1}{\rho} \frac{\partial f}{\partial \varphi} \varphi_1 + \frac{\partial f}{\partial z} z_1$	$\frac{\partial f}{\partial r} r_1 + \frac{1}{r} \frac{\partial f}{\partial \theta} \theta_1 + \frac{1}{r \sin\theta} \frac{\partial f}{\partial \varphi} \varphi_1$
$\nabla \cdot \mathbf{A}$	$\frac{A_\rho}{\rho} + \frac{\partial A_\rho}{\partial \rho} + \frac{1}{\rho} \frac{\partial A_\varphi}{\partial \varphi} + \frac{\partial A_z}{\partial z}$	$\frac{2}{r} A_r + \frac{\partial A_r}{\partial r} + \frac{A_\theta}{r} \cot\theta + \frac{1}{r} \frac{\partial A_\theta}{\partial \theta}$ $+ \frac{1}{r \sin\theta} \frac{\partial A_\varphi}{\partial \varphi}$
$\nabla^2 f$	$\frac{1}{\rho} \frac{\partial f}{\partial \rho} + \frac{\partial^2 f}{\partial \rho^2} + \frac{1}{\rho^2} \frac{\partial^2 f}{\partial \varphi^2} + \frac{\partial^2 f}{\partial z^2}$	$\frac{1}{r^2} \frac{\partial}{\partial r} \left(r^2 \frac{\partial f}{\partial r} \right) + \frac{\cot\theta}{r^2} \frac{\partial f}{\partial \theta} + \frac{1}{r^2} \frac{\partial^2 f}{\partial \theta^2}$ $+ \frac{1}{r^2 \sin^2 \theta} \frac{\partial^2 f}{\partial \varphi^2}$

The flux ϕ of a vector \mathbf{A} through a closed surface S is given [1] as $\oint_S \mathbf{A} \cdot d\mathbf{S}$ where $d\mathbf{S}$ is an outward normal vector. For a closed surface S , bounding a volume Ω , the surface and volume integrals are related by Gauss' theorem, sometime also called the *divergence theorem*, viz.

$$\int_{\Omega} \nabla \cdot \mathbf{A} dV = \oint_S \mathbf{A} \cdot d\mathbf{S}$$

The consideration of fluid flow is convenient for interpreting this result. As noted above, if \mathbf{A} is the rate of flow per unit area then the total outward flow from a volume Ω is $\oint_{\Omega} \nabla \cdot \mathbf{A} dV$. This must equal $\oint_S \mathbf{A} \cdot d\mathbf{S}$, the rate of fluid flow through the surface S enclosing the volume Ω .

On making [1–3] a specific choice of \mathbf{A} , one gets two interesting identities, known as Green's theorems.

$$(i) \int_{\Omega} (\phi \nabla^2 \psi + \psi \nabla^2 \phi) dV = \oint_S (\phi \nabla \psi) \cdot d\mathbf{S}$$

and

$$(ii) \int_{\Omega} (\phi \nabla^2 \psi - \psi \nabla^2 \phi) dV = \oint_S (\phi \nabla \psi - \psi \nabla \phi) \cdot d\mathbf{S}$$

substituting $\psi = 1$ in the second result, one obtains

$$\int_{\Omega} \nabla^2 \phi dV = \oint_S (\nabla \phi) \cdot d\mathbf{S}.$$

Stokes' theorem relates the line integral of a vector function \mathbf{A} to the surface integral of $\nabla \times \mathbf{A}$. For a surface S bounded by a simple closed path C ,

$$\int_C \mathbf{A} \cdot d\mathbf{l} = \int_S (\nabla \times \mathbf{A}) \cdot d\mathbf{S}.$$

References

1. D D Fitts, *Vector Analysis in Chemistry*, McGraw-Hill, Tokyo (1974).
2. P Lorrain and D Corson, *Electromagnetic Fields and Waves*, Freeman, San Francisco (1970).
3. R P Feynman, R B Leighton and M Sands, *The Feynman Lectures on Physics*, Addison-Wesley, New York (1964) Vols. 1 and 2.

Appendix D

Ab Initio Methods and Gaussian Basis Sets

The exact analytic solution of the time-independent Schrödinger equation for atoms and molecules has been possible only for hydrogen-like atoms and one-electron diatomic molecules such as H_2^+ . Hence, it is necessary to turn to approximate methods for treating many-electron systems. The usual starting framework is the Born–Oppenheimer approximation [1] wherein use is made of the fact that the motion of nuclei takes place on much longer time scales than that of electrons. Good approximations, as far as electrons are concerned, are thus obtained by holding the nuclei fixed. The total molecular wave function within this framework is adequately described by a product

$$\Phi(\{\mathbf{r}_i, \mathbf{R}_\alpha\}) \equiv \psi_{el}(\{\mathbf{r}_i, \mathbf{R}_\alpha\}) \cdot \phi_N(\{\mathbf{R}_\alpha\}) \quad (D.1)$$

if $(m_e/m_\alpha)^{1/4} \ll 1$, m_e and m_α being respectively the mass of electron and α 'th nucleus. The electronic and nuclear wave functions are described by ψ_{el} and ϕ_N respectively and $\{\mathbf{r}_i\}$ and $\{\mathbf{R}_\alpha\}$ denote the electronic and nuclear co-ordinates. Even within this simplified framework, the many-electron Schrödinger equation cannot be solved exactly due to the presence of electron–electron repulsion term in the electronic Hamiltonian [2]. This interelectronic interaction is treated in an average way within the approximation due to Hartree, generalized later by Fock [3]. Here, it is assumed that each electron is moving in the effective potential provided by the nuclei and other electrons. This potential is obtained with the help of self-consistent field (SCF) approximation, which is derived by employing the variation principle [4]. For simplicity, we shall explicitly deal here with the simple case of closed shell systems only. In this case, the Hartree–Fock (HF) treatment normally begins with a single-determinantal approximation for the wave function. For example, such a Slater determinant for an N -electron system can be written in terms of N spin-orbitals $\chi_1, \chi_2, \dots, \chi_N$ as

$$\Phi(\mathbf{x}_1, \mathbf{x}_2, \dots, \mathbf{x}_N) = \frac{1}{\sqrt{N!}} \begin{vmatrix} \chi_1(\mathbf{x}_1) & \chi_2(\mathbf{x}_1) & \dots & \chi_N(\mathbf{x}_1) \\ \chi_1(\mathbf{x}_2) & \chi_2(\mathbf{x}_2) & \dots & \chi_N(\mathbf{x}_2) \\ \vdots & \vdots & & \vdots \\ \chi_1(\mathbf{x}_N) & \chi_2(\mathbf{x}_N) & \dots & \chi_N(\mathbf{x}_N) \end{vmatrix} \quad (D.2)$$

Here \mathbf{x}_i represents space and spin co-ordinates of the electron i . Since a determinant retains its numerical value but changes sign on an interchange of two columns, it can be readily verified that such a wave function is antisymmetric with respect to interchange of two electrons, i.e.,

$$\Phi(\mathbf{x}_1, \mathbf{x}_2 \dots \mathbf{x}_i \dots \mathbf{x}_j \dots \mathbf{x}_N) = -\Phi(\mathbf{x}_1, \mathbf{x}_2 \dots \mathbf{x}_j \dots \mathbf{x}_i \dots \mathbf{x}_N) \quad (\text{D.3})$$

In Eq. D.2, each spin-orbital is described as a product of space (\mathbf{r}) and spin (ω) parts, viz. $\chi_i(\mathbf{x}) = \psi_i(\mathbf{r})\alpha(\omega)$ or $\psi_i(\mathbf{r})\beta(\omega)$ where α and β correspond to functions of an unspecified spin variable ω .

The HF equations are obtained by minimizing energy subject to orthonormality constraint on the molecular orbitals. Roothaan [3] derived them in special form by expanding the molecular orbitals (MOs) ψ_i 's as a linear combination of fixed atomic orbitals (AOs) or basis functions. Two kinds of basis functions commonly employed in HF-SCF calculations are Slater-type [5] and Gaussian-type [6]. A comparison of the simplest (s -type orbital) function of the STO and GTO types centred at the origin is shown in Fig. D.1. Here

$$\varphi_{STO}(r) = (\alpha^3/\pi)^{1/2} \exp(-\alpha r)$$

and

$$\varphi_{GTO}(r) = (2\beta/\pi)^{3/4} \exp(-\beta r^2) \quad (\text{D.4})$$

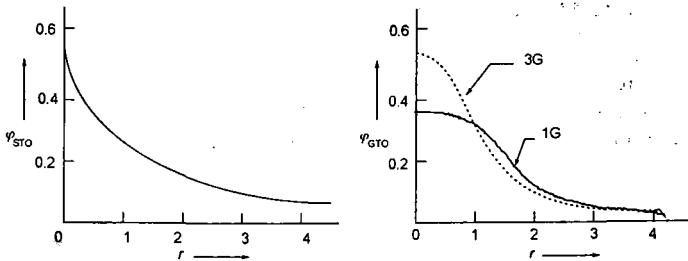


Fig. D.1 A schematic comparison of $\varphi_{STO}(\alpha = 1)$ with φ_{GTO} . This represents a least-square fit of the STO to a single Gaussian (1G) and to three Gaussians (3G) with appropriately chosen exponents and coefficients.

102 Electrostatics of Atoms and Molecules

It can be seen from Fig. D.1 that the major differences between these two functions occur at small as well as large r . At $r = 0$, φ_{STO} shows a *cusp* [6(c)], viz.

$$\left. \frac{\partial \varphi_{STO}}{\partial r} \right|_{r=0} = -\alpha \varphi_{STO}(0) \quad (D.5)$$

whereas

$$\left. \frac{\partial \varphi_{GTO}}{\partial r} \right|_{r=0} = 0 \quad (D.6)$$

For large values of r , on the other hand, φ_{GTO} dies out much more rapidly than φ_{STO} . The cusp and the exponential decay shown by the STOs are rigorously desirable attributes. On expanding φ_{STO} in terms of several Gaussians, a good numerical approximation to the former is obtained though the cusp conditions are never satisfied. However, since the required integrals over Gaussian type functions (GTFs) are easily and compactly evaluated by virtue of the Gaussian product theorem [6], these functions are most widely used. The basis functions (termed as *contractions*) are taken as fixed linear combination of primitive Gaussians (PGs) φ_p

$$\varphi_p(\mathbf{r}) = N x_p^l y_p^m z_p^n \exp(-\alpha |\mathbf{r} - \mathbf{R}_p|^2) \quad (D.7)$$

$$\psi_i = \sum_p C_{ip} \varphi_p \quad (D.8)$$

where \mathbf{R}_p is a centre of φ_p and $x_p = x - X_p$ etc.

Let us illustrate the so-called product theorem for two s -type Gaussians [i.e. $l = m = n = 0$ in Eq. D.7], viz.

$$\varphi_s(\mathbf{r}_A) = (2\alpha/\pi)^{3/4} \cdot e^{-\alpha(r-\mathbf{R}_A)^2}$$

and $\varphi_s(\mathbf{r}_B) = (2\beta/\pi)^{3/4} \cdot e^{-\beta(r-\mathbf{R}_B)^2}$

The product of these two is again a Gaussian, viz.

$$\varphi_s(\mathbf{r}_A) \cdot \varphi_s(\mathbf{r}_B) = K_{AB} \varphi_s(\mathbf{r}_C) \quad (D.9)$$

where

$$K_{AB} = [2\alpha\beta/\{(\alpha + \beta)\pi\}]^{3/4} \cdot \exp[-\alpha\beta(\mathbf{R}_A - \mathbf{R}_B)^2/(\alpha + \beta)] \quad (\text{D.10})$$

and

$$\varphi_s(\mathbf{r}_C) = (2\gamma/\pi)^{3/4} e^{-\gamma(\mathbf{r}-\mathbf{r}_C)^2} \quad (\text{D.11})$$

with $\gamma = (\alpha + \beta)$ and $\mathbf{r}_C = (\alpha\mathbf{R}_A + \beta\mathbf{R}_B)/(\alpha + \beta)$; i.e., the centre of the product Gaussian $\varphi_s(\mathbf{r}_C)$ lies on the line joining the centres of the two individual ones. This theorem is illustrated by plotting the two different Gaussians as well as the product of the two in Fig. D.2.

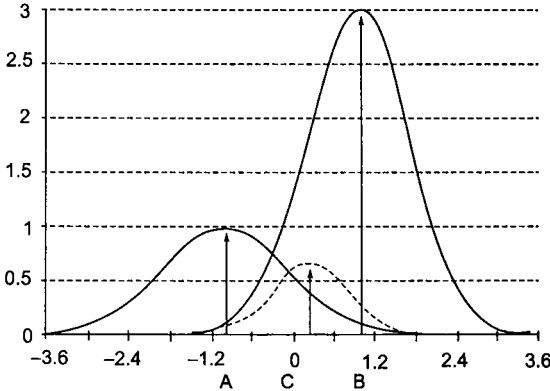


Fig. D.2 A representation of the Gaussian product theorem. The product of the two Gaussians (in one dimension) $\varphi_A(x)$ and $\varphi_B(x)$ is a Gaussian with its centre C on the line joining the centres A and B . The Gaussian centred on A ($x_A = -1.0$) is $\varphi_A = \exp(-0.6 \times (x + 1.0)^2)$ and the one centred on B ($x_B = 1.0$) is $\varphi_B = 3 \times \exp(-(x - 1.0)^2)$.

As a result of the Gaussian product theorem, even the most intricate four-centre two-electron integral is readily reduced to a two-centre one. Such integrals are then easily evaluated using the Gauss transform or Fourier transform method [6].

With the use of basis functions, the HF equations emerge as a set of matrix equations also known as the Roothaan equations. For closed-shell molecules, these are of the form

$$\mathbf{F} \mathbf{C} = \mathbf{E} \mathbf{S} \mathbf{C} \quad (\text{D.12})$$

where \mathbf{F} is the effective one-electron Hamiltonian (matrix) operator, called the Fock operator, \mathbf{S} stands for the overlap matrix and \mathbf{C} denotes the coefficient matrix. A column matrix \mathbf{E} gives the eigenvalues ε_i which were shown by Koopmans to be good approximations to the corresponding ionization potentials. The magnitude of ε_i is thus termed as the Koopmans' or vertical ionization potential.

This treatment for closed-shell systems is termed as the restricted Hartree-Fock (RHF) scheme. The corresponding equations for the open shell case are called as Pople-Nesbet [7] equations and they form the basis of the unrestricted Hartree-Fock (UHF) method.

A major task in the HF calculations is the evaluation of one- and two-electron integrals over the basis. Among these, the two-electron integrals (ERIs) are more computer-intensive and mammoth in number [8]. The evaluation of these integrals forms a real "bottleneck" in *ab initio* HF-SCF programs. It is found convenient to introduce a matrix \mathbf{P} from the corresponding real, occupied MO coefficients, for the RHF method, viz.

$$P_{ij} = 2 \sum_a^{occ} C_{ia} C_{ja} \quad (\text{D.13})$$

The integrals are required along with the density matrix \mathbf{P} (Eq. D.13) to set up the Fock matrix \mathbf{F} given by

$$F_{ij} = h_{ij} + \sum_{k,l}^N P_{kl} \left[\langle ij|kl \rangle - \frac{1}{2} \langle ik|jl \rangle \right] \quad (\text{D.14})$$

where h is the one-electron Hamiltonian, $\langle ij|kl \rangle$ is the ERI and N is the number of basis functions. The ERI $\langle ij|kl \rangle$ for real-valued basis functions $\{\varphi_i\}$ is defined by

$$\langle ij|kl \rangle = \int \varphi_i(1) \varphi_j(1) \frac{1}{r_{12}} \varphi_k(2) \varphi_l(2) d^3 r_1 d^3 r_2$$

Since matrix \mathbf{F} depends on \mathbf{P} and indirectly on \mathbf{C} through Eq. D.13, the Roothaan equation is nonlinear and must be solved iteratively. Equation D.12 is a pseudo-eigenvalue equation since the matrix elements F_{ij} themselves depend on the spatial wave function. Hence, an iterative scheme called self-consistent field (SCF) procedure is required to be followed wherein a new set of coefficients is obtained by diagonalizing the current Fock matrix. From these coefficients, the new density matrix \mathbf{P} is set up and the process continued till convergence. In order to reduce the scheme to a standard eigenvalue problem, viz. $\mathbf{FC} = \mathbf{CE}$, an extra step, viz. orthogonalization of the basis is necessary. The SCF procedure briefly described above is represented in a flow-chart shown in Fig. D.3.

In order to minimize the number of linear coefficients involved (which all need to be optimized) during the SCF scheme, several GTOs are often conveniently grouped together in the form of contractions. The basis sets

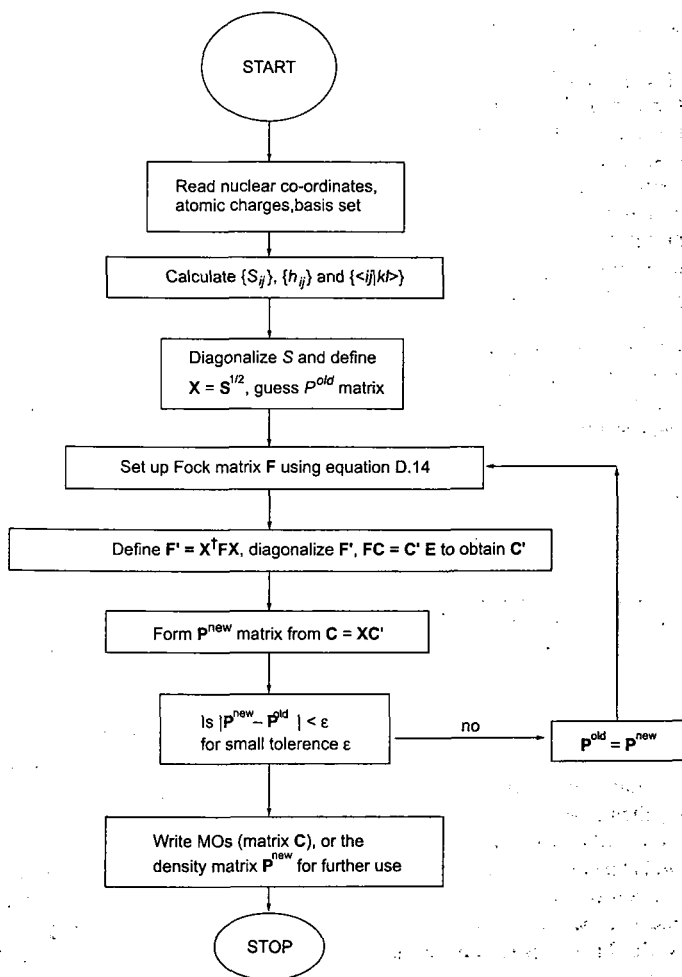


Fig. D.3 A flow chart representing a typical restricted Hartree-Fock program.

are given a label depending upon how many primitive Gaussians and contractions of which type (*s*, *p*, *d*, *f* etc.) are employed. For example, a minimal basis set is one in which only one contraction is used per atomic orbital. Thus, for the H and He atoms, a minimal basis set consists of only one *s*-type contraction. For atoms from Li to Ne, five contractions (one each for 1*s* and 2*s* orbitals, and three for the 2*p* orbitals, i.e. one each for 2*p_x*, 2*p_y*, and 2*p_z*) constitute the minimal basis set. A *double zeta* (DZ) or *triple zeta* (TZ) basis set employs two and three contractions per orbital respectively. These naturally yield better i.e. lower, energy expectation values. For a split-valence basis (SV), the core orbitals are represented by one contraction each whereas two contractions are employed for each valence orbital. In the so-called 3-21G basis set, one contracted Gaussian of three primitives represents the inner shell whereas two contractions (one containing two primitives and another diffuse function containing one primitive with a small value of the exponent) describe the valence shell. The addition of polarization functions to a DZ basis results into DZP type and TZ into TZP one. Similarly, in the 6-31G* basis, additional six *d*-type functions are included (to each atom other than H) over and above those in the 6-31G one. If three more *p*-type functions are added to each H atom, a 6-31G** basis results. The directional effects are better described on inclusion of such polarization functions.

As an illustration, consider 6-31G, 6-31G* and 6-31G** level calculations for the methane molecule. The H atom in a 6-31G basis is represented by 4 primitives (2 contractions: the first with 3 and the other with 1 primitive). The carbon atom has each inner shell of 6 PGs (1*s* orbital) and valence shells (2*s* and 2*p* orbitals) each with 2 contractions (3 and 1 PG respectively) i.e. the total number of contractions for the carbon atom is nine, described in terms of 22 PGs. Thus, a 6-31G level calculation of CH₄ entails 17 contractions and 38 PGs. In a 6-31G* (6-31G**) calculation, this number would be 23(44) and 45(56) respectively.

For more details on Gaussian basis sets, a reference may be made to Szabo and Ostlund [8(a)] and Poirier *et al.* [8(b)]. A worker in molecular quantum mechanics must familiarize himself with the jargon of basis sets and their labels.

Many molecular properties can also be evaluated in terms of closed-form algebraic expressions for the Gaussian orbital basis. For example, the electron density $\rho(\mathbf{r})$ also emerges as a sum of appropriately defined Gaussians within that basis. The corresponding electronic contribution to MESP at \mathbf{r}_2 can be readily evaluated employing the integral transformation

$$\frac{1}{r_{12}} = \frac{1}{\sqrt{\pi}} \int_0^{\infty} s^{-1/2} \exp(-sr_{12}^2) ds \quad (\text{D.15})$$

followed by an integration

$$\int \frac{G_C(\mathbf{r}_1)}{r_{12}} d^3 r_1 \quad (D.16)$$

Here $G_C(\mathbf{r}_1)$ represents a Gaussian centred at \mathbf{C} as a product of two Gaussians at \mathbf{A} and \mathbf{B} . The contributions to MESP due to the products of the Gaussian orbitals centred at \mathbf{A} and \mathbf{B} are tabulated in the following tables.

Table D.1 Electrostatic potential at $\mathbf{r} \equiv (x, y, z)$ due to a product of unnormalized s - and p -type Gaussians at different centres \mathbf{A} and \mathbf{B} . Here, $\mathbf{C} = (\alpha\mathbf{A} + \beta\mathbf{B})/(\alpha + \beta)$.

Type	MESP
$s^A s^B$	$2KF_0$
$s^A p_x^B$	$2K \left[(x - C_x)F_1 + \frac{\alpha}{\alpha + \beta} (A_x - B_x)F_0 \right]$
$p_x^A s^B$	$2K \left[(x - C_x)F_1 + \frac{\beta}{\alpha + \beta} (A_x - B_x)F_0 \right]$
$p_x^A p_x^B$	$K \left[\begin{aligned} & \left[2(\alpha - \beta)(A_x - B_x)(x - C_x) - 1 \right] \frac{F_1}{\alpha + \beta} + 2(x - C_x)^2 F_2 \right] \\ & + \left[1 - \frac{2\alpha\beta}{(\alpha + \beta)} (A_x - B_x)^2 \right] \frac{F_0}{\alpha + \beta} \end{aligned} \right]$
$p_x^A p_x^B$	$2K \left[\begin{aligned} & \left[\alpha(A_y - B_y)(x - C_x) - \beta(A_x - B_x)(y - C_y) \right] \frac{F_1}{\alpha + \beta} \\ & - \frac{\alpha\beta}{(\alpha + \beta)^2} (A_x - B_x)(A_y - B_y)F_0 + (x - C_x)(y - C_y)F_2 \end{aligned} \right]$

where

$$K = \frac{\pi}{\alpha + \beta} \exp \left[\frac{-\alpha\beta}{\alpha + \beta} \sum_{x,y,z} (A_x - B_x)^2 \right];$$

$$F_m = F_m(t) = \int_0^1 u^{2m} \exp(-tu^2) du$$

and $t = (\alpha + \beta)(\mathbf{r} - \mathbf{C})^2$

Table D.2 Electrostatic potential produced by a concentric pair of unnormalized Gaussians. For details of notations, cf. Table D.1.

Type	MESP
$s^A s^A$	$\frac{2\pi}{\alpha + \beta} F_0$
$s^A p_x^A$	$\frac{2\pi}{\alpha + \beta} [(x - A_x) F_1]$
$p_x^A p_x^A$	$\frac{\pi}{\alpha + \beta} \left[\frac{F_0}{\alpha + \beta} - \frac{F_1}{\alpha + \beta} + 2(x - A_x)^2 F_2 \right]$
$p_x^A p_y^A$	$\frac{2\pi}{\alpha + \beta} [(x - A_x)(y - A_y) F_2]$

Apart from the HF-SCF method, more accurate computational methods have been designed starting from HF-related approximation. These include: Configuration Interaction (CI), Multi-Configuration SCF (MC-SCF), Coupled Cluster (CC), Møller-Plesset (MP) Perturbation Theory, etc. [9]. Thus a molecular wave function can be calculated at various levels of theoretical sophistication such as HF, CI, MC-SCF, MP2 or MP4 etc. However, for the study of one-electron properties such as $\rho(\mathbf{r})$, HF-SCF level (implemented at double-zeta polarized basis set) calculations are normally found to be adequate (see page 13 of Ref. [10]). Such a theoretical study is made possible by many 'ready-made' *ab initio* packages, such as GAUSSIAN [11], HONDO [12], MICROMOL [13], TURBOMOLE [14], DISCO [15], INDMOL [16], GAMESS [17], etc. which are available and run on various computational platforms ranging from personal computers, RISC-workstations to parallel/vector architectures.

References

1. M Born and J R Oppenheimer, *Ann. Phys.* **84**, 457 (1927).
2. E Clementi and J Mehl, Symp. Quantum Chem. and Biochem., Israel Academy of Science, Jerusalem (1974).
3. (a) D R Hartree, *Proc. Cambridge Phil. Soc.* **24**, 89 (1928). (b) V Fock, *Z Physik* **61**, 126 (1930). (c) J C Slater, *Phys. Rev.* **35**, 210 (1930). (d) C C J Roothaan, *Rev. Mod. Phys.* **23**, 69 (1951).
4. S T Epstein, *The Variational methods in Quantum Chemistry*, Academic, New York (1974).

5. E Clementi, A D Maclean, D L Raimondi and M Yoshimine, *Phys. Rev.* **133**, A1274 (1964).
6. (a) S F Boys, *Proc. Roy. Soc.* **A200**, 542(1950). (b) I Shavitt in: *Methods in Computational Physics*, eds. B Alder, S Fernbach, and M Rotenberg, Academic, New York (1963) Vol. 2. p.1. (c) A Kato, *Commun. Pure Appl. Math.* **10**, 151 (1957).
7. J A Pople and R K Nesbet, *J. Chem. Phys.* **22**, 571 (1954).
8. (a) A Szabo and N S Ostlund, *Modern Quantum Chemistry: Introduction to Advanced Electronic Structure Theory*, Macmillan, New York, (1982). (b) For a comprehensive introduction and detailed tabulation of basis sets, see R Poirier, R Kari and I G Csizmadia, *Handbook of Gaussian basis sets: A Compendium for Ab initio Molecular Orbital Calculations*, Elsevier, Amsterdam (1985).
9. An excellent overview of many of these methods is included in: E Clementi, Ed. *Modern Techniques in Computational Chemistry, MOTECC-90*, ESCOM, Amsterdam (1990).
10. L C Snyder and H Basch, *Molecular wave functions and properties: tabulated from SCF calculations in Gaussian basis sets*, John Wiley, New York (1972).
11. GAUSSIAN 94: M J Frisch, G W Trucks, H B Schlegel, P M W Gill, B G Johnson, M A Robb, J R Cheeseman, T Keith, G A Paterson, J A Montgomery, K Raghavachari, M A Al-Laham, V G Zakrzewski, J V Ortiz, J B Foresman, J Cioslowski, B F Stefanov, A Nanayakkara, M Challacombe, C Y Peng, P Y Ayaia, W Chen, M W Wong, J L Andres, E S Replogle, R Gomperts, R L Martin, D J Fox, J S Binkley, D J DeFrees, J Baker, J J P Stewart, M Head-Gordon, C Gonzalez, and J A Pople, Gaussian Inc., Pittsburgh, PA, U.S.A. (1995).
12. HONDO: M Dupuis, A Farazdel, S P Karna and S A Maluendes, IBM Corporation, Scientific and Engineering Computations Dept. 48B/428, Kingston, New York 12401, U.S.A.
13. MICROMOL: S M Colwell and N C Handy, University of Cambridge, Cambridge, U. K.; see also S M Colwell, A R Marshall, R D Amos and N C Handy, *Chem. Britain* **21**, 665 (1985).
14. TURBOMOLE: R Ahlrichs, M Bär, M Häser, H Horn and C Kölmel, Electronic structure calculations on workstation computers: the program system TURBOMOLE, *Chem. Phys. Letters* **162**, 165 (1989).
15. DISCO: J Almlöf, K Faegri, M Feyereisen and K Korsell, Electronic Structure Calculations in Quantum Chemistry: Massively Parallel Algorithms, *SIAM News*, p.14, January 1993.
16. INDMOL: The sequential and parallel *ab initio* package developed by Gadre *et al.*; cf. (a) R N Shirsat, A C Limaye, and S R Gadre, *J. Comput. Chem.* **14**, 445 (1993). (b) A C Limaye and S R Gadre, *J. Chem. Phys.* **100**, 1303 (1994).
17. GAMESS: M W Schmidt, K K Baldridge, S T Boatz, S T Elbert, M S Gordon, J J Jensen, S Koseki, N Matsunaga, K A Nguyen, S Su, T L Windus, M Dupuis and J A Montgomery, *J. Comput. Chem.* **14**, 1347 (1993).

Appendix E

Introduction to Semi-empirical Methods

The molecular orbital (MO) theory has been presented in Appendix D with an *ab initio* viewpoint. As seen there, the first step in the *ab initio* HF-SCF method is the evaluation of a large number of integrals over the basis functions. This is followed up by the SCF procedure. The first step, especially the evaluation of the two-electron integrals is a major bottleneck of *ab initio* quantum chemistry. The evaluation of numerous difficult integrals is circumvented in the more approximate treatments, known as *semi-empirical methods*. In these methods, recourse is made of experimental data rather than resorting to rigorous evaluation of integrals. A semi-empirical theory for treating π electron systems viz. the Hückel molecular orbital (HMO) method, has attained the status of a celebrated model in organic chemistry [1]. Within this theory, the σ framework is ignored and only π electrons are explicitly treated. An MO ψ_i is expressed as a linear combination of π -AOs, $\{\phi_p\}$ (cf. Appendix D) i.e. $\psi_i = \sum C_{ip} \phi_p$. For obtaining the MO coefficients $\{C_{ip}\}$ and energies $\{E_i\}$, the roots of the secular determinantal equation $\text{Det}(H_{ij} - ES_{ij}) = 0$ are required. Here $H_{ij} = \int \phi_i^* \hat{H} \phi_j d^3r$ and $S_{ij} = \int \phi_i^* \phi_j d^3r$ denote the Hamiltonian and overlap matrix elements respectively. All the integrals H_{ij} are assumed to be equal, and assigned a parameter α (termed as Coulomb integral). Further, the non-diagonal matrix elements H_{ij} are set equal to a parameter β (called the bond integral) if the orbitals ϕ_i and ϕ_j are on neighbouring atoms; otherwise they are ignored (set equal to 0). The parameter β is assigned appropriate values based on spectroscopic ($\beta \sim 3.5$ eV) or thermodynamic ($\beta \sim 77$ kJ mol⁻¹) measurements. The overlap integrals S_{ij} are approximated as δ_{ij} (δ_{ij} denotes the Kronecker delta). This theory has been extensively applied for obtaining bonding and reactivity features of organic molecules from the 1940s to 1960s.

Several extensions of the Hückel theory have been developed. The one due to Pariser, Pople and Parr (PPP) corrects the shortcomings of HMO in treating the excited states and molecular geometries, still retaining its π electron basis. This approximation is based on the Roothaan equations (cf. Appendix D), with appropriate approximations made while evaluating the one- and two-electron integrals involved. The most noteworthy of these is the zero differential overlap (ZDO) approximation. In the ZDO

approximation, the interaction of the orbitals centered on different atoms is neglected. Under this approximation, the electron repulsion integrals (ERIs) are simplified by the formula

$$\langle ij|kl \rangle = \langle ii|kk \rangle \delta_{ij} \delta_{kl} \quad (\text{E.1})$$

where δ_{ij} denotes the Kronecker delta. The PPP method may thus be viewed as the HMO + SCF approach, with incorporation of CI, if desired. The method has been applied to many chemical problems in the sixties with good success.

In the next phase of development of semi-empirical theories, the extended Hückel theory (EHT) is the most noteworthy. This method is applicable to any conjugated or non-conjugated molecule wherein only valence electrons are treated. EHT is also based on Roothaan's equations, but does not make use of self-consistency. The diagonal elements of the Fock matrix are obtained from the valence-state ionization energies of the respective atoms. For example, the diagonal Fock matrix elements involving $2s$ and $2p$ orbitals of carbon atom are taken to be -21.4 and -11.4 eV respectively, and the one for hydrogen atom $1s$ orbital is, of course, taken as -13.6 eV. The off-diagonal elements are estimated employing

$$F_{ij} = K(F_{ii} + F_{jj})S_{ij}/2 \quad (\text{E.2})$$

where K is an empirical constant and S_{ij} are the overlap integrals. Such an approximation is termed as Wolfsberg-Helmholtz relation[5]. The EHT method proceeds with geometry optimization by minimizing the weighted sum of the occupied orbital energies. Many predictions of MO orbital energies given by EHT were later borne out by *ab initio* calculations. However, it was not found suitable for treating excited states. An important use of EHT is made for generating the initial guess to density matrix within many modern-day *ab initio* packages.

Pople and Dewar pioneered further progress in the semi-empirical methods. Pople and co-workers formulated [6, 7] the complete neglect of differential overlap (CNDO) method in 1965. Here also, (like the EHT) only the valence-shell orbitals of atoms are treated, simplifying ZDO approximation (Eq. E.1). The diagonal and off-diagonal Fock matrix elements (cf. Eq. D.14) within the ZDO framework are given as

$$\begin{aligned}
 F_{ii} &= H_{ii} - \frac{1}{2} P_{ii} \langle ii | ii \rangle + \sum_k P_{kk} \langle ii | kk \rangle \\
 F_{ij} &= H_{ij} - \frac{1}{2} P_{ij} \langle ii | jj \rangle \quad (\text{for } i \neq j)
 \end{aligned}
 \tag{E.3}$$

This approximation greatly simplifies the computation of the wave function, as many of the ERIs are eliminated (all three- and four-centre integrals become zero). For the remaining integrals the use of experimental data is made. Depending on the extent of ZDO approximation, the semi-empirical methods are called as CNDO (complete neglect of differential overlap), MNDO (modified neglect of differential overlap) etc. In the CNDO method developed by Pople *et al.* [6, 7], only valence electrons are treated explicitly, the ZDO approximation is used fully, and the remaining ERIs are approximated as $\langle ii | jj \rangle = \gamma_{AB}$ (for all i on atom A and all j on atom B) where γ_{AB} is the average electrostatic repulsion between any electron on A and any electron on B . For large internuclear distances, $\gamma_{AB} \cong (R_{AB})^{-1}$. Using this, the Fock matrix elements simplify to

$$\begin{aligned}
 F_{ii} &= H_{ii} - \frac{1}{2} P_{ii} \gamma_{AA} + \sum_B P_{BB} \gamma_{AB} \\
 \text{and } F_{ij} &= H_{ij} - \frac{1}{2} P_{ij} \gamma_{AB}
 \end{aligned}
 \tag{E.4}$$

where P_{BB} is the total electron density associated with atom B which is given as $P_{BB} = \sum_{i \in B} P_{ii}$ (where i runs from 1 to all AOs on atom B). Further, the Fock matrix elements expressed in terms of experimental parameters are given by

$$\begin{aligned}
 F_{ii} &= -\frac{1}{2} (I_i + A_i) + \left\{ (P_{AA} - Z_A) - \frac{1}{2} (P_{ii} - 1) \right\} \gamma_{AA} + \sum_{B \neq A} (P_{BB} - Z_B) \gamma_{AB} \\
 F_{ij} &= \beta_{AB} - \frac{1}{2} P_{ij} \gamma_{AB}
 \end{aligned}
 \tag{E.5}$$

where I_i and A_i are experimentally determined ionization potential and electron affinity respectively for i 'th orbital, and Z_A is the core charge of atom

A. Here β_{AB} is a parameter that depends only on the nature of atoms A and B. Using these approximations, an iterative procedure is carried out until self consistency is achieved in the Fock matrix elements. Some other related semi-empirical methods representing improvement over CNDO are also available. Within the INDO (intermediate neglect of differential overlap) method, fewer ERIs are neglected as compared to the CNDO method since interactions of different AOs on the same atom are not neglected. The CNDO and INDO methods yield fairly good bond lengths and bond angles, somewhat erratic dipole moments and poor dissociation (or binding) energies [6, 7].

The MNDO (modified neglect of differential overlap) [8] method given by Dewar is parameterized to yield good geometry as well as binding energies. This method is widely used for calculating properties of organic molecules as well as for scanning the ground-state potential energy surface during a chemical reaction. AM1 (Austin Model 1) is an improved version of MNDO given by Dewar *et al.* [8, 9] to reproduce intermolecular hydrogen bonding in a biological system. The PM3 method [9] is parametrized to give better heats of formation without loss of accuracy in molecular geometry and dipole moments. Thus several semi-empirical methods have been designed to serve different purposes. These methods are available collectively in the form of packages. For instance, MNDO, AM1 and PM3 methods are contained in the package MOPAC. The most widely used semi-empirical packages these days are AMPAC and MOPAC [10, 11]. Thus the wave function employing semi-empirical methods can be obtained for large molecules in reasonable time, and molecular properties including various electronic moments, molecular electron density as well as electrostatic potential can be calculated using this wave function. A brief account of the electrostatic properties obtained from semi-empirical wave functions is given in Chapter 2.

References

1. (a) E Hückel, *Z. Phys.* **70**, 204 (1931); *ibid* **76**, 628 (1932). (b) For a detailed summary of the Hückel theory, see R. McWeeny, *Coulson's Valence*, ELBS, London (1979) and F L Pilar, *Elementary Quantum Chemistry*, McGraw Hill, New York (1990).
2. (a) R Pariser and R G Parr, *J. Chem. Phys.* **21**, 466, 767 (1953). (b) J A Pople, *Trans. Faraday Soc.* **49**, 1475 (1953).
3. R Hoffmann, *J. Chem. Phys.* **39**, 1397 (1963).
4. R Hoffmann and W N Lipscomb, *J. Chem. Phys.* **36**, 2179 (1962); *ibid* **37**, 3489 (1962).

114 *Electrostatics of Atoms and Molecules*

5. B M Wolfsberg and L Helmholtz, *J. Chem. Phys.* **20**, 837 (1952).
6. (a) J A Pople, D P Santry and G A Segal, *J. Chem. Phys.* **43**, S129 (1965).
(b) J A Pople and G A Segal, *J. Chem. Phys.* **43**, S136 (1965); *ibid* **44**, 3289 (1966).
7. For details see J A Pople and D L Beveridge, *Approximate Molecular Orbital Theory*, McGraw-Hill, New York (1970).
8. M J S Dewar, *Science* **187**, 1037 (1975).
9. M J S Dewar, E G Zoebisch, E F Healy and J J P Stewart, *J. Amer. Chem. Soc.* **107**, 3902 (1985).
10. J J P Stewart, *J. Comput. Chem.* **10**, 209 (1989).
11. The package AMPAC, Semichem, Shawnee, Kansas, U.S.A.

Appendix F

Molecular Electron Density and Density Functional Theory

F.1 Molecular Electron Density

Among various molecular properties of chemical interest, the molecular electron density (MED) distribution, $\rho(\mathbf{r})$, has been found to be of great conceptual value. The MED can be extracted from the corresponding many-particle wave function $\psi(\mathbf{x}_1, \mathbf{x}_2, \dots, \mathbf{x}_N)$ as

$$\rho(\mathbf{r}) = N \sum_{\sigma} \int |\psi(\mathbf{x}, \mathbf{x}_2, \dots, \mathbf{x}_N)|^2 d^3r_2 \dots d^3r_N \quad (\text{F.1})$$

Here, the summation runs over all spin coordinates, integration over all but one spatial coordinates (\mathbf{x} stands for position and spin), and N is the total number of electrons. The electron density $\rho(\mathbf{r})$ has a probabilistic interpretation. The probability that an electron is found in an infinitesimally small volume element d^3r around \mathbf{r} is proportional to $\rho(\mathbf{r})d^3r$.

Within the simplest HF framework wherein the wave function ψ is expressed in the form of a Slater determinant constructed from the MOs which are in turn expressed as linear combinations of the AOs $\{\phi_i\}$ (cf. Appendix D), $\rho(\mathbf{r})$ takes the form

$$\rho(\mathbf{r}) = \sum_{\mu\nu} P_{\mu\nu} \phi_{\mu}(\mathbf{r}) \phi_{\nu}^*(\mathbf{r}) \quad (\text{F.2})$$

Here \mathbf{P} is the corresponding charge density bond order matrix. Normally, linear combinations of Gaussians are employed almost by default (cf. Appendix D) in modern quantum chemical programs. Since the product of two Gaussians is another Gaussian, $\rho(\mathbf{r})$ finally emerges as a weighted sum of Gaussians.

The MED $\rho(\mathbf{r})$ fulfills all the requirements for being a faithful descriptor of the structure of a molecule. It has a direct dependence on the corresponding molecular wave function, is invariant to all the unitary transformations of the MOs and represents an observable molecular property that can be determined by a combination of X-ray (cf. Section 2.2) and neutron diffraction experiments [1, 2].

The MED is normally visualized in terms of its three-dimensional isosurfaces or through a set of contours in specified planes. In Fig. F.1 are shown such electron density contour maps for some molecules at their equilibrium geometries. Figure F.1(a) depicts the MED contour map for the H_2 molecule. It may be noticed that the MED contours are almost spherical in the vicinity of the nuclei. However, a clear indication of the build-up of charge density is seen in the so-called 'bonding region'. Similar contour maps for the Li_2 and N_2 molecules are depicted in Figs. F.1(b) and F.2(a) respectively.

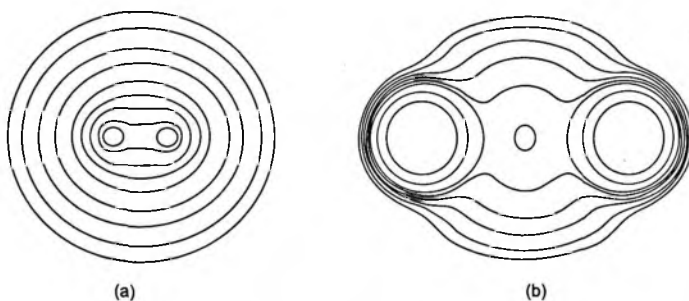


Fig. F.1 *Electron density contours for (a) H_2 (the contour values from outward direction to atom centres are 0.002, 0.004, 0.01, 0.02, 0.05, 0.09, 0.15, 0.25 and 0.32 a.u. respectively) and (b) Li_2 (the corresponding contour values are 0.004, 0.0047, 0.006, 0.0075, 0.01, 0.012, 0.028 and 0.1 a.u. respectively) molecules in a plane containing the internuclear axis.*

The general characteristics of MEDs noted above are clearly borne out by these cases as well. A particularly noteworthy distinctive feature is exhibited by the Li_2 molecule, in contrast to the MED contours of H_2 and N_2 . The contours engulfing both the nuclei display an inward dip for H_2 and N_2 whereas those for Li_2 show an outward 'bulge'. This feature is displayed by only a few other molecules and has been termed *non-nuclear maximum* in recent literature [3, 4]. The MED contour map for the lithium fluoride molecule is displayed in Fig. F.2(b). What happens on pulling the atoms in LiF apart has been discussed in a classic paper by Wahl *et al.* [5]. They have pictorially demonstrated that around the equilibrium bond length, the contour maps (Fig. F.2(b)) resemble those of Li^+ and F^- superposed together. However, at large internuclear separations, the contour maps appear as though they are superpositions of the corresponding *atomic* ones.

Going further to a typical polyatomic molecule, viz. H_2O , similar features are seen in the MED contour maps (Fig. F.3). Figure F.3(a) describes the MED distribution in the plane of the molecule, whereas that in the perpendicular plane passing through the O atom is shown in Fig. F.3(b). It may be noticed, however, that in the latter figure, there is no trace of the so-called 'rabbit ears' (viz. the lone pairs) of the water molecule!

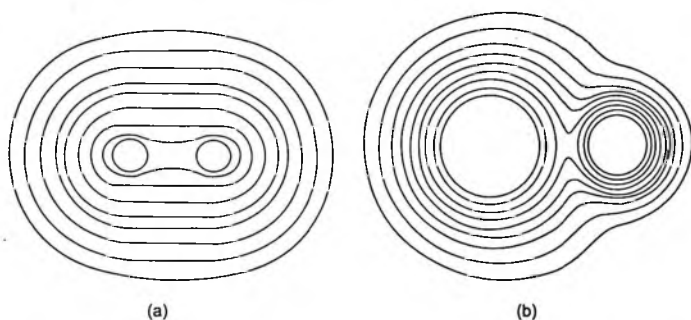


Fig. F.2 Electron density contours for (a) N_2 (the contour values from outward direction to atom centres are 0.0033, 0.008, 0.02, 0.05, 0.09, 0.2, 0.4, 0.64 and 1.3 a.u. respectively) and (b) LiF (the corresponding contour values are 0.0022, 0.006, 0.014, 0.025, 0.04, 0.07, 0.11, 0.2 and 0.32 a.u. respectively) molecules in a plane containing the internuclear axis.

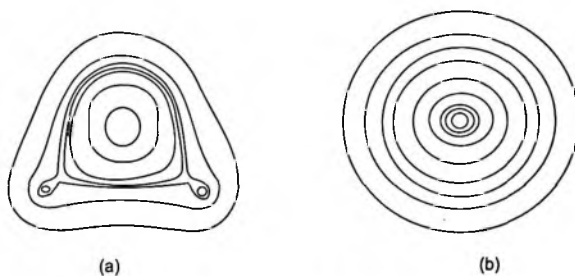


Fig. F.3 Electron density contours for (a) H_2O molecule in the molecular plane (the contour values from outward direction to centre of oxygen atom are 0.1, 0.25, 0.39, 0.415, 0.5, 0.8 and 4.0 a.u. respectively) and (b) H_2O molecule in a plane perpendicular to the molecular plane.

F.2 Density Functional Theory

An alternative approach, and certainly an attractive one, to the wave function-based treatments such as HF-SCF, CI or MP2 is offered by the density functional theory (DFT). Foundations of DFT [6, 7] have been laid in the last thirty years, though it is beginning to be utilized extensively for computational purposes only since 1990 or so. It offers substantial computational advantage over the HF-SCF, CI or MP2 methods and has been found to be particularly useful for a study of large molecules and clusters. DFT employs the MED as a basic variable for describing the ground states of atoms, molecules and solids. Though several functionals of $\rho(\mathbf{r})$ have historically been employed for atomic and molecular systems (e.g. the Thomas-Fermi model and its numerous variants), the DFT was formally born with the seminal contribution of Hohenberg and Kohn (HK) [6].

Hohenberg and Kohn [6] showed in 1964 that for the non-degenerate ground state of a collection of electrons moving under the influence of an external potential V and their mutual repulsion, the electron density $\rho(\mathbf{r})$ is a unique functional of V and conversely. A functional is defined as a one-one or many-one map from a set of functions to a set of numbers (or functions). For example, $\int \rho(\mathbf{r})d^3r$ or $\int \rho^{5/3}(\mathbf{r})d^3r$ are functionals of $\rho(\mathbf{r})$. Similarly, the energy expectation value that is used in the Rayleigh-Ritz variational principle, viz. $\int \psi^* \hat{H} \psi d^3r / \int \psi^* \psi d^3r$ is a functional of the trial wave function ψ , where \hat{H} denotes the Hamiltonian operator.

As a consequence of the first HK theorem, the ground state energy, $E[\rho]$, and in fact all the ground state properties, turn out to be functionals of the ground state $\rho(\mathbf{r})$. The energy functional $E[\rho]$ can hence be expressed as a sum of a universal functional, $F[\rho]$ and the interaction energy of the electron density with the so-called external potential $V(\mathbf{r})$, viz. $E_v[\rho] = \int V(\mathbf{r})\rho(\mathbf{r})d^3r + F[\rho]$. The functional $F[\rho]$ is a universal one since it does not depend on the external potential. This functional is in fact the sum of the kinetic energy and electron-electron repulsion functionals viz. $F[\rho] = T[\rho] + V_{ee}[\rho]$. If the universal functional $F[\rho]$ is known (that is a big 'if' indeed!), it provides a variational framework, viz. $E_v[\rho_{g.s.}] \leq E_v[\rho]$, for an arbitrary trial density ρ , which obeys certain conditions. The equality in the above variational bound is attained for $\rho = \rho_{g.s.}$. This is the second HK theorem which leads to an operational variational equation

$$\delta\{E_v[\rho] - \mu \int \rho(\mathbf{r})d^3r\} = 0 \quad (\text{F.3})$$

for determining the electron density by minimization of the energy functional subject to the condition of the constancy of the number of electrons. The Lagrange parameter μ in Eq. F.3 is called the chemical potential, in analogy with classical thermodynamics.

Although these theorems have placed the DFT on a firm footing, it should be pointed out that they are only existence type results. They do not provide us with the form of the energy functional. The search for the exact HK functional has been going on for decades. However, now it seems to be generally agreed that such an exact form may never be found! The stress in contemporary work is on finding practically more accurate descriptions of the energy functional for atoms, molecules and solids.

A practical, orbital-based DFT method for the determination of $\rho(\mathbf{r})$ is offered by the Kohn–Sham (KS) scheme [8]. This treatment is somewhat similar in spirit to the Hartree–Fock theory. The ground state energy within the KS method is given by

$$E[\rho] = -\frac{1}{2} \sum_i \int \psi_i(\mathbf{r}) \nabla^2 \psi_i(\mathbf{r}) d^3r - \sum_\alpha Z_\alpha \int \frac{\rho(\mathbf{r})}{|\mathbf{r} - \mathbf{r}_\alpha|} d^3r + \frac{1}{2} \iint \frac{\rho(\mathbf{r})\rho(\mathbf{r}')}{|\mathbf{r} - \mathbf{r}'|} d^3r d^3r' + E_{xc}[\rho] \quad (\text{F.4})$$

Here, ψ_i 's (assumed to be real) denote the so-called Kohn–Sham orbitals, yielding the ground state density, $\rho(r) = \sum_{i=1}^{occ} |\psi_i(r)|^2$ and the first term on the r.h.s. represents the *non-interacting* (Kohn–Sham) kinetic energy. The second term stands for nuclear–electron interaction and the third one denotes the direct Coulomb repulsion of the electrons. The last term is the so-called exchange–correlation energy i.e. the non-classical part of the electron–electron interaction. The KS equations are obtained by minimizing the energy functional in Eq. F.4 where $\rho(\mathbf{r})$ is given in terms of the KS orbitals $\{\psi_i\}$ as seen above. The KS equations are expressed as

$$\left\{ -\frac{1}{2} \nabla^2 - \sum_\alpha \frac{Z_\alpha}{|\mathbf{r} - \mathbf{r}_\alpha|} + \int \frac{\rho(\mathbf{r}') d^3r'}{|\mathbf{r} - \mathbf{r}'|} + V_{xc}(\mathbf{r}) \right\} \psi_i(\mathbf{r}) = \epsilon_i \psi_i(\mathbf{r}) \quad (\text{F.5})$$

Here, $\{\epsilon_i\}$ denote the orbital energies. $V_{xc}(\mathbf{r})$ in Eq. F.5 is the functional derivative of the exchange–correlation energy, viz. $V_{xc} = \delta E_{xc}[\rho] / \delta \rho$ (See [7] for the definition of functional derivatives). The form of Eq. F.5 resembles

that of the Hartree–Fock equations. However, there are a few subtle differences. The KS orbitals have no particular physical significance, except that they allow a computation of $\rho(\mathbf{r})$ as pointed out above. There is no ‘molecular wave function’ defined within the KS framework. For example, the ‘wave function’ cannot be obtained by stacking the KS orbitals in a Slater determinant form or otherwise. Furthermore, the orbital energies $\{\varepsilon_i\}$ do not represent the Koopmans’ ionization potential. They, on the other hand, obey an interesting theorem, called Janak’s theorem, viz. $\partial E/\partial n_i = \varepsilon_i$ [7]. The problem again, as with the Hohenberg–Kohn treatment, is that $E[\rho]$ is not exactly known. This ignorance gets naturally reflected in the exchange correlation functional, $E_{xc}[\rho]$ and hence in the corresponding potential, $V_{xc}(\mathbf{r})$. Further, the sum $\sum_i \langle \psi_i | -\frac{1}{2}\nabla^2 | \psi_i \rangle$ (called $T_s[\rho]$, the Kohn–Sham kinetic energy) does not represent the entire kinetic energy [7].

Many approximate functional forms of $E_{xc}[\rho]$ are hence being explored for a study of atoms, molecules and solids [7, 9]. A particularly popular method in earlier literature was the so-called local density approximation, wherein $E_{xc}[\rho]$ is expressed as

$$E_{xc}[\rho] = \int \rho(\mathbf{r}) \varepsilon_{xc}(\mathbf{r}) d^3r \quad (\text{F.6})$$

Here, $\varepsilon_{xc}(\mathbf{r})$ is the exchange correlation energy per electron of a homogeneous electron gas with density $\rho(\mathbf{r})$. In retrospect, it may be commented that Slater’s X_α method, extremely popular in the sixties and seventies, was one of the earlier schemes of this type. More accurate (and, needless to say, more complicated!) functionals are now being developed, the most popular one at the time of writing this monograph being the B3LYP [14, 15] (Becke, Lee, Yang and Parr). Two local functionals employed in the GAUSSIAN 94 package share the Slater terms for exchange but differ in the treatment of correlation: one by Vosko–Wilk–Nusair [10] and the other by Perdew [11]. A non-local method in the package combines the Becke [12] and Perdew [13] functionals for exchange and correlation respectively. The package further offers three non-local DFT methods sharing Becke’s [14] functional for exchange while the correlation is described by Perdew [11], Lee–Yang–Parr [15] and Perdew–Wang [16] functionals. DFT is thus closer in spirit to *ab initio* methods than to semi-empirical ones since it generally does not employ experimental parameters (except in the calculation of some functionals wherein some experimental data is employed). The DFT is being increasingly utilised since 1990 for molecular calculations.

F.3. Topographical Features of MED

From the computational view point, it is very easy to calculate the MED, $\rho(\mathbf{r})$, once the molecular wave function is available [17]. The MED is a real, non-negative and continuous scalar function of the position vector \mathbf{r} and allows a visual distinction between different (reactive) sites in the molecule. The quantitative characterization of this scalar field is carried out by topographical investigations (see Appendix G for an introduction to topography). Bader *et al.* [21] in their pioneering work have successfully exploited the topography of $\rho(\mathbf{r})$ and the details of the Laplace field $\nabla^2\rho(\mathbf{r})$ for a crisp and compact description of molecular structure. It may be noted that at every (point) nucleus, MED attains a maximum. Further, due to the cusp condition, the $\nabla\rho(\mathbf{r})$ is discontinuous at the nucleus and does not qualify to be a 'true' (3, -3)-type critical point (CP) (cf. Appendix G). However, there exists a function homeomorphic to $\rho(\mathbf{r})$ which is identical to the latter almost everywhere but possessing true (3, -3) CPs at the nuclei. Their studies have revealed [4, 21] that a chemical bond is represented by a (3, -1) CP, a ring in a molecular frame shows a (3, +1) signature and a cage gives rise to a (3, +3) CP in $\rho(\mathbf{r})$. Some simple examples are presented in Fig. F.4, to illustrate the topography of the MED. Figure F.4(b) depicts the MED CPs for the formaldehyde (H_2CO) molecule wherein the (pseudo) (3, -3) CPs at the nuclei and the (3, -1) bond saddles are seen. Conspicuous by their absence are (3, +3) minima denoting the lone pairs.

Figure F.4(a) shows the MED maxima at the nuclei and the (3, -1) bond CP for the HF molecule. In Fig. F.5 the MED topography for diborane (B_2H_6) and cyclopropane (C_3H_6) molecules is depicted. Apart from the maxima at the nuclei and the (3, -1) bond saddles, the (3, +1) ring CPs are seen in this figure. Cage CPs, viz. (3, +3) minima make their appearance for molecules such as cubane.

As seen above, the scalar field of MED exhibits a rather simple topographical pattern. Further important and useful features could be unearthed by studying the Laplacian of $\rho(\mathbf{r})$ viz. $\nabla^2\rho(\mathbf{r})$. It has been pointed out [19] that the region where $\nabla^2\rho(\mathbf{r}) < 0$, shows charge concentration whereas the region where $\nabla^2\rho(\mathbf{r}) > 0$ describes charge depletion. Detailed investigations of the Laplace field of $\rho(\mathbf{r})$ are carried out for atomic as well as molecular systems [4, 18]. Chemical applications such as locating sites of electrophilic attack with the help of $\nabla^2\rho(\mathbf{r})$ are also reported in the literature [18].

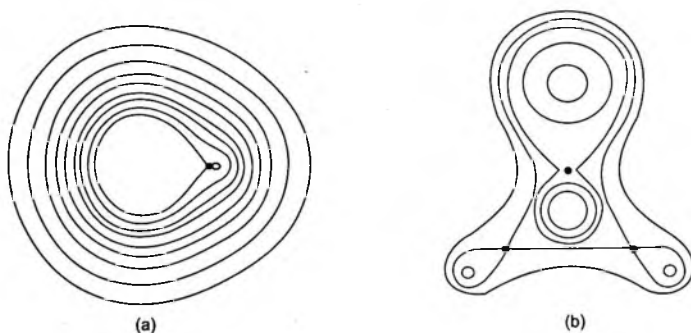


Fig. F.4 Electron density contours for (a) HF molecule (the contour values from outward direction to atom centres are 0.0015, 0.0055, 0.015, 0.03, 0.053, 0.1, 0.15, 0.25 and 0.4 a.u. respectively) showing maxima at nuclei and (3, -1) bond CP (•) near H atom and (b) Formaldehyde (H_2CO) molecule in the molecular plane showing maxima at nuclei and (3, -1) bond CPs. The corresponding contour values are 0.2, 0.297, 0.42, 0.8 and 3.0 a.u. respectively.

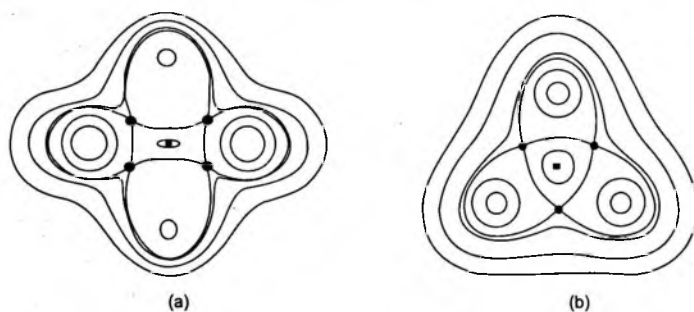


Fig. F.5 Electron density contours for (a) B_2H_6 molecule in the plane containing two boron (on X-axis) and two hydrogen atoms. The contour values from outward direction to atom centre are 0.05, 0.08, 0.114, 0.12, 0.35 and 2.0 a.u. respectively. (b) C_3H_6 molecule in the plane containing three carbon atoms. The bond CPs are shown by • and ring CPs by ◻. The corresponding contour values are 0.06, 0.12, 0.22, 0.25, 0.5 and 8.0 a.u. respectively.

Other parameters such as bond ellipticity [4, 18] and bond order which are expressed in terms of eigenvalues of the Hessian matrix and electron density at the corresponding bond CP are useful in the study of molecular

structure. The bond ellipticity (ε) is given as $\varepsilon = (\lambda_1/\lambda_2 - 1)$ where λ_1 and λ_2 are the eigenvalues ($\lambda_1, \lambda_2 < 0$) (cf. Appendix G) at the bond CP. For a (partial) π bond it turns out that $\varepsilon > 0$ and for a triple bond it is close to zero. The ellipticity has been found useful for describing π character of a bond and further constructing the bond paths. The value of $\rho(\mathbf{r})$ at the bond CP has been used to determine the bond order (n) by an empirical equation [4],

$$n = \exp[a \rho(\mathbf{r}) - b]$$

where a and b are constants. For the case of hydrocarbons, these constants are determined so that the n values of 1, 2 and 3 are obtained for ethane, ethylene and acetylene respectively. Further, the position of a bond CP gives the measure of bond polarity [7]. Collard and Hall [20] have pointed out that a change in structure is reflected in the variation in the number and nature of CPs in $\rho(\mathbf{r})$. In such a case, the system must pass through a catastrophe point. In particular, Bader *et al.* [21] have studied the nature of catastrophes during the C_{2v} dissociation of H_2O molecule. The same reaction has been investigated by exploring the topography of momentum space electron density by Kulkarni and Gadre [22]. In summary, molecular structural parameters and reactivity patterns can be elucidated with the help of the MED and its topography.

References

1. P Becker, *Electron Density and Magnetization Densities in Molecules*, Nato Advanced Study Institutes, series B: Phys. Vol. 48, Plenum, New York (1980).
2. (a) P Coppens and M B Hall, *Electron Density Distribution and the Chemical Bond*, Plenum, New York (1981). (b) P Coppens, *J. Phys. Chem.* **93**, 7979 (1989).
3. W L Cao, C Gatti, P J McDougall and R F W Bader, *Chem. Phys. Letters* **141**, 380 (1987).
4. R F W Bader, *Atoms in Molecules: a Quantum Theory*, Clarendon, Oxford (1990).
5. A C Wahl, P Bertoincini, K Kaiser and R Land, *Intern. J. Quantum Chem. Symp.* **3**, (Part II), 499 (1970); A C Wahl, *Science* **151**, 961 (1966).
6. P Hohenberg and W Kohn, *Phys. Rev.* **136**, B864 (1964).
7. R G Parr and W Yang, *Density Functional Theory of Atoms and Molecules*, Oxford, New York (1989).
8. W Kohn and L J Sham, *Phys. Rev.* **140**, A1133 (1965).

124 *Electrostatics of Atoms and Molecules*

9. (a) S Borman, *Chem. Eng. News* p 2 (1990). (b) T Ziegler, *Chem. Rev.* **91**, 651 (1991).
10. S H Vosko, L Wilk and M Nusair, *Can. J. Phys.* **58**, 1200 (1980).
11. J P Perdew and A Zunger, *Phys. Rev.* **B23**, 5048 (1981).
12. A D Becke, *Phys. Rev.* **A38**, 3098 (1988).
13. J P Perdew, *Phys. Rev.* **B33**, 8822 (1986).
14. A D Becke, *J. Chem. Phys.* **98**, 5648 (1993).
15. C Lee, W Yang and R G Parr, *Phys. Rev.* **B37**, 785 (1988).
16. J P Perdew and Y Wang, *Phys. Rev.* **B45**, 13244 (1992).
17. M Breitenstein, H Dannohl, H Meyer, A Schweig, R Seeger, U Seeger, W Zittlau, *Int. Rev. Phys. Chem.* **3**, 335 (1983).
18. K Kraka and D Cremer, in *Theoretical Models of Chemical Bonding Part 2, The Concept of the Chemical Bond*, Ed. Z. B. Maksić, Springer, New York (1990).
19. P M Morse and H Feschbach, *Methods of Theoretical Physics*, McGraw Hill, New York, Vol. 1, p.6 (1953).
20. K Collard and G G Hall, *Intern. J. Quantum Chem.* **12**, 633 (1979).
21. R F W Bader, T T Nguyen-Dang and Y Tal, *J. Chem. Phys.* **70**, 4316 (1979).
22. S A Kulkarni and S R Gadre, *J. Amer. Chem. Soc.* **115**, 7434 (1994).

Appendix G

Topographical Concepts

The geographical topographical maps are familiar to all of us normally from our school days. The dictionary meaning of the word *topography* (Greek *topos* = place + *graphia* = mapping) is: a detailed description (mapping) of a small area. Such a map usually describes the physical features of a region by showing contours representing elevation [1] and noting various other features such as roads, streams, etc. Mathematically, such contours are curves of the type $h(x, y) = \text{constant}$ where h is the elevation. Figure G.1 shows the relation between the heights of two hills with an adjoining valley and the corresponding topographical contour map. It may be seen that the hill-tops A and B reduce to the innermost points in the contour map. The contours representing heights of 400 m and above are disjoint. However, those depicting 300 m and lower values engulf both the peaks. Such maps offer a convenient means for the depiction of a function of several variables.

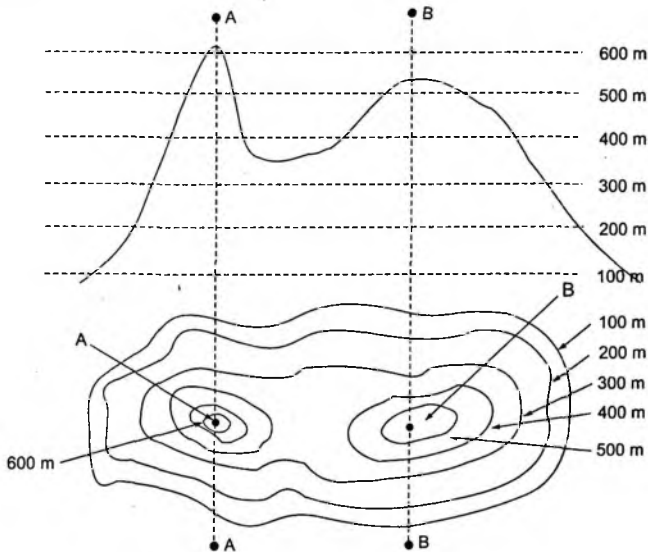


Fig. G.1 A schematic topographical map of two hills and the adjoining valley. Six contours with heights from 100 m to 600 m are shown.

Topography is widely employed for investigating potential energy surfaces which are useful in the studies of reaction dynamics. Further, a topographical approach employing the values of the electronic energy and its partial derivatives is found useful in locating minima while implementing geometry optimization of molecules. Special methods are used for locating transition states which are so crucial for studying reaction mechanisms and chemical dynamics. In this monograph, we have depicted contour maps of the scalar fields, such as the electron density, electrostatic potential, bare-nuclear potential, etc. for a variety of molecules.

The detailed topographical features of a scalar function $f(x_1, x_2, \dots, x_n)$ of several variables are quantitatively described in terms of its first and second order partial derivatives. In particular, these features may be summarized by the number and nature of the critical points (CPs). A CP, P , is a point at which all the first order partial derivatives of the function (assuming differentiability) or the gradient of the field is zero, viz.

$$\nabla_i f(x_1, x_2, \dots, x_n)|_P = 0$$

$$\text{i.e. } \left. \frac{\partial f}{\partial x_i} \right|_P = 0 \text{ for } i=1, 2, \dots, n \quad (\text{G.1})$$

Thus, the CPs for a given scalar field may be located by minimizing the magnitude of the first partial derivatives of it with respect to the variables. The nature of a CP is decided by the signs of eigenvalues of the corresponding Hessian matrix at that CP. The elements of the Hessian matrix (for a general discussion, see Ref. [2–5]) are given by

$$H_{ij} = \left. \frac{\partial^2 f}{\partial x_i \partial x_j} \right|_P \quad (\text{G.2})$$

If none of the eigenvalues of the Hessian matrix is zero, then that particular CP is said to be non-degenerate. On the other hand, a CP for which at least one of the eigenvalues of the Hessian matrix is zero, is called a degenerate one. A non-degenerate CP is characterized by two numbers, R (rank) and σ (signature). Here the former stands for the number of non-zero eigenvalues at the CP whereas the latter denotes the excess of the positive eigenvalues

over the corresponding negative ones. The CP is then labelled as an (R, σ) CP. In the case of a function of two variables, $f(x, y)$, consider a non-degenerate CP, viz. $R = 2$. There are only three possible σ values: $-2, 0$ and $+2$, representing a maximum, saddle and minimum respectively. For a function of three variables, $f(x, y, z)$, the rank of a non-degenerate CP is 3 and the signature σ can assume only four different values: $-3, -1, +1$ and $+3$, as there are only three eigenvalues for such a Hessian matrix. This results in four types of non-degenerate CPs, viz. $(3, -3), (3, -1), (3, +1)$ and $(3, +3)$. The $(3, -3)$ CP is one at which all three eigenvalues are negative, corresponding to a local maximum of the function. The CPs of the type $(3, -1)$ and $(3, +1)$ denote saddle points while a $(3, +3)$ CP represents a local minimum in the function.

We now consider several simple examples in one and two dimensions in order to illustrate the degenerate and non-degenerate CPs.

- i) For the function $f(x) = -x^2, f'(0) = 0$. Hence $x = 0$ is a critical point. However, $f''(0) = -2$. Hence $x = 0$ is a non-degenerate CP, which is actually a maximum.
- ii) Let $g(x) = -x^4$. Here, $g'(0) = g''(0) = 0$. Therefore, $x = 0$ represents a degenerate CP, viz. a maximum, since the function is negative at all the points in the neighbourhood of $x = 0$ whereas $g(0) = 0$. It may be noted that the 'usual criterion of $g'' < 0$ ' for a maximum fails here since the CP under reference happens to be a degenerate one.
- iii) Consider $h(x, y) = x^2y^2$ for which $h_x = \partial f / \partial y = 2xy^2$ and $h_y = \partial f / \partial x = 2x^2y$. Thus, the lines $x = 0$ and $y = 0$ represent the CPs. The corresponding Hessian matrix is given by

$$H = \begin{bmatrix} 2y^2 & 4xy \\ 4xy & 2x^2 \end{bmatrix}$$

The CP at $(0, 0)$ is thus a degenerate one. By inspection, one may verify that it is a *degenerate minimum*.

- iv) For the function $r(x, y) = x^3 - 3xy^2$; $r_x = \partial r / \partial x = 3x^2 - 3y^2$; $r_y = \partial r / \partial y = -6xy$. Thus, there is an (isolated) CP at $(0, 0)$. The corresponding Hessian matrix is $\begin{bmatrix} 6x & -6y \\ -6y & -6x \end{bmatrix}$, the determinant of which vanishes at $(0, 0)$. Thus this CP is also degenerate.

An interesting result regarding non-degenerate CPs is given by Morse's lemma, which states that a non-degenerate CP is necessarily isolated. Example (i) above illustrates this lemma. Is the converse of this theorem true? That is, is every isolated CP always a non-degenerate one? The answer to this question is certainly in the negative. This is exemplified by the case (iv) above where the CP at $(0, 0)$ is indeed an isolated one, but is still degenerate.

A useful way of describing the nature of a function is given by the so-called *phase portraits*. Here, the nature of the function is scrutinized in the vicinity of critical points and depicted with the help of arrows and curves which point in the direction of increase of the function. Figure G.2 shows the qualitative phase portraits for non-degenerate CPs A, B, C of the types $(2, -2)$, $(2, +2)$ and $(2, 0)$ respectively. The first one (Fig. G.2(a)) is a maximum and hence, all the arrows in its neighbourhood are seen to point towards it. Similarly, all the arrows point away from the point B in Fig. G.2(b). However, Fig. G.2(c) represents a mixed pattern in this respect since it depicts a saddle of type $(2, 0)$.

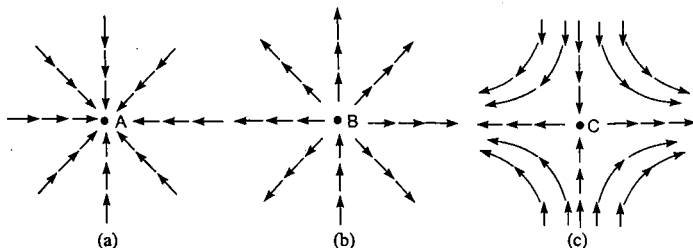


Fig. G.2 Phase portraits for $(2, -2)$, $(2, +2)$ and $(2, 0)$ critical points A, B and C respectively. The arrows point in the direction of increase of the function.

As seen earlier, a function of two variables has three possible CPs of rank 2, viz. $(2, +2)$ minimum; $(2, -2)$ maximum and $(2, 0)$ saddle. If the numbers of these CPs are denoted as n_{+2} , n_{-2} and n_0 respectively, then a non-negative, well-behaved function (such as the electron density or electron momentum density) obeys [5] the so-called Hopf–Poincaré theorem, viz.

$$n_{+2} - n_0 + n_{-2} = 1 \quad (\text{G.3})$$

As an example of a simple function of three variables in which a non-degenerate CP occurs, consider $f(x, y, z) = ax^2 + by^2 + cz^2$ where a , b and c are *distinct non-zero real numbers*. This function has for its partial

derivatives, $f_x = 2ax$, $f_y = 2by$ and $f_z = 2cz$. All these first order partial derivatives are zero at the point $(0, 0, 0)$ indicating the occurrence of a CP at $(0, 0, 0)$. The matrix of second order partial derivatives (Hessian matrix) is

$$H = \begin{bmatrix} H_{xx} & H_{xy} & H_{xz} \\ H_{yx} & H_{yy} & H_{yz} \\ H_{zx} & H_{zy} & H_{zz} \end{bmatrix} = \begin{bmatrix} 2a & 0 & 0 \\ 0 & 2b & 0 \\ 0 & 0 & 2c \end{bmatrix}$$

It can be seen from the elements of this Hessian matrix that it is a diagonal matrix with non-zero diagonal elements, implying that the CP is a non-degenerate one with rank 3. The nature of the CP is decided by the signs of a , b and c .

A function of three variables, viz. $f(x, y, z) = -x^4 y^4 z^4$ provides an example of a degenerate CP. The function f shows a CP at $(0, 0, 0)$ with all the eigenvalues of the Hessian matrix equal to zero; the CP is thus a degenerate one and the function shows a numerical maximum at $(0, 0, 0)$ though it is not a $(3, -3)$ CP.

In three dimensions, the numbers of non-degenerate CPs of a non-negative function obey the Hopf–Poincaré relation, viz.

$$n_{+3} - n_{+1} + n_{-1} - n_{-3} = 1 \quad (\text{G.4})$$

Here, a notation similar to the one used above is employed, viz. n_{+3} stands for the number of CPs of type $(3, +3)$ etc.

Studies on topography of the molecular electron density have been pioneered by Bader and co-workers [6]. These studies have led to valuable insights on bonding and electron localization features in molecules. The topographical concepts have been widely employed in chemistry including quantum chemistry and crystallography for extracting these two features. Bader *et al.* have also investigated, in detail, the change in the number and nature of critical points in the scalar field of molecular electron density during the course of several chemical reactions. For some specific examples of applications of topographical concepts to MED, see Appendix F. Study of such a change, in general, forms the basis of catastrophe theory [7]. In this theory, the discontinuities of an appropriate scalar field are isolated and analyzed. As Thom [7] puts it, "We must concede that the universe we see is a ceaseless creation, evolution and destruction of forms, and that the purpose of science is to foresee this change of form and, if possible, explain it".

References

1. *Van Nostrand's Scientific Encyclopedia*, Ed. D. M. Considine, van Nostrand Reinhold, New York (1976).
2. I Stewart, *Sci. Amer.* **264**, 123 (1991) (This reference presents an enjoyable introduction to topographical concepts written in the style of Gulliver's Travels).
3. (a) T Poston and I Stewart, *Catastrophe Theory and its Applications*, Pitman, London (1978). (b) T Poston and I Stewart, *Taylor Expansions and Catastrophes*, Research notes in mathematics: 7, Pitman, London (1976).
4. P T Saunders, *An Introduction to Catastrophe Theory*, Cambridge University press, Cambridge (1980).
5. K Collard and G G Hall, *Intern. J. Quantum Chem.* **12**, 623 (1977).
6. See, R W F Bader, *Atoms in Molecules: A Quantum Theory*, Oxford University Press, Oxford (1990) and references therein.
7. R Thom, *Structural Stability and Morphogenesis*, Benjamin, New York (1975).

Index

A

ab initio packages 108
DISCO, GAMESS,
GAUSSIAN,
HONDO, INDMOL,
TURBOMOLE, MICROMOL
acetylene 34, 58
Alhambra-Luque-Orozco model 68
ammonia 55
ammonium nitrate 71
AMPAC 113
anions 51–54
atomic orbitals 101
atomic units 8, 90
Austin model-1 (AM1) 113

B

ball-and-stick models 33
Balázs' theorem 42–44
banana bonds 57
bare-nuclear potential 17, 47
 similarity with electron density 47
 similarity with electrostatic
 potential 47–48
Becke–Yang–Lee–Parr
 (BLYP) functional 120
benzene molecule 34, 35, 57, 58
bond ellipticity 123
bond order 115
bond polarity 123
Born–Oppenheimer
 approximation 100
Buckingham–Fowler model 67

C

catalysis 72
catastrophe theory 123, 129
cationic radius 54

charge density bond order matrix 115
charges
 Löwdin 22
 Mulliken 22
 potential-derived atomic
 charges (PD-AC) 22
complete neglect of differential overlap
 (CNDO) 111, 113
conservation of charge 2
contour 8
contour plots 8
contracted Gaussian functions 106
Coulomb's Law 1
 experimental verification 2, 3
Coulombic forces 3, 4
covalent radius 54
critical point (CP) 126
 degenerate 58, 126, 129
 rank 126, 129
 signature 126, 129
cumulative atomic multipole
 moments (Camm) 21
cusp condition 102, 121
cyanide ion 52
cyclopropane 47, 57, 121
cylindrical co-ordinates 97, 98
cytosine 35, 64

D

decane 35
decavanadate ion, $[V_{10}O_{28}]^{6-}$ 34
degenerate critical point 56, 126–128
density functional theory (DFT) 20, 118
 Hohenberg–Kohn theorem 118
 Kohn–Sham scheme 119
density matrix 104
diazirine 47
diborane 121
dipole moment 8, 9
distributed multipole moments
 (DMM) 67
divergence theorem 14

132 *Electrostatics of Atoms and Molecules*

divergence theorem 14
drugs 79
DZ, DZP, DZ2P (Gaussian)
basis set 106

E

Earnshaw's theorem 16
electric field 8
energy 14, 15
point charge 11
electron affinity 54
electronegativity 46
electron momentum density 123
electron repulsion integrals (ERI) 111
electronic energy 44
molecules 45
electrophilic attack 63
electrostatic field 4–8, 72
electrostatic potential 6–9, 16
electronegativity 54
at nuclei 44
continuous charge
distribution 12
point charges 6–9
EPIC model 68
ethylene 59
enzymes 73
equipotential surface 7, 8
exchange-correlation potential 119
extended Hückel method 111

F

Fermi momentum 40
fluoride ion 49, 50
Fock operator (matrix) 104
formaldehyde 23
fragmentation approach 28
fujasite 72
fullerenes 35, 60
functional 118–120

G

Gauss' theorem 13, 14, 98
Gaussian basis sets 100–102
Gaussian-type orbitals (GTO)
29, 101, 105
Gaussian product theorem 102

gravitational field 14
gravitational forces 1, 2
Green's theorem 87, 98
guanine 35, 64

H

Hamiltonian 100
Hammett constant 75
Hartree-Fock (HF) theory 100, 101
Hellmann-Feynman theorem 44, 45
Hessian matrix 126, 127
high-energy molecules 70
Hohenberg-Kohn theorem 118
homoconjugation 65
Hopf-Poincaré theorem 128
Hückel theory 110
hydrophobicity 75
hydroxide ion 52
hydrogen chloride 58
hydrogen cyanide 58
hydrogen fluoride 58
hydrogen molecule 56

I

intermediate neglect of
differential overlap (INDO) 113
intermolecular interactions 67–70
ionization potential 104, 112
isodensity surface 65
isopotential surfaces 68

J

Janak's theorem 120

K

Keggin ion 73
Kohn-Sham kinetic energy 119, 120
Kohn-Sham scheme 119
Kohonen network 76
Koopmans' ionization potential 120

L

Laplace's equation 15
Laplacian 7, 32, 56, 96
Laplacian operator 7, 56, 96

lattice energy 77
 lithium molecule (Li_2) 116
 Legon–Millen rules 67
 Lindquist ion 73
 lone pairs 25, 35, 55, 56
 Löwdin charges 25

M

maximum of a function 127, 128
 medicinal chemistry 79
 MESP for a product of
 Gaussians 107, 108
 minimal basis set 106
 minimal surface 34, 54
 minimum of a function 127, 128
 modified neglect of differential
 overlap (MNDO) 25, 29
 molecular anions 51, 52
 molecular electron density 20
 bond critical point 121
 cage critical point 121
 contours 116
 Laplacian 121
 non-nuclear maxima 116
 ring critical point 121
 molecular electrostatic field
 (MEF) 19, 43, 44
 molecular electrostatic potential
 (MESP) 17, 44, 45
 electron localisation 18
 Gaussian charge density 106
 experimental determination 19, 30
 semi-empirical wave
 function 29
 molecular mechanics of clusters
 (MMC) model 68
 molecular orbital 26
 molecular wave function 26
 MOPAC 113
 Morse's lemma 128
 Mulliken Charges 70
 multipole moments 20

N

neon atom 49
 nitrogen molecule 56
 non-degenerate critical point 128, 129
 non-nuclear maxima 51

nucleophilic attack 65
 nitroaromatics 71
 nitrate ion 54

O

oil-water partition coefficient 76

P

parallel program 28
 Pariser–Parr–Pople (PPP) method 110
 π -facial selectivity 65
 phase portraits 128
 PM3 method 29
 point charges 21
 point charge models 22
 Poisson equation 24
 Poisson–Boltzmann equation 77
 polyatomic anions 52
 Pople–Nesbet equations 104
 potential-derived atomic charges
 (PD-AC) 22
 primitive Gaussians (PG) 21
 principle of superposition 3

Q

quadrupole moment 11
 quantitative structure–activity
 relationship (QSAR) 79
 quantization of charge 2, 4
 quarks 2

R

regioselectivity 65
 restricted Hartree–Fock (RHF)
 theory 104
 ring critical points 121
 root mean square deviation (RMSD) 23
 Roothaan equations 103

S

saddle point 55
 scalar field 72

134 *Electrostatics of Atoms and Molecules*

self consistent field (SCF)
approximation 108, 109

semi-empirical methods
AMI, AMPAC, Hückel theory,
Extended Hückel method, PPP
theory, MOPAC, PM3, Zero
differential overlap (ZDO) 113

shells 106

signature of a critical point 126, 127

Slater determinant 100

Slater-type orbitals (STO) 101

Slater's X_α method 120

S_N2 reaction 65

spherical polar co-ordinates 96

spin orbital 100, 101

split-valence basis 106

Stokes' theorem 99

structure-activity relationship
(SAR) 75

T

Teller's theorem 42

Thomas-Fermi (TF) theory
molecular nonbinding 39-42

Thomas-Fermi atomic model 39-42

topography 125

bond ellipticity 123

molecular electron density 47

molecular electrostatic potential 49-51

molecular electron momentum
density 128

two-electron integrals (ERI) 104

TZ, TZP, TZ2P (Gaussian)
basis-sets 106

U

UNIPROP 28

UNIVIS 34

unrestricted Hartree-Fock (UHF)
theory 104

V

van der Waals complexes 67
radii 67

surface 67

vector 91-99

field 8

products 92-95

vertical ionization potential 104

visualization 33-35

contours 33-35

isosurfaces 35

pixel plots 33

ball-and-stick models 33

W

water molecule 25, 47, 117

Wolfsberg-Helmholtz
approximation 111

Z

zeolites 72, 73

zero differential overlap (ZDO) 110